Faculty of Science and Technology

Past methane emissions in the earliest Pleistocene on Yermak Plateau, NW Svalbard.

Karianne Heimdal
Geo-3900
Master thesis in Geology
May 2016
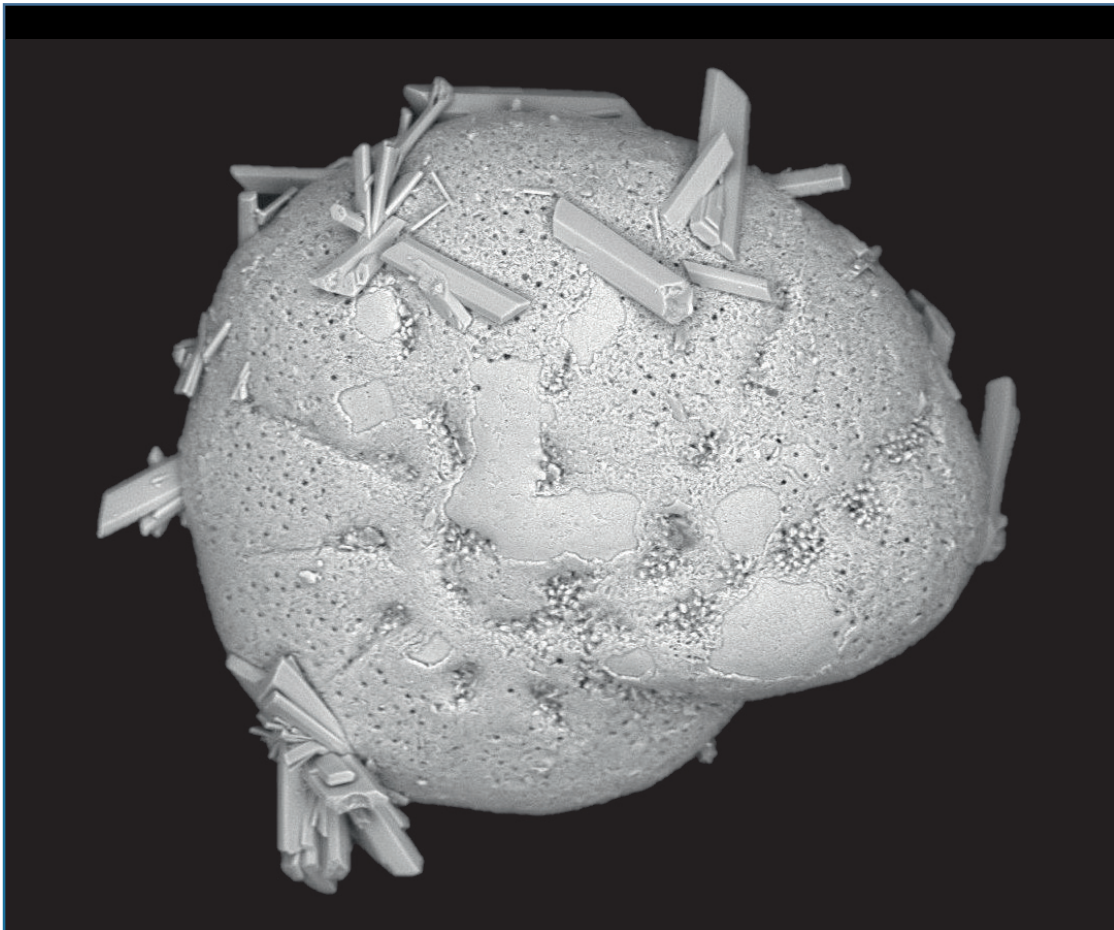
Abstract

Hole 912A (Ocean Drilling Program (ODP) Leg 151) drilled on the Yermak Plateau (eastern Arctic Ocean) is used to investigate past methane emissions in the earliest Pleistocene. Preliminary work showed depleted $\delta^{13}C$ values at 93-96 meters below sea floor (mbsf), and an increase in methane concentration between 11, 5 and 23 mbsf. A secondary sampling focused on intervals between 10 and 23 mbsf (core 912A-2H and 912A-3H) and between 78 and 116,6 mbsf (core 912A-10X, 912A-11X and 912A-13X). The results are divided into intervals, where several intervals show depleted $\delta^{13}C$ values in foraminifera test. Depleted calcite $\delta^{13}C$ values in interval II from 13,05 to 20,18 mbsf could imply an early effect of diagenesis due to a suggested modern day sulfate-methane transition zone (SMTZ) located between 13 to 23 mbsf. Extremely negative calcite $\delta^{13}C$ values in sediments represented in interval III and IV (71,96 to 97 mbsf) have been interpreted as being due to secondary methane-derived authigenic carbonates. This clearly indicates that the benthic foraminifera record past methane seepage events on the Yermak Plateau. The result is consistent with other studies that attribute anomalous carbon isotopic depletions in marine sediments to release of methane from destabilized methane hydrates. The mechanism for gas hydrate dissociation is suggested to be associated with an ice shelf retreat after ~1.5 Ma (millions of years before present) of the Svalbard-Barents ice sheet, and temperature changes due to increased inflow of warmer water currents through the Fram Strait.

Acknowledgements

To start with, I would like to thank my scientific advisors Prof. Giuliana Panieri and Dr. Jochen Kneis, who supervised me with great enthusiasm. They have shared their expertise, experience and provided great support during this master thesis. Together with CAGE (Centre for Arctic Gas Hydrate), they made it possible for me to travel to the IODP (International Ocean Discovery Program) core Repository in Bremen to collect samples. In addition, thanks to Soma Baranwal for giving me preliminary work for this master thesis. I`m grateful to Prof. Jürgen Mienert for organizing a CAGE cruise I took part in from Tromsø to the north of Svalbard during my master preparation.

I would also like to thank Trine Dahl, Ingvild Hald and Karina Monsen for all their expertise and help at the Geology Department Laboratory at the University of Tromsø. Moreover, many thanks to Kai Mortensen for administrative work. He has always had an open door during all my five years at the University.

I would like to thank my fellow students through my five years at the University of Tromsø. These people are greatly responsible both for my growth as a student and development as a person. During these five years we had many field trips together, shared hours of scientific discussions, helped each other, and just had fun enjoying life in general –Silje Røde, Maren Galguften Lunsæter, Frank Jakobsen, Gert Høgseth, Ida Kristin Danielsen, Nora Dahl, Ida Grindal Skagseth, Carina Nilsen, Halldis Lea, Sinthuja Sriharan and others.

I owe an immeasurable gratitude to my parents for their everlasting support, and my love Marius for being my cliff.

Karianne Heimdal

Tromsø, 13th of May 2016

Table of Contents

1.1 Objective of the study

The aim of this study is to reconstruct early Pleistocene paleoclimatic changes and assess potential methane emissions into the water column in the Arctic-Atlantic gateway region. This is done by using geochemical measurements of benthic and planktonic foraminifera in Ocean Drilling Program (ODP) Hole 912A (Yermak Plateau). Additional chronological control will be obtained using δ^{18} O of planktic/benthic foraminifera, while δ^{13}C will be scrutinized for evidence of methane emissions. Previous geochemical measurements of foraminifera and other sedimentological inferences for past climatic changes obtained from Hole 912A will be integrated with this new information and discussed in a regional/global contexts.

The motivation for investigating the core was based on preliminary data from Hole 912A that showed: (1) An increase in methane concentration between 11, 5 and 23 mbsf in core 912A-2H and 912A-3H (Stein, R. et al. 1995) (2) A negative excursion of δ^{13}C in benthic foraminifera was observed between 93-96 mbsf in core 912A-11X.

By revisiting ODP Hole 912A, additional sampling was proceeded in the mentioned intervals for further investigation.

1.2   Background

1.2.1   North Atlantic-Arctic Gateways

The north Mid Oceanic Ridge in the Atlantic Ocean represent the opening of the Norwegian-Greenland Sea, and defines the boundary between the American- and the Eurasian plate (Figure 1). The ridge is represented by both extensional and transform offset. The Fram Strait is a deep passage situated between Greenland and Svalbard, and is the only deep water connection of the Arctic Ocean to the rest of the world`s oceans (Thiede, J. et al. 1996) The opening of the Fram Strait induced deep-water exchange between the Arctic and the Atlantic Oceans, and forced long-term paleoclimatic changes(Jakobsson, M. et al. 2007). Therefore, knowledge of the evolution of the Fram Strait is a key to understanding global oceanic circulation (Spiegler, D. 1993). The Fram Strait opening was due to the propagation of seafloor spreading of the northern Greenland Sea into the Eurasian Basin. Evidence suggest that the oceanic crust formation started at ca. 53-56 Ma (Stein, R. 2008). According to published tectonic models, it took about ~30 million years until the gateway was fully opened. Evidence suggest that the ventilation between Atlantic- and Arctic Ocean began during the late early Miocene at about 18.2 Ma ago and was completed ca. 0.7 Ma later (Jakobsson, M. et al. 2007). The complex system of fracture zones along the ridge provide the link to the global current circulation system, expressed by the exchange of warm Atlantic and cold Arctic water masses (Stein, R. 2008). The Svalbard archipelago east of the Fram Strait, is part of the Barents Sea continental shelf, and is situated between 76-81°N. The western part of the Svalbard margin is characterized by a narrow shelf and a steep slope of 4-5°, carved by glacially eroded troughs (Slubowska-Wodengen, M. et al. 2007).
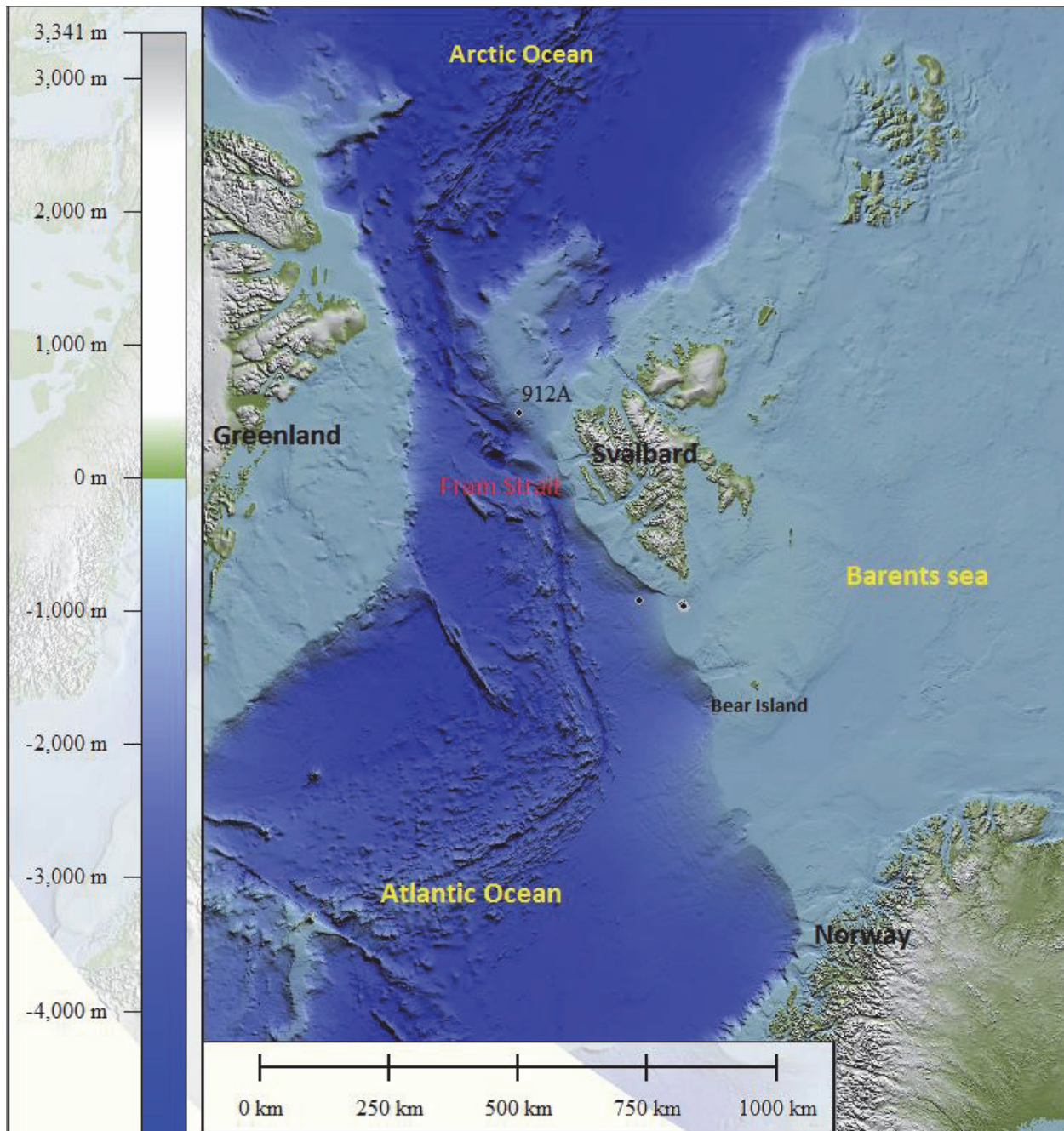
Figure 1: Map of the North Atlantic-Arctic Gateway from IBCAO modified with place names, and the investigated Hole 912A. (Jakobsson, M. et al, IBACO).

1.2.2 Oceanography

The Atlantic water is the largest source of heat, mass, and salt to the Arctic Ocean via the Fram Strait. The Fram Strait (Figure 1) is 2500 meter deep, and plays a major role in the global thermohaline circulation, due to deep water renewal, deep water ventilation and the seasonal ice cover which transfer latent heat to the atmosphere (Aagaard, K. et al. 1987, Thiede, J. et al. 1996). Atlantic Water (AW) from lower latitudes bring warm and saline water northwards, and is transported across the Greenland-Scotland Ridge and flows toward the coast of Norway as the North Atlantic Current (NAC) (Slubowska-Wodengen, M. et al. 2007). The NAC is characterized as relatively warm (>3°C) with salinity slightly above 35‰ (Loeng, H. 1991). When the current flows northwards as the Atlantic Norwegian Current (NwAC) it follows the continental slope of the Norwegian margin (Figure 2). The upper mixed layer cools with of the exchange of heat with the atmosphere, and the density increases. When the current reaches the latitude of the Bear Island Channel it splits into two currents; one enters the Barents Sea as the North Cape Current (NCaC), while the other continues as the West Spitsbergen Current (WSC) toward the Fram Strait (Aagaard, K. et al. 1987, Meincke, J. et al. 1997). By the time the current reaches the Fram Strait, the average temperature loss is 5°C and the salinity dropped with 0,3‰ (Manley, T. O. 1995). At around 79°N the WSC splits into three streams: the Svalbard Branch (SB), Yermak Branch(YB) and the Return Atlantic Current (RAC) (Bourke, R. H. et al. 1988). The SB flows along the Svalbard shelf and the continental slope, were it divides into several series of complex topographically controlled branches in the upper 300 meters of the water column (Manley, T. O. 1995). The primary branch travel north-east along the north coast of Svalbard and eventually submerge below the edge of the summer sea ice and circulates in to the Arctic Ocean. It is estimated that 20% of the WSC is brought to the Arctic Ocean trough the SB, and therefore this branch is the major supplier of warm saline water into the Arctic Ocean (Bourke, R. H. et al. 1988). The second branch follows the western flank of the Yermak Plateau as the YB. It follows the lower continental slope at the 1000-m contour, along the seaward edge of the plateau, and then rejoins the SB somewhere northeast of Spitsbergen (Cokelet, E. D. et al. 2008). The RAC makes a U-turn and flows southward to join the cold East Greenland Current (EGC) (Figure 2), which travels southwards from the Arctic Ocean along the Greenland margin (Bourke, R. H. et al. 1988, Muench, R. D. et al. 1992). Low salinity and density Polar Surface Water (PSW) is mainly created in the Arctic Ocean. This is due to atmospheric transport of water

vapor from lower latitudes and large run-off from the continents surrounding the Arctic Ocean. The EGC transports the fresh cold waters southwards through the Fram Strait and the Denmark Strait into the North Atlantic Ocean (Rudels, B. et al. 2005). The modern day estimation is that ~1,160 km³ of annual liquid freshwater is transported in the EGC from the Arctic Ocean. (Stein, R. 2008). Changes in the freshwater transport rates can result in changes of the deep-water formation and influence the global thermohaline circulation and ventilation (Broecker, W. S. 1997). It is suggested that change in freshwater input along with the sea-ice cover and earth albedo has triggered climate changes in the past (Driscoll, N. W. and Haug, G. H. 1998). Because of this important mechanism for the global thermohaline circulation it makes the Arctic very sensitive to changes in flow patterns, and an important place for investigation of paleoclimate. An overview of the major currents in the North Atlantic Ocean is shown in Figure 2.
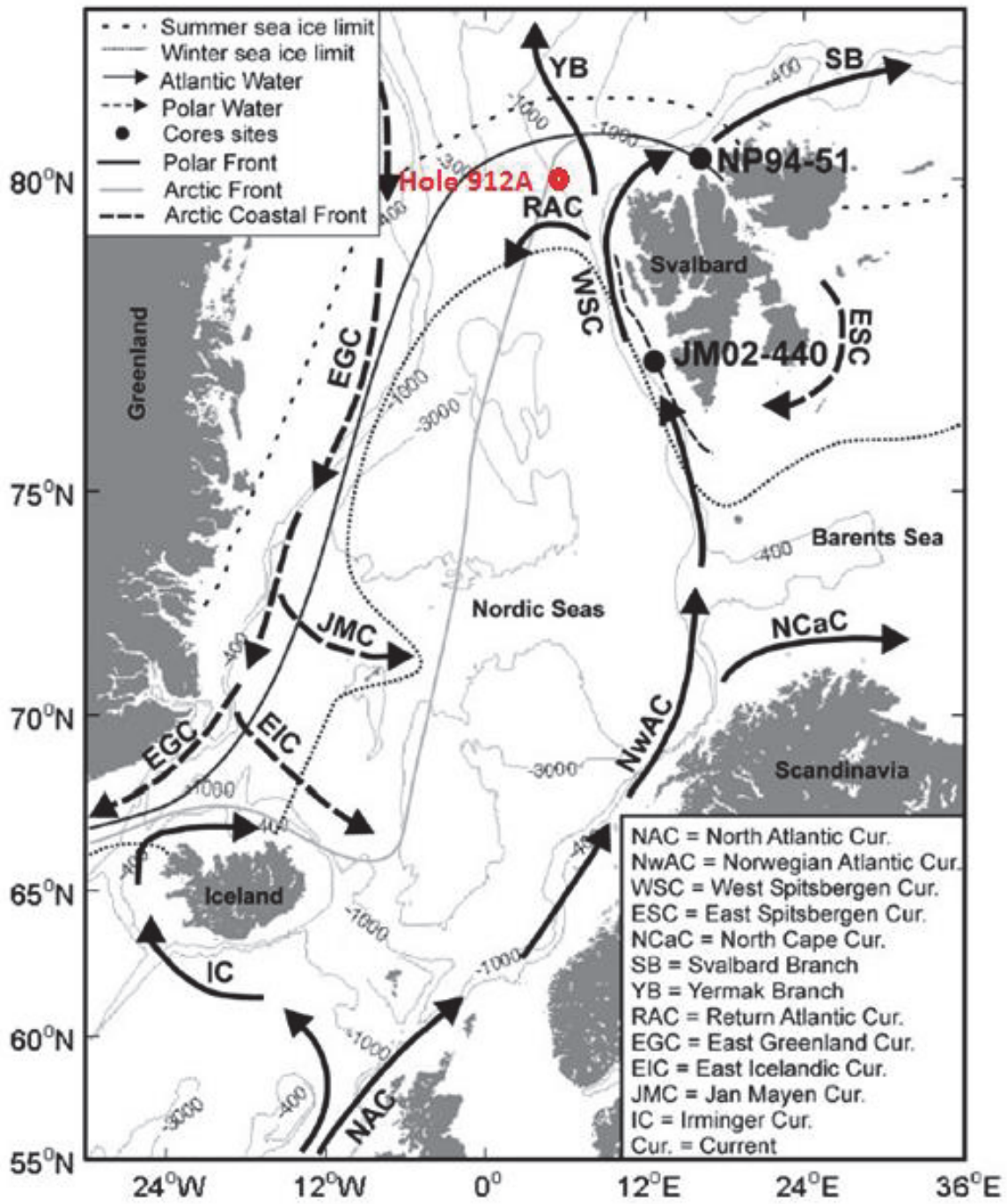
Figure 2: Overview of the major currents in the North Atlantic Ocean. Hole 912A are shown in red. Figure modified from Slubowska-Woldengen et al., 2007.

1.2.3   Quaternary period

The geological record is divided into periods, which again can be subdivided into epochs. The Quaternary period is the most recent major subdivision of the geological record, and can be subdivided into the Pleistocene and Holocene, see Figure 3 (Lowe, J. J. et al. 1997). The start of the Quaternary period coincides with the base of Gelasian Stage which is the Marine Isotope Stage (MIS) 103, and has been calibrated to ~2.58 Ma (Gibbard, P. L. et al. 2010). The start of Holocene is 11, 700 years before AD 2000 (Lowe, J. J. et al. 1997). The conventional subdivision of the Quaternary is into glacial and interglacial stages, with further subdivisions into stadial and interstadial episodes. Glacial stages are colder periods with presence of major extensions of ice sheets and glaciers. Interglacial periods are usually recognized as warmer intervals with temperatures at the thermal maximum as high as or even higher than those experienced during the Holocene. Stadials are viewed as shorter time intervals where it was cold, with occurrence of local ice advances. Interstadials are relatively short-lived periods of warmer climate coinciding with glacial periods (Lowe, J. J. et al. 1997). The Quaternary period has shown distinctive changes between repeated warm and cold periods (Lowe, J. J. et al. 1997).

(Emiliani, C. 1955) pioneered one of the most powerful tools in Quaternary stratigraphy and paleoenvironmental reconstructions, which is the oxygen isotope analysis. Oxygen isotopes from calcareous microfossils in deep sea records have been extracted to identify over 100 marine oxygen isotope stages during the past 2.5 Ma. Working from the most recent time, each isotopic stage has been assigned a number where even numbers denotes glacials (cold episodes), and uneven numbers denotes interglacials. Detailed age control for isotope records around the world have been established by "stacking" a great number of records (Gupta, B. K. S. and Barun, K. 1999). The LR04 stack for example, contains over 38,000 individual δ^{18} O measurements from 57 globally distributed sites, sampled at many different laboratories. Because this stack incorporates information from so many sites, accurately reflects changes in global climate (Lisiecki, L. E. and Raymo, M. E. 2005). Figure 3 shows the formal division of the Quaternary period, constructed by the International Commission on Stratigraphy's Subcommission on Quaternary Stratigraphy, in partnership with International Union for Quaternary research (Gibbard, P. and Cohen, K. M. 2008).

Figure 3: Global chronostratigraphical correlation table for the last 2.7 million years. (International Commission on Stratigraphy), Cambridge, England (Cohen K.M. & Gibbard, P. 2011).

1.3 Isotopes

Isotopes has become one of the most widely used methods for paleoenvironmental reconstructions. Changes in isotopes can be used to reconstruct paleoclimate and paleoceanographic conditions, together with ocean paleocirculation patterns, ice-volume, sea-level and the carbon cycle, and how these record varies with time (Katz, M. E. et al. 2010) and the principles behind the methods will now be introduced.

1.3.1   Carbon isotopes

Carbon (C) has three naturally occurring isotopes, which is atoms of the same number but different atomic weight. ^{12}C and ^{13}C are stable isotopes, while ^{14}C is unstable and therefore radioactive (Armstrong, H. and Brasier, M. 2005). The carbon cycle describes the movement of carbon between biota (living or dead), the atmosphere, the hydrosphere and the lithosphere (Gupta, B. K. S. and Barun, K. 1999, Harnung, S. E. and Johnson, M. S. 2012). Most of the carbon exchange between the Earth`s surface and the atmosphere occurs via carbon dioxide ($CO_2$ ). At the Earth`s surface, carbon is mainly found in two main carbon reservoir: organic matter and sedimentary carbonates (Compton, J. S. and Mallinson, D. J. 1996). The ratio between the lighter and heavier isotopes (i.e. ^{13}C/^{12}C) is expressed as the delta (δ) value pr. thousand (‰) showed by the equation;

$$\delta^{13}C = \frac{(^{13}C/^{12}C)\ sample - (^{13}C/^{12}C)\ standard}{(^{13}C/^{12}C)\ standard} \times 1000$$

The terms heavier/lighter, positive/negative, or enriched/depleted refer to the increase/decrease in the heavy isotope ^{13}C (Armstrong, H. and Brasier, M. 2005).

The δ^{13}C in deep water reflects: (1) time of exposure to organic matter decay, (2) amount of organic matter decayed in the deep water, and (3) the rapidity of organic matter decay, which is temperature dependent (Gupta, B. K. S. and Barun, K. 1999). This technique provide a powerful method for the reconstruction of oceanic circulation.

The δ^{13}C are effected by several major controls, listed in Table 1. Global shifts are related to changes in terrestrial vegetation and/or burial/oxidation of sedimentary organic matter, and the

interrelated influences of export production, respiration at depth and the age of the deep water (Gupta, B. K. S. and Barun, K. 1999). The marine reservoir effect (MRE) is the carbon age offset at any point in time between samples formed in the terrestrial biosphere, which is in equilibrium with the atmosphere, and marine organisms that absorbs carbon from the ocean. This offset exists because of the lack of carbon exchange between the deep water and the atmosphere (Ascough, P. L. et al. 2006). The planktonic foraminifera living in the surface water builds tests (shells) of calcium carbonate ($CaCO_3$), and has $\delta^{13}C$-values that is more or less in equilibrium with the surface waters. Benthic foraminifera living et the sea floor are exposed to old bottom waters, and can have depleted $\delta^{13}C$-values. Table 1 show the main processes determining seawater $\delta^{13}C$ at any study site (shown in white), and the determining fractionations between $\delta^{13}C$ of carbonate in seawater (shown in gray) (Gupta, B. K. S. and Barun, K. 1999).

Table 1: The list show the effects on δ^{13} in benthic and planktonic foraminifera due to global and local impact and typical magnitude (Gupta, B. K. S. and Barun, K. 1999).

Carbon isotopes Process	Deep/ Benthic	Surface/ Planktonic	Impact and typical magnitude
photosynthesis		√	global, but locally variable; <1‰
respiration	√	√	local; <1‰
export production	— causes gradients —		function of photosynthesis, respiration, 'age' of deep water
'age' of deep water	√		along deep water path; up to >1‰
shifts in terrestrial vegetation	√	√	global; >1‰
burial/oxidation sedimentary organic matter	√	√	global; >1‰
equilibrium fractionation	√	√	everywhere; <1‰ to negligible (uncertain!)
depth habitat/vertical migrations		√	up to 1‰ depending on local temperature gradient
microhabitat effect		√	1‰ or more depending on local gradient in pore-water (very strong near gas-hydrate seepage)
growth-related effects		√ (some)	species (or specimen?) specific <1‰
photosynthetic symbiont effect		√	specimen specific <1‰
vital effect	√	√	species specific <1%, not well known for Foraminifera
changing carbonate ion concentration	√	√	<1‰, poorly known for natural conditions

1.3.2   Oxygen isotopes

Oxygen is the most abundant chemical element on Earth. It consists of three stable isotopes; ^{16}O, ^{17}O, ^{18}O, but only two are of importance in oxygen isotope analysis (^{16}O and ^{18}O) of

marine deposits (Lowe, J. J. et al. 1997). The deviation of a standard ratio of oxygen isotopes $^{18}O/^{16}O$ can be measured in the calcium carbonate tests of the foraminifera (Katz, M. E. et al. 2010). Oxygen isotope ratios are expressed as positive or negative values relative to the standard. The equation used are (Armstrong, H. and Brasier, M. 2005);

$$\delta^{18}O = \frac{(^{18}O/^{16}O)\ sample - (^{18}O/^{16}O)\ standard}{(^{18}O/^{16}O)\ standard} \times 1000$$

The standard normally applied for marine environments are measured in Pee Dee Belemnite rostrum (PDB) for the analyses of carbonates, and Standard Mean Ocean Water (SMOW) for analyses of water, ice and snow (Lowe, J. J. et al. 1997). The oxygen isotopic composition of the foraminifera tests reflects the ^{18}O of the seawater (δw), where the foraminifera calcifies the test, as well as the temperature-dependent fractionation during the calcification process. In turn, the δw is the function of 1) global ice volume and 2) global/regional river water input and evaporation/precipitation patterns for shelf and surface waters, especially towards higher latitudes (Katz, M. E. et al. 2010).

The isotopic composition of ocean waters can be reconstructed from the ratio between ^{18}O and ^{16}O, of carbonate shells and skeletons preserved in deep sea sediments (Lowe, J. J. et al. 1997). Because the foraminifera calcifies in seawater, it reflects the global ice volume, region/local river water input, evaporation/precipitation for shelf, and surface waters (Katz, M. E. et al. 2010). The ratios of oxygen isotopes are measured in relative deviations of $\delta^{18}O$ ‰ from a laboratory standard.

There are significant evidences of variations in the $\delta^{18}O$ in ocean waters varied in quasi-cyclic fashion during glacial and interglacial periods. This is due to the natural fractionation of oxygen isotopes during evaporation of water from the sea surface. Evaporation of water into the atmosphere leads to fractionation of oxygen isotopes, as the lighter $H_2{}^{16}O$ molecules is drawn to the atmosphere in preference to the heavier $H_2{}^{18}O$ (Lowe, J. J. et al. 1997). The lighter $H_2{}^{16}O$ travel with the water vapor to lower latitudes, while the less heavy $H_2{}^{18}O$ precipitates as rain. This leads to an enrichment of ^{16}O in high latitude clouds and snow (Armstrong, H. and

Brasier, M. 2005). This means that carbonates in marine sediments will have higher ratio between ^{18}O and ^{16}O in glacial periods, compared to interglacial periods, shown in Figure 4 (Armstrong, H. and Brasier, M. 2005).
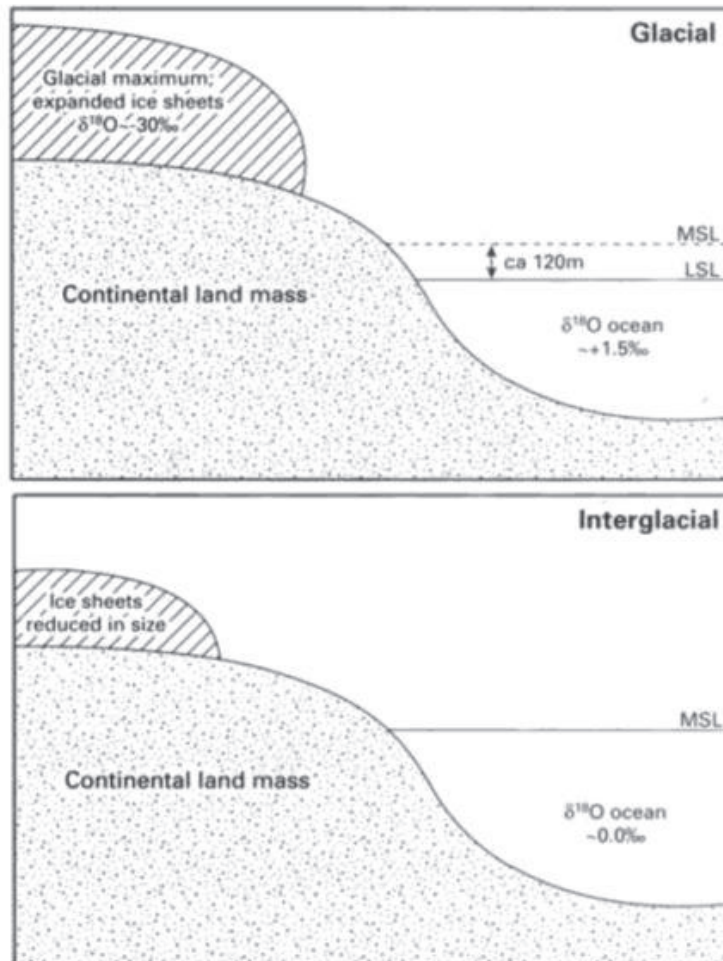
Figure 4: Variations in surface water oxygen isotope ratios during glacial maxima and interglacial with minimal ice-cover (Lowe, J., et al., 1997). In a glacial period the seawater will contain higher amounts of $\delta^{18}O$, than in an interglacial period.

1.4 Methane hydrates

Gas hydrates are solid compounds composed of natural gas and water. The water molecules are linked through hydrogen bonding, and create cavities that can enclose a large variety of gas molecules (Kvenvolden, K. A. 1988, Englezos, P. 1993). They occur naturally in pore space of different type of marine sediments where the chemical and physical criteria are met (Bunz, S. et al. 2003). Typical natural gas molecules include methane, ethane, propane and carbon dioxide. Methane (CH_4) appears to be the most common naturally occurring type. When the gas contains mainly methane (>99, 9 %), they are called methane hydrates (Kvenvolden, K. A. 1988). The interest of gas hydrates can be explained by three factors: (1) future energy resource (2) submarine geohazards (3) the factor in global climate change (Kvenvolden, K. A. 1993).

The occurrence of gas hydrates in nature are controlled by several factors: water temperature, geothermal gradient, depth below sea surface, pore water salinity and the concentrations of other dissolved chemicals and the composition of the gas (Judd, A. and Hovland, M. 2009).

Figure 5 shows a diagram of gas hydrate stability, defined by water temperature and pressure. Because the exact composition of gas and water in sediment pore spaces is not normally known, the diagram show a pure methane and pure water system to predict the depth and temperature regime (Kvenvolden, K. A. 1993). According to the diagram, the upper depth limit for methane hydrates are 150 meters where the surface temperature are below 0°C (Polar Regions). The zone where the gas hydrates are stable is called the gas-hydrate stability zone (GHSZ). The depth of this zone depends on the geothermal gradient, bottom water temperature, pressure (water depth), gas composition, pore
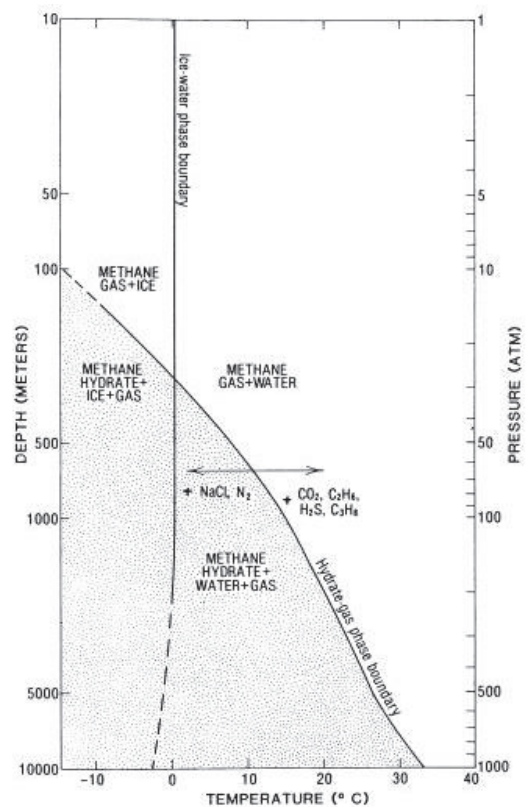
Figure 5: Phase diagram showing zones in which different phases of gas and water are stable in respect to depth, temperature and pressure of pure methane and pure water (Kvenvolden, K. A. 1993).

water salinity, and the physical and chemical properties of the host rock (Kvenvolden, K. A. 1995, Dickens, G. R. and QuinbyHunt, M. S. 1997, Bunz, S. et al. 2003).

1.4.1   Microbial, Thermogenic, and Abiotic Methane

Microbial methane gas is produced during diagenesis of sediments by microbial communities (Archaea) at relatively low temperatures (60-120°C). Methane produced this way are very dry, and generally indicate a shallow gas source in rocks and reservoir (Hunt, J. 1996). The production of microbial gas is further explained in the next section 1.4.2. Thermogenic gas is produced in deeper rocks by thermal cracking of organic matter at higher temperatures (190-200°C). This type of gas is often associated with oil reservoirs (Hunt, J. 1996). Both microbial and thermogenic methane is derived from biological compounds, and is often referred to as biotic methane (Etiope, G. 2015). Abiotic gas are produced by chemical reactions and do not require presence of organic matter. It is produced under a wide range of temperatures, and include magmatic processes and gas-water rock reactions. Around half of the atmospheric methane is generated by anaerobic respiration (Harnung, S. E. and Johnson, M. S. 2012). The origin of the methane gas can be detected by analyzing the stable isotopes of $\delta^{13}C$ and hydrogen ($^2H/^1H$). The result can be plotted into an empirical diagram showed in Figure 6, were the origin of the gas can be distinguished (Bernard, B. B. et al. 1978).
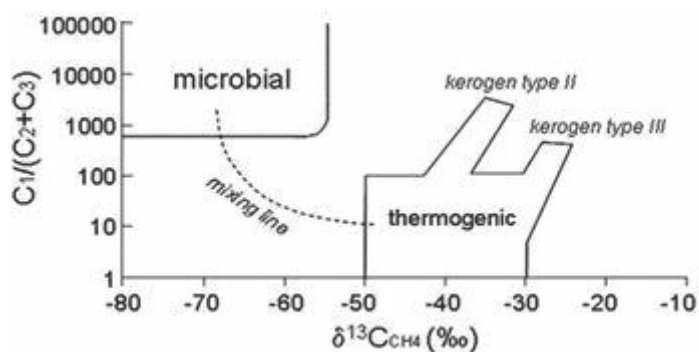
Figure 6: Bernard diagram (Bernard et al. 1978 redrawn by Etiope, G., 2015). An empirical diagram that differentiates the genetic fields of microbial and thermogenic gas. Microbial gas are generally characterized by $\delta^{13}C$ values lower than -50‰. Thermogenic methane has a range between -50 to -30‰, but can reach values down to -20‰. Abiotic methane has a wide range and overlap parts of both microbial and thermogenic methane.

1.4.2 Sulfate-methane transition zone (SMTZ)

The sulfate transition zone is a horizon in the sediment column where sulfate and methane coexist. This is a diffusion-controlled interface with enhanced microbial activity by the strict anaerobe Archaea (Harrison, B. K. et al. 2009, Judd, A. and Hovland, M. 2009). The ocean contain dissolved sulfate due to diagenesis of marine sediments, and the sulfate depletes with depth in the sediments (Borowski, W. S. et al. 1999, Harrison, B. K. et al. 2009). When methane increases with depth and encounter pore water with sulfate, anaerobic oxidation of methane occurs due to equation (1): $CH_4 + SO_4{}^{2-} \rightarrow HS^- + HCO_3{}^- + H^2O$ (Panieri, G. et al. 2016 and references therein). The SMTZ divides a distinct sediment interval both the sulfate reaction and the methanogenesis is the dominant form of microbial respiration. The depth of the SMTZ depends on the methane flux (Garming, J. F. L. et al. 2005, Panieri, G. et al. 2016) showed in Figure 7.
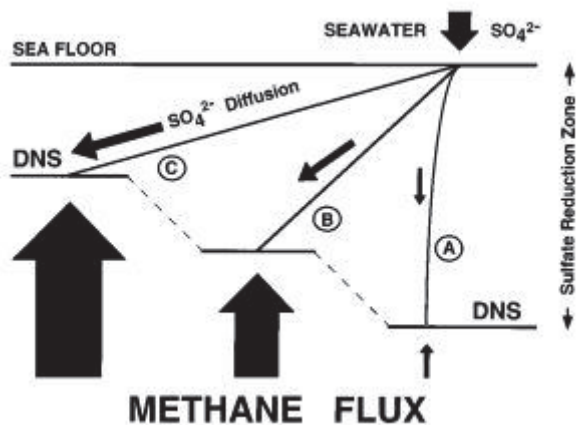
Figure 7: Diagram shows the how the upward methane flux controls the depth of no sulfate (DNS). The methane flux arrow size is proportional to the upward methane flux. A) Show the typical sulfate reduction of in situ organic sedimentary matter. B) and C) show the rate of sulfate consumption and steepness of sulfate gradients controlled by flux of methane from below (Borowski, W. S. et al. 1996).

In environments with methane seeps, the carbon isotopic signature in authigenic calcium carbonate has shown to be highly negative ($\delta^{13}C_{DIC}$ lower than -40‰), relative to normal marine environment where $\delta^{13}C$ is at -1‰ to 1‰ (Panieri, G. et al. 2016). This is caused by the metabolic coupling between Archaeas that oxidize methane at the SMTZ. Anaerobic oxidation of methane (AOM) is one potentially output. The production of bicarbonate from AOM can induce

the precipitation of calcium carbonate according to equation (2): $Ca^{2+} + 2HCO_3^- \rightarrow CaCO_3 + CO_2 + H_2O$ (Consolaro, C. et al. 2015). The so-called methane-derived authigenic carbonates can precipitate in different shapes like slabs, crusts, nodules, chimney, and pipes, with typical negative δ 13C values (Snyder, G. T. et al. 2007).

Dissolved inorganic carbon (DIC) derived from oxidation of methane (CH_4) in the pore space of adjacent sediments, are observed to give negative δ ^{13}C values in benthic foraminifera tests (Wefer, G. et al. 1994, Panieri, G. et al. 2009, Consolaro, C. et al. 2015) Most of the methane emitted at the seafloor escape in the water column and are consumed by methanotrophic aerobic microbes. Because of this, negative values are often not found in planktonic foraminifera. Although after deposition on the seafloor, benthic and planktonic foraminifera can be affected by alteration due to the precipitation of AOM derived authigenic carbonates on their tests, often referred to as secondary overgrowth (Torres, M. E. et al. 2003, Millo, C. et al. 2005, Panieri, G. et al. 2009). The use of foraminifera to trace past and present methane seepage is a subject of current debate (Panieri, G. et al. 2016). Preliminary data reveals a series of large negative excursions in benthic foraminiferal δ^{13}C, interpreted to result from incorporation of ^{13}C-depleted carbon from methane emissions during the primary biomineralization of the tests, and likely ingestion of ^{13}C-depleted methanotrophic microbes (Panieri, G. 2006). Up to 90% or more of the methane that reaches the SMTZ in the sediments close to the seafloor, may be consumed by anaerobic methane oxidation (Ruppel, C. 2011).

1.4.3   Global occurrence of methane

It is known that gas hydrates, containing mostly methane, has been formed naturally in sediments and exists in regions associated with meeting of the restricted physical and chemical criteria for stability (Englezos, P. 1993, Judd, A. and Hovland, M. 2009). Methane hydrates exist in vast quantities within and below the permafrost zone and in subsea sediments in the Arctic, Antarctic, and tropical and subtropical oceans (Englezos, P. 1993). The occurrence of methane hydrates can be divided into five geographic sectors (Ruppel, C. 2011) shown in Figure 8.
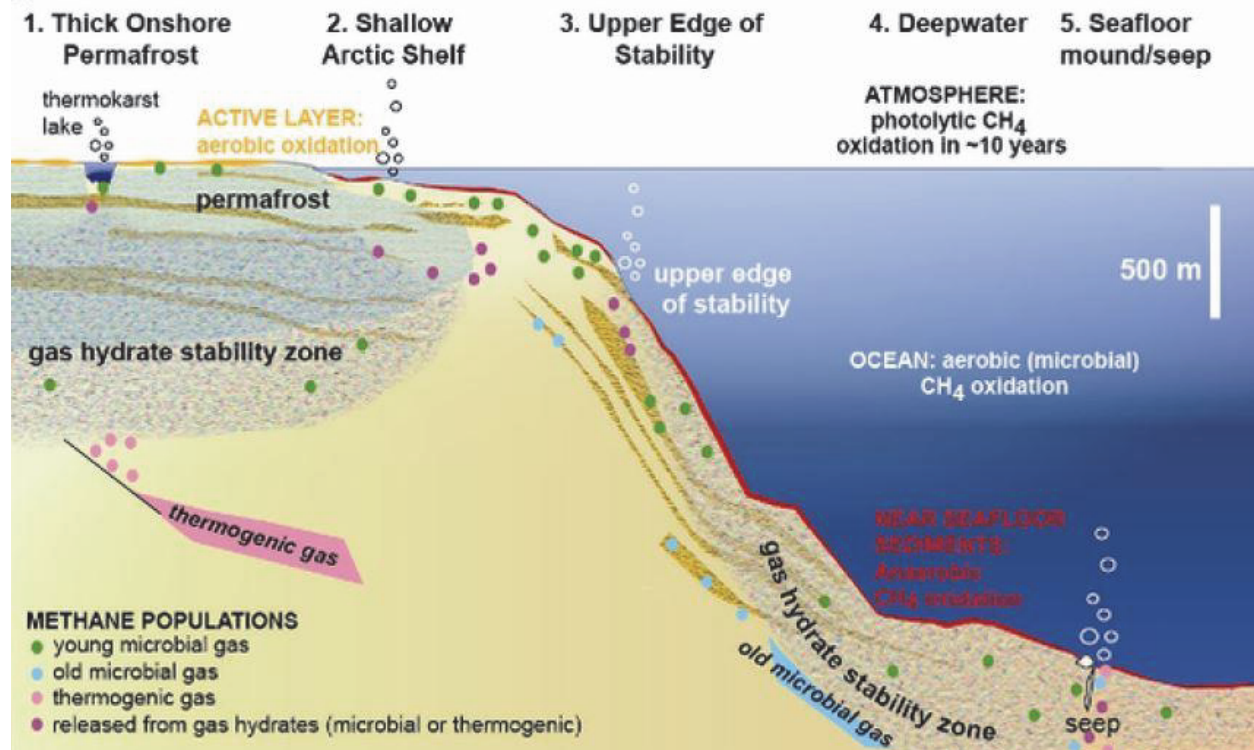
Figure 8: Cross-section from high latitude ocean margin. Sector 1 and 2 show onshore permafrost and shallow offshore subsea permafrost. Sector 3 show the upper continental slope, down to a deep water marine gas hydrate system in sector 4, and an area of deep gas seeps on the right in sector 5.

Gas hydrates are present in thick continuous permafrost sediments onshore in sector 1 (Ruppel, C. 2011). In sector 2 there are sediments on shallow marine arctic shelfs, which is often underlain by permafrost and associated with gas hydrates. These sediments formed in Pleistocene time, when these regions was exposed to much colder annual temperatures (Ruppel, C. 2011). In sector 3, the gas hydrates are present in the upper continental slope. The GHZS is situated near the surface and is vulnerable for gas hydrate dissociation driven by warming and imprinting of intermediate ocean waters. The dissolution of CH_4 consist in bubbles or oxidation in the water column, and should prevent the methane from being released into the atmosphere in this area. The deep water gas hydrates in section 4 constitute most of the global inventory of methane. These hydrates have generally low susceptibility to temperature changes over shorter time scales. If some of the CH_4 is released, it is suggested that much of it can be trapped in newly formed gas hydrate. Relatively pure gas hydrates can occur in seafloor mounds as shown in sector 5. These are shown in Figure 8 as a deep water phenomena, but can often occur at the

17

upper continental slope. They can dissociate by the warming and imprinting of overlaying waters.

The global water circulation keep the ocean bottom waters relatively cold (generally <10°C) all over the world. It is estimated that 99% of gas hydrates occurs in sediments of marine continental margins at saturations as high as 20% to 80% (Ruppel, C. 2011). The methane hydrates in the Arctic Ocean is deposited in shallow water depths close to shelf edges, and are stabilized by the cold temperatures (Biastoch, A. et al. 2011). The Arctic region is highly sensible to climate change, and the effect of rising temperatures is probably more extreme (Spielhagen, R. F. et al. 2011). Gas emissions of methane gas has been associated with global warming, due to hydrate decomposition as a result of higher bottom water temperatures (Etiope, G. 2015).

1.4.4   Methane and past Warming Events

Methane is a powerful greenhouse gas (GHG), and is ~20 times more potent than CO_2 (Ruppel, C. 2011). Methane hydrates are highly sensible to climate change, and a potential increase in temperature or decrease in pressure will destabilize the methane hydrate, causing it to decompose and release methane into the atmosphere and the ocean (Kvenvolden, K. A. 1995). Past gas seepage can be investigated by looking at geochemical and geological features in stratigraphic sequences or ice cores (Etiope, G., 2015). A series of rapid increased atmospheric methane concentration the last 400,000 years seem to have been accompanied by periods of rapid warming (Brook, E. J. et al. 1996, Blunier, T. and Brook, E. J. 2001). Changes in sources or sinks in methane could have caused variations in atmospheric methane concentration (Etiope, G., 2015). Large negative carbon isotopic excursions (CIE), recorded both in marine and terrestrial sediments during the Paleocene-Eocene Thermal Maximum at ~54,95 Ma, has been interpreted as reflecting widespread release of microbial carbon from dissociating marine methane hydrates (Zachos, J. C. et al. 2005). Two main hypotheses has been suggested to explain the rapid increase in methane concentrations, (1) emissions from tropical wetlands and (2) the clathrate gun hypothesis (Etiope, G., 2015 and reference therein). The first hypothesis propose a sudden increase in temperature and precipitation due to expansion of wetland (Chappellaz, J. et al. 1990). The second hypothesis advocates for sudden emissions of methane gas from hydrates in shallow sediments, which decomposed due to oscillations of intermediate water temperatures

(Dickens, G. R. 2003). Both hypotheses are highly debated, and there is a distinctive need for research to find a plausible mechanism to explain the increase of methane during the Quaternary period. Some studies have already suggested that the gas hydrates in water depths up to 400 meters are already effected by ongoing ocean warming in the Arctic Ocean (Shakhova, N. et al. 2010, Ferre, B. et al. 2012).

2 Materials and methods

The Ocean Drilling Program (ODP) Leg-151 drilled Site-912 on the Yermak Plateau in late summer 1993 (Myhre, A. et al. 1995). Leg-151 was conducted by the drill vessel JOIDES Resolution, and was escorted by the Finnish icebreaker Fennica. Site 912 is located on the southwestern slope of the Yermak Plateau with water depth of 1050 meter (Thiede, J. et al. 1995). Three holes were drilled at this site, named 912A, 912B and 912C. The material used in this study is from Hole 912A.
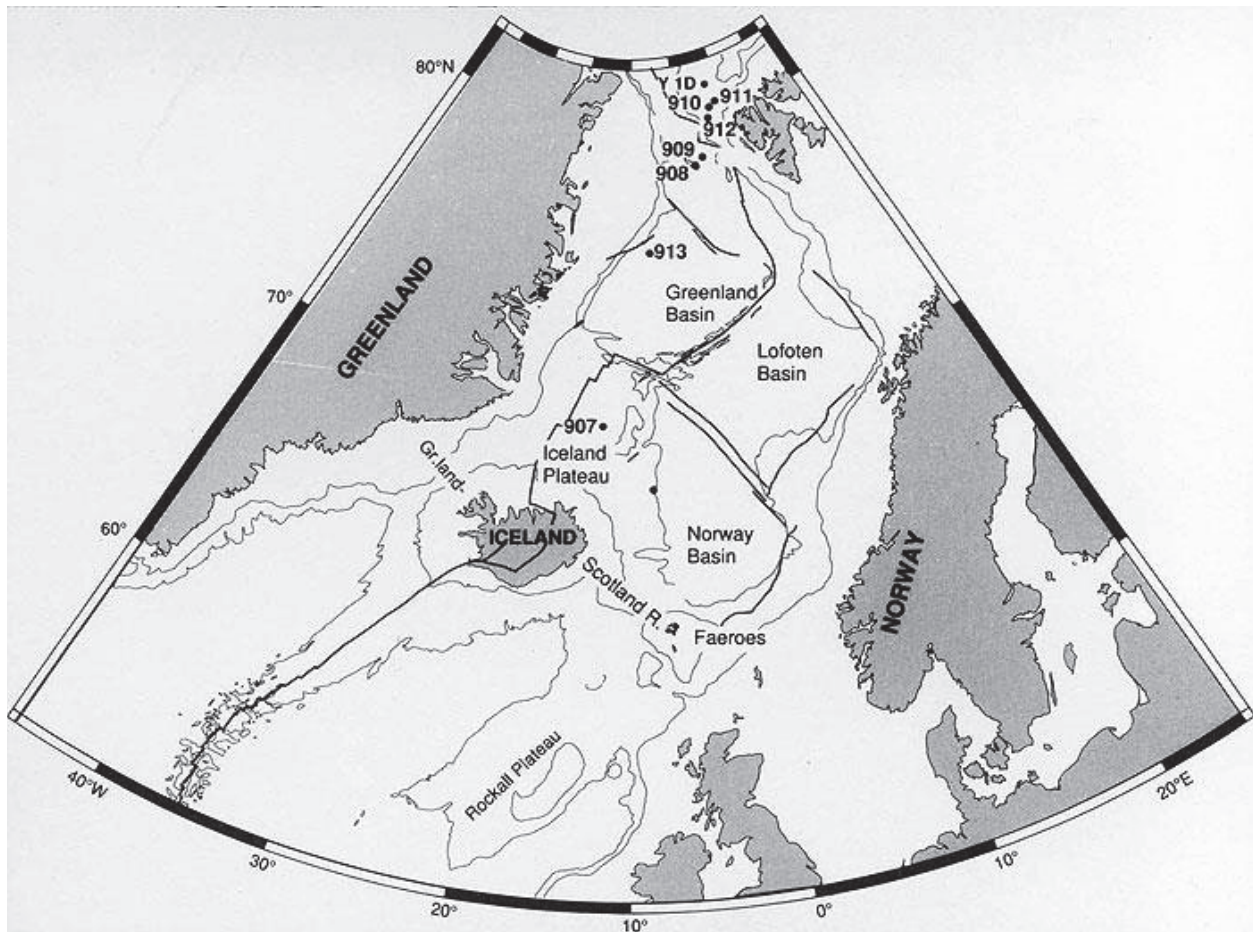
Figure 9: Map showing the sites of Leg 151, drilled by the ODP in 1993. Northeast of Svalbard lies the Site 912, which is used in this study (Myhre, A.M., Thiede, J., Firth, J.V., et al. 1995).

2.1 Hole 912A

The coring was conducted by JOIDES Resolution, a uniquely outfitted dynamically positioned drillship with a floating laboratory. The total length of the cored section was 145, 4 meters, in a total of 16 cores. Recovered length of the section was 118, 37 meters and the recovery was 81, 4%. The water depth at this site was 1047, 4 meters below rig floor. An advanced hydraulic piston corer (APC) was used for the first eight cores (912A-1H to 912A-8H), while an extended core barrel (XCB) assembly was run on the last eight cores (912A-9X to 912A-16X) (Myhre, A. M. et al. 1995). Details of core, length, depth and recovery are shown in Table 2.

Table 2: The coring summary of Hole 912A are shown due to core number, time, depth (in meter below sea floor), and length cored and recovered (Myhre et al. 1995).

Core	Date (1993)	Time (UTC)	Depth (mbsf)	Length cored (m)	Length recovered (m)	Recovery (%)
151-912A-						
1H	Aug. 27	1750	0.0–4.0	4.0	4.00	100.0
2H	Aug. 27	1805	4.0–13.5	9.5	9.93	104.5
3H	Aug. 27	1825	13.5–23.0	9.5	9.90	104.2
4H	Aug. 27	1915	23.0–32.5	9.5	10.06	105.9
5H	Aug. 27	1940	32.5–42.0	9.5	10.05	105.8
6H	Aug. 27	2010	42.0–51.5	9.5	10.23	107.7
7H	Aug. 27	2055	51.5–61.0	9.5	10.33	108.7
8H	Aug. 27	2120	61.0–70.5	9.5	10.28	108.2
9X	Aug. 27	2250	70.5–78.0	7.5	8.72	116.3
10X	Aug. 27	2335	78.0–87.6	9.6	8.01	83.4
11X	Aug. 28	0035	87.6–97.2	9.6	9.62	100.2
12X	Aug. 28	0215	97.2–106.9	9.7	0.00	0.0
13X	Aug. 28	0245	106.9–116.5	9.6	8.44	87.9
14X	Aug. 28	0325	116.5–126.1	9.6	0.00	0.0
15X	Aug. 28	0415	126.1–135.8	9.7	8.65	89.2
16X	Aug. 28	0510	135.8–145.4	9.6	0.15	1.6
Coring totals				145.4	118.37	81.4

2.1.1 Location of Hole 912

The Yermak Plateau is located on the eastern flank of the Fram Strait in the marginal Arctic Ocean. It forms forms the western part of the Barents Shelf, and is bounded by the Arctic Ocean to the north and the Svalbard archipelago to the south. The southern part of the Yermak Plateau has water depths of about 600-800 meter deep, with more shallow parts of less than 500 meter in the southernmost part. The basement morphology show a basement with a graben looking structures. Over the basement there are sediments with a thickness <1 km to >4 km thick (Mattingsdal, R. et al. 2014).
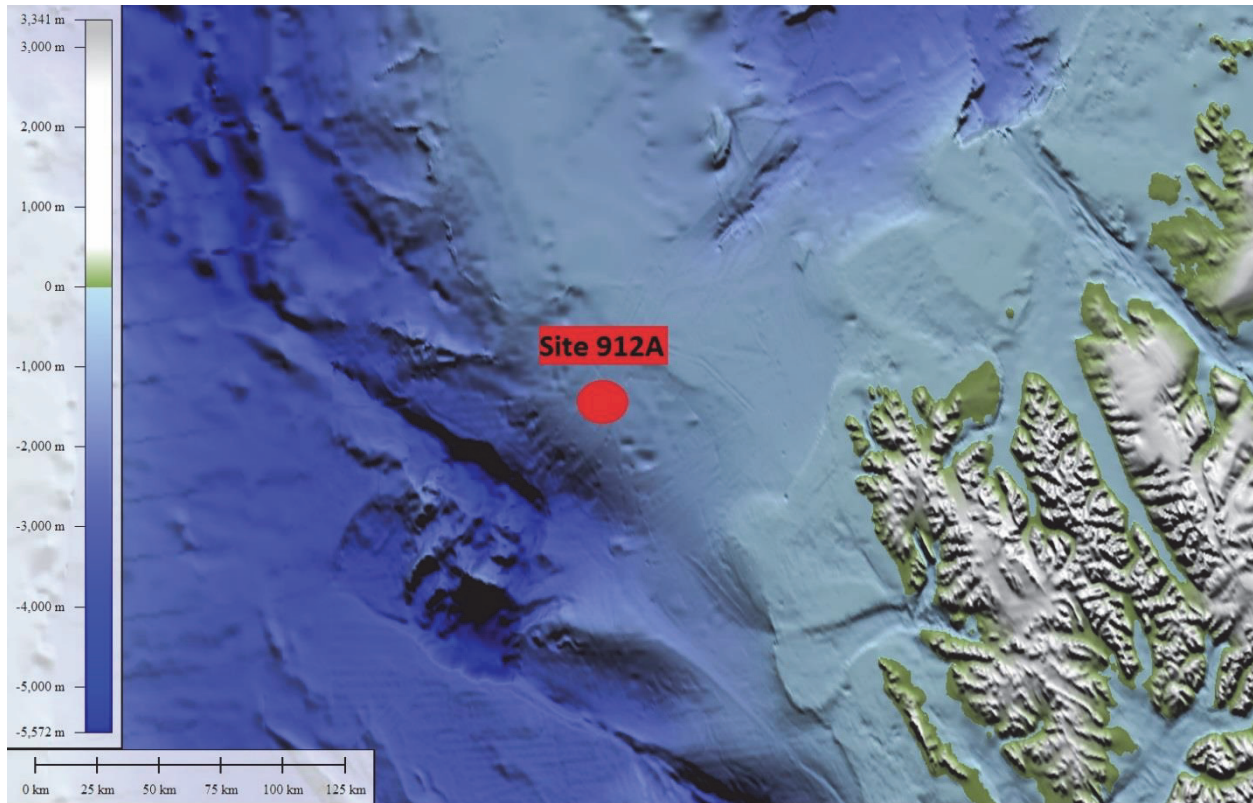
Figure 10: The location of the Site 912A, located on the southwestern part of the Yermak Plateau.

2.2 Description of Hole 912A

Myhre et al (1995) describes the stratigraphy of Hole 912A into two subunits 1A and 1B. The upper unit 1A has a thickness of 40 meters and is dominated by 1.5m layers of olive gray layers of clay and dark layers of clay. Despite the difference in color, the sediments composition do not change. Fining up sequences are common above 12 meters below seafloor (mbsf), with a thickness of 20 cm. They contain dark gray clay and are normally graded from clayey mud to silty clay. There are some evidences of bioturbation. Carbonate grains are in varying abundance throughout the core in clay and silt sizes. The highest abundance of carbonate grains appear in mud layers, and are represented in four dark gray mud layers in unit A. The coarse fraction dominating the sequence is quartz. Dropstones (diameter >1 cm) are observed in every core. The average in each core is about 15 dropstones, with the highest average is found near the part closest to the surface bottom at 30mbsf (Figure 11). Most of the dropstones is comprised of sedimentary rocks, but metamorphic and volcanic rocks are also present. Traces of foraminifera and nanofossils are found in the mud layers.

Subunit 1B has a thickness of 169 meters, and consist mainly of silt and clay, with some layers of silty mud and clayey mud. These layers of mixed mud are brownish in color, and the contact are usually gradational. Some sections contain iron-monosulfide, which appear as black sediments. The coarse fraction is dominated by quartz, same as subunit 1A. The rate of dropstone is lower in this unit. The average dropstones in each core ranges from 0 to 11 (Figure 11). The main type of dropstone is siltstone and sandstones. The igneous and metamorphic rocks found in subunit 1A is rare in this subunit. The content of inorganic carbonate varies from 1% to 12% throughout the unit (Myhre, A. M. et al. 1995).
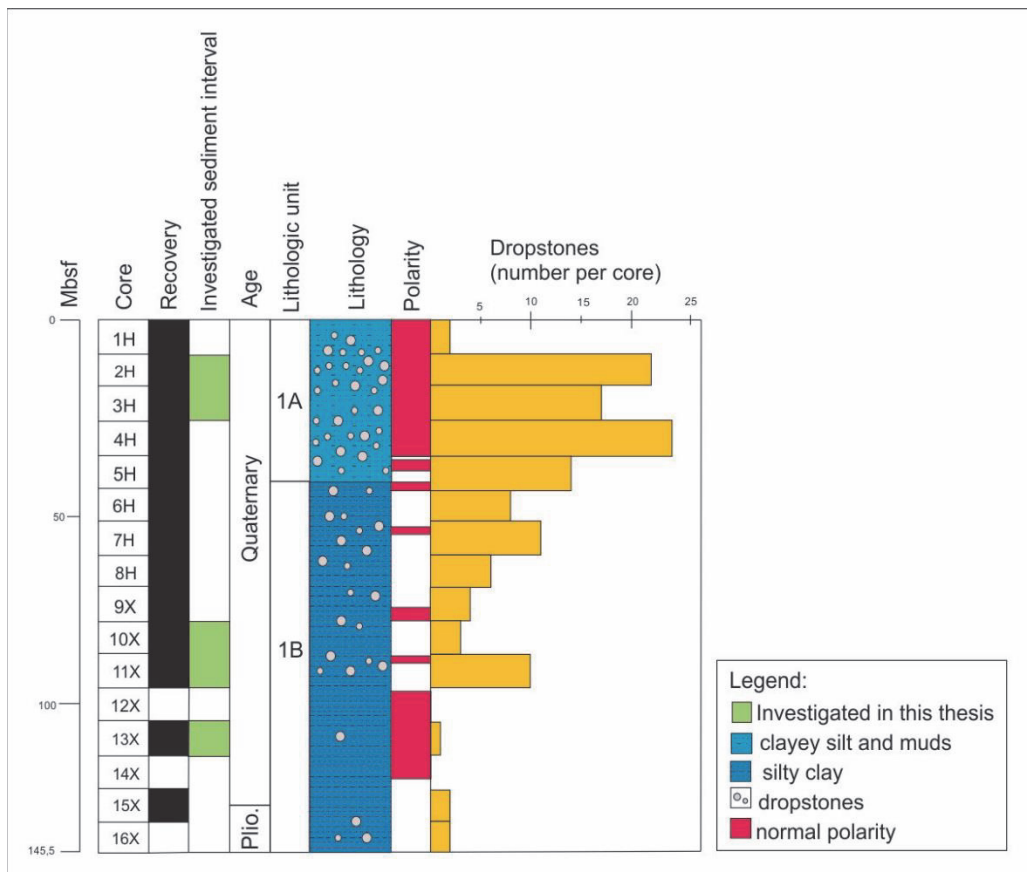
Figure 11: overview of cores at Hole 912A with depth, recovery, age, subunit 1A and 1B, lithology, polarity and number of dropstones. Redrawn form information and figures from (Myhre, A. M. et al. 1995).

2.3   Magnetostratigraphy and Biostratigraphy

Myhre et al (1995) found that siliceous microfossils are absent throughout the whole sequence, with some exceptions of reworked diatoms, silicoflagellates and rare radiolarians. Dinoflagelates are scarce, but terrestrial pollen and spores are common throughout the cores in Hole 912A. Age-diagnostic species was found, despite poorly preserved calcareous nanofossils and low species diversity. Samples from 151-912A-1H to 151-921A-4H contained *Gephyrocapsa* sp. This findings were correlated to the NN19 to NN21 Zones in the upper Quaternary period (Figure 12). Samples from 151-912A-5H to 151-912A-9X contained *Pseudoemiliana lacunosa, Gephyrocapsa caribbeanica* and *Gephyrocapsa oceanica.* These are assigned to the Quaternary Zone NN19, based on occurrence of *G. caribbeanica* together with *P. lacunosa*. Large specimens of *Gephyrocapsa* are found in 151-912A-8H and 151-912A-9X, and are correlated to the Quaternary Zone NN19. Below 151-912A-9X the samples contain *Gephyrocapsa, Crenalithus doronicoiides* and *Coccolithus pelagicus*. In this interval there is an absence of *G. caribbenica* and *G. oceanica*. Based on this, it is indicated that this interval can be correlated with Zone NN18 to NN19. The planktonic foraminifera *Neogloboquadrina pachyderma sinistral* are found in Core 151-912A-1H to -4H, and indicate a Quaternary age (Myhre, A. M. et al. 1995).

Myhre et al (1995) discussed the transition zone of sediments between the Pliocene and the Quaternary age, based on reworked diatoms. An interpretation done in conjunction with the findings of calcareous nannofossils and planktonic foraminifera, suggest the transition to be at 135, 8 mbsf (Core 151-912A-15X-CC). There was no recovery in the core between 97,2-106,9mbsf (Core 151-912A-12X-CC), 116,5-126,1mbsf (Core 151-912A-14X-CC), and 135,8-145,4mbsf (Core 151-912A-16X-CC), so the boundary are uncertain because of missing sediments in core sample (Myhre, A. M., et al. 1995).

Paleomagnetic studies provided significant temporal constrains for the sedimentary column with the identification of major chronozones and several short sub-chronozones. The inclination in terms of normal and reversed polarity has been interpreted and are shown as age-depth fix points in Figure 12 together with the biostratigraphy. The Brunhes/Matuyama reversal is interpreted to an age of 0,78 Ma (millions of years before present) and correlates with 24,6 mbsf in Core 912A-

3H. The top of Jaramillo subchron is poorly defined at ca 30 mbsf in core 912A-4H (Myhre, A., M. 1995). The Jaramillo base reversal is well defined at 36,5 mbsf interpreted to an age of 1,07 Ma in core 912A-5H. The Cobb Mountain subchrone is interpreted to be between 53,8 mbsf to 54,7 mbsf and is dated to an age of 1,20 Ma. The Olduvai Top is interpreted to be at 107,1 mbsf in core 912-13X with an age of 1,78 Ma. The Olduvai Base is interpreted to be at 121,6 mbsf in core 912A-14X with an age of 1,95 Ma (Myhre, A., M. 1995).
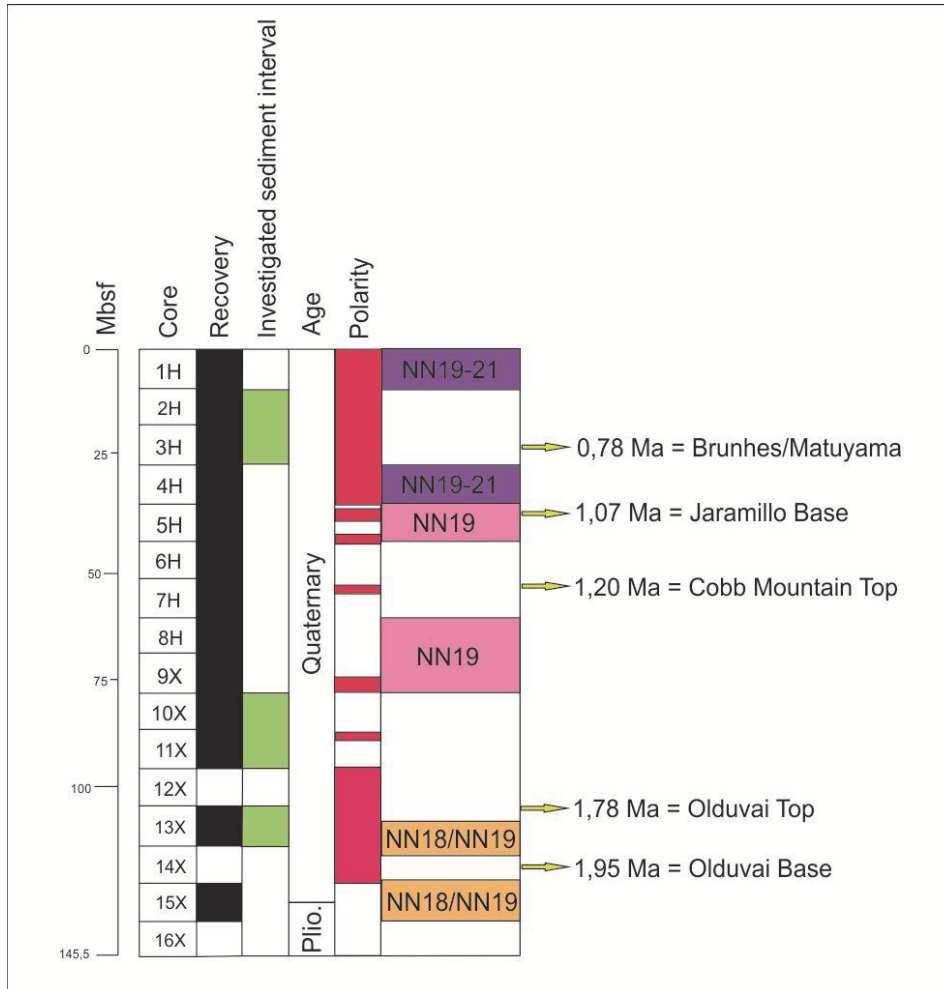
Figure 12: Biostratigraphy of Hole 912A redrawn from (Myhre, A. M. et al. 1995) and added datum from (Mattingsdal, R. et al. 2014).

2.4 Hydrocarbon measurements

Concentrations of methane, ethane and propane was monitored in every core by using standard ODP vacutainer and headspace-sampling techniques on Hole 912A (Stein, R. et al. 1995). The upper 11, 5 meters of the sedimentary sequence contained low methane concentrations of 8-18 ppm. Between 11, 5 meters and 23 meters below sea floor, the methane concentration increase distinctly from 18 to 40,000 ‰. The methane concentration increases immediately below the depth at which sulfate falls to zero (Stein, R. et al. 1995).

Figure 13: Methane concentration in Site 912A in ppm considering depth. (Stein, R. et al. 1995)

The ratio between methane and ethane are high, ranging from 4300‰ to 13,000‰, with a decreasing trend downhole (Myhre, A. M. et al. 1995).

2.5 Previous work and sampling strategy

Preliminary work had already been conducted on Hole 912A (Baranwal, S., unpublished data). Samples had been taken at 68-72 and 146-150 cm in every section of the core. In total, 154 samples were dried and sieved in size fraction 63μm and 100μm. A total number of 58 samples from the interval 0-20 meter below sea floor (mbsf) and 92-134 mbsf, was sent for stable isotope analyses. The result revealed strong negative excursions of $\delta^{13}C$ values in some intervals in Hole 912A. Analyses of *Cassidulina reniforme* showed a low negative peak in $\delta^{13}C$ (-8,82 ‰ VPDB) at 96, 37 mbsf in core 912A-11X section 6. *Cassidulina neoteretis* revealed negative values at 93, 56 mbsf (-13, 34 ‰ VPDB) in core 912A-11X section 4, and at 96, 37 mbsf (-9, 39 ‰ VPDB) in core 912A-11X section 6. The results from the preliminary work is showed in Figure 14. More detailed data are shown in the appendix 1.
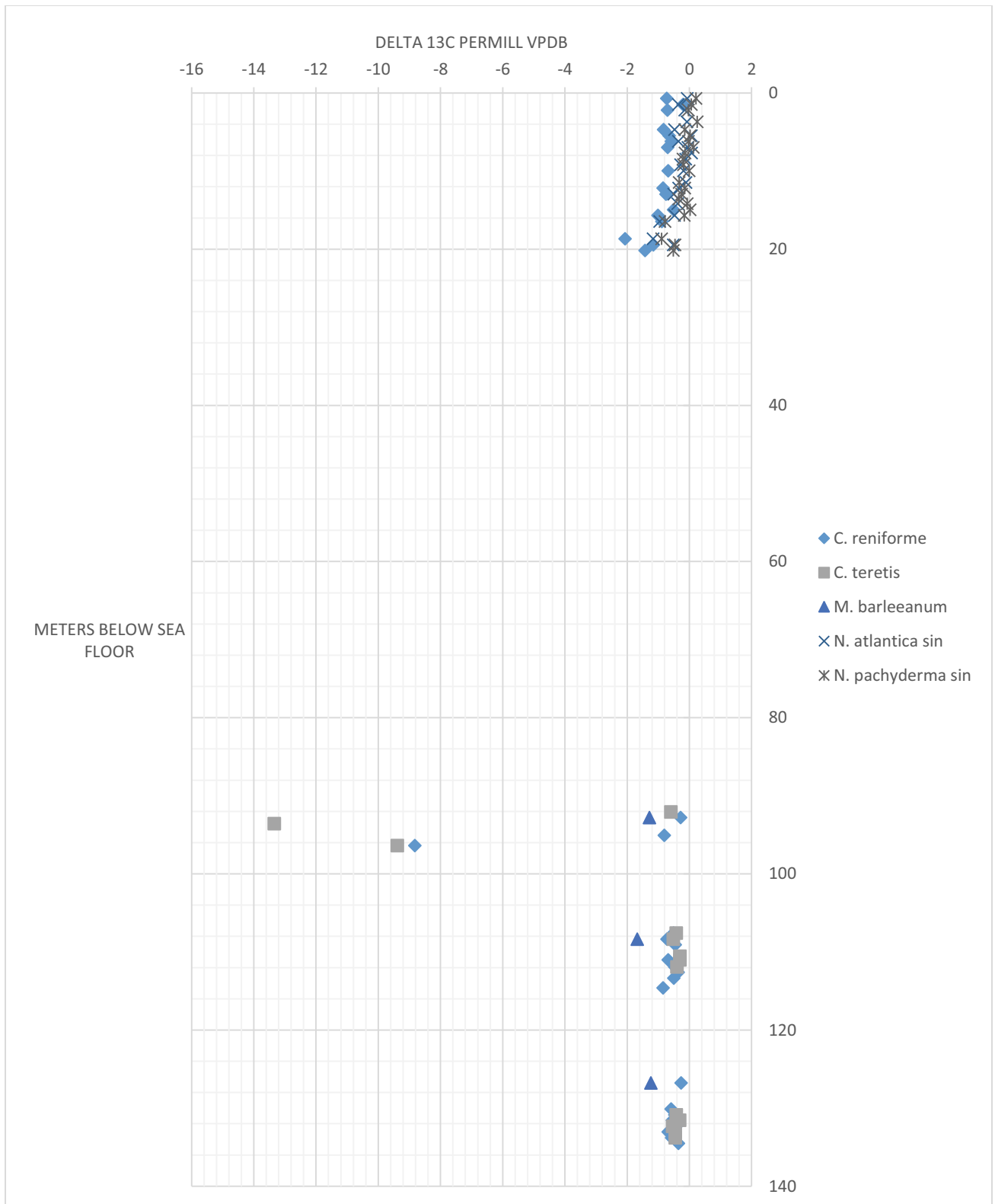
Figure 14: The graph show the δ¹³C values from foraminifera and depth below sea floor, conducted during preliminary work (Baranwal, S., unpublished data).

Based on the preliminary work, additional sampling was done in November 2015 at the ODP Core Repository in Bremen, Germany. The focus on the second sampling was based on the negative values found in Hole 912A (Figure 14). The additional samples was taken in core 912A-10X from sections 1 to 5, core 912A-11X sections 1 to 7, and core 912A-13X sections 1 to 5. Samples was also taken in core 912A-2H section 5, 6 and 7 and core 912A-3H section 1, 2 and 3, due to a previously seen increase in concentration of methane. Each sample was cut into 4 cm slices using a knife. The equipment was cleaned between each sampling. The samples were put in plastic bags, and labelled. A total of 167 samples was taken.

The samples was brought from Bremen to Arctic University of Tromsø (UiT). As the samples was already dry (naturally because of long storage), distilled water was added in each plastic bag before they went in the freezer at the Geology Department Laboratory. The samples was then freeze dried in a Christ: Alpha 1-4.

Every other sample of the core 912A-10X, 912A-11X and 912A-13X from the additional sampling was picked out for sieving, a total of 67 samples and additional 9 samples were picked out from core912A-3H. Two thirds of the samples was wet sieved using 63µm size fraction. The remaining one third was labelled in plastic bags for storage. After every sieving process of the wet sieved samples, the residues were removed from the sieves, using distilled water, into glass and dried. The samples were sieved again with size fractions of 63µm and 125µm, dried, labeled and weighed. The 125µm samples was analyzed by a binocular microscope. The remaining samples (96 samples) from the prelaminar work, was also analyzed.

2.6 Micropaleontological analyses

The handpicking of the foraminifera from both preliminary and additional sampling was conducted on the sieved samples of fraction 100µm and 125µm. Samples was evenly spread on a picking trail consisting of 45 equal squares, and analyzed with a binocular microscope (Leica CLS150X-MZ12$_5$). Planktonic and benthic foraminifera were picked from each sample and transferred to a slide and labeled. A total of 230 samples was analyzed with the binocular microscope. Many of the samples did not contain significant material to be analyzed.

Each slide with picked foraminifera was labeled with the sample number. Foraminifera suitable for analysis of oxygen and carbon isotopes were sorted by species and transferred into a slide. Only undamaged foraminifera with no evident contaminations of secondary minerals were used. The samples were sent to the Stable Isotope Laboratory at Oregon State University in the USA. The laboratory required a minimum of 10 foraminifera of the same species in each sample to conduct analyzes.

2.7   Stable isotope analyzes

Stable isotopes values (δ^{18} C and δ^{13}) were determined using a MAT252 mass spectrometer coupled to a Kiel-III carbonate preparation device (Figure 15), at the Stable Isotope Laboratory at Oregon State University (McKay, J. 2015). During the preparation, samples were induced with ~105% orthophosphoric acid at 70°C for 5 minutes. The evolved CO_2 and H_2O gasses were trapped in colfinger 1, the non-condensable gases was removed, and the CO_2 was transferred into a second coldfinger 2. The H_2O was retained in coldfinger 1, and when the second tapping was complete, the CO_2 was thawed and transferred via a capillary into MAT252 mass spectrometer, where the analyzed by a dual inlet mass spectrometry. Precision for δ^{18} O are ±0,05‰, and for δ^{13}C are

Figure 15: Figure 16: Picture of the Kiel-III preparation device in Oregon State University (McKay, J. 2015)

±0,03‰ (McKay, J. 2015). The table of the samples sent to the Stable Isotope Laboratory are added appendix 2.

2.8   Scanning Electron Microscopy investigations

A selection of specimens was examined via Scanning Electron Microscopy (SEM) at the Geology laboratory at the University of Tromsø, to further describe their preservation. Based on the results of the micropaleontological analyses and the $\delta^{13}C$ values, specimens from intervals with negative $\delta^{13}C$ values and bad preservation were picked together with specimens from intervals with $\delta^{13}C$ in normal range (1 to -1‰) with good preservation. This was done for comparison with foraminiferal test showing carbon values reflecting a normal marine environment unaffected by methane seepages.

3　Foraminifera

Foraminifera are a single-celled protozoa that live on the seafloor or amongst the marine plankton in the water column. They are adapted to tolerate a certain range of salinity and temperatures, and are found in most marine environments (Armstrong, H. and Brasier, M. 2005). The foraminifera comprised a soft body (protoplasm) enclosed in a test composed of various organic matter, minerals (calcite or aragonite with the chemical formula $CaCO_3$) or agglutinated (foreign particles held together by various cements) components (Lowe, J. J. et al. 1997). Ecology is the study of the relationship between the environment and the living organism. Excellent preservation and prolific production of foraminifera fossils in the oceanic sediments has probably produced one of the best fossil records on earth (Kucera, M. 2007). The foraminifera depend on different factors, such as chemical, physical and biological parameters of the environment. Important physical parameters are temperature, currents and pressure. Chemical parameters are salinity, oxygen, alkalinity, organic and inorganic substances. The biological parameter is migration due to food supply (Murray, J. W. 2001) As the foraminifera tests are composed of $CaCO_3$, signals of stable isotopes of carbon and oxygen can be measured and interpreted (Faure, G. and Mensing, T. M. 2005). It is proven that carbon-isotopic compositions of foraminifera tests can in some species record distinct ^{13}C-depletions inherited from methane (Gupta, B. K. S. and Aharon, P. 1994, Wefer, G. and Heinze, P.-M. 1994, Gupta, B. K. S. et al. 1997, Barbieri, R. and Panieri, G. 2004, Millo, C. et al. 2005, Panieri, G. et al. 2009, Panieri, G. et al. 2012). The variations in ^{13}C of foraminiferal tests are likely a result of incorporation of ^{13}C-depleted carbon in the presence of methane emissions at the seafloor during biomineralization of the carbonate foraminifera tests and subsequent secondary mineralization (Panieri, G. et al. 2014). This means that foraminifera in environments with methane seeps record geochemical information from which past methane emissions events may be reconstructed. The foraminifera are grouped into planktonic or benthic, depending on their habitat. They are then classified on a number of characteristics; the rhizopodial (the cytoplasmic extensions used in locomotion and feeding), degree and form of coiling, numbers of chambers, numbers of pattern of apertures, and the surface ornamentation (Lowe, J. J. et al. 1997).

3.1 Benthic foraminifera

Benthic foraminifera live at, or few centimeters from the seafloor. They are most abundant in the upper one cm of the sediment and on the sediment surface, which is referred to the epifaunal microhabitat. They can also live deeper in the sediments, most in the upper 5cm, but can be found up to 20 cm deep in the sediments, referred to as the infaunal microhabitat (Katz, M. E. et al. 2010). Because of this, they give information about the conditions on the seafloor. The abundance of the species is controlled by temperature, food supply and oxygen (Schmiedl, G. et al. 1997). Their tests can be composed of different minerals, however, calcareous tests are the most abundant form (Armstrong, H. and Brasier, M. 2005). Benthic foraminifera are sensitive to environmental changes, and can be used to reconstruct modern and ancient marine environments. The calcareous species can be used for radiocarbon dating, isotope analysis and can provide insight into paleoceanographic changes through time. They also give information about previous glacial histories and the sedimentary environment.

3.1.1 *Cassidulina neoteretis* (Seidenkrantz, 1995)

C. neoteretis is in the order *Rotaliina*, superfamily *Cassidulinacea*. The test is convex with arranged chambers coiled in a plane spiral (Armstrong, H. and Brasier, M. 2005). It is a shallow infaunal species, that prefers fine-grained, terrigenous mud that is rich in organic material (Mackensen, A. and Hald, M. 1988). The *C. neoteretis* are often found in glaciomarine environments with stable salinity and temperature. It is often confined to areas influenced by cool Atlantic Water (Chauhan, T. et al. 2016). *C. neoteretis* is found to be abundant in the continental slope of Norway, where the bottom water has a temperature of c. -1°C with salinities ~34,92‰ (Mackensen, A. and Hald, M. 1988).

3.1.2 *Cassidulina reniforme* (Nørvangi, 1945)

C. reniforme is an abundant species on the Arctic shelfs (Polyak, L. et al. 2002), and it considered an Arctic species. It is infaunal and requires a silty muddy substrate, and is associated with seasonal ice cover and is frequently found in glasiomarine environments (Mackensen, A. et al. 1985, Mackensen, A. and Hald, M. 1988, Hald, M. and Korsun, S. 1997). The species prefers cold Intermediate Waters, with high salinity and low temperatures (<2°C) (Steinsund, P. I. and

Hald, M. 1994, Hald, M. and Korsun, S. 1997, Polyak, L. et al. 2002). It is typical in waters where there is little influx of temperate waters (Osterman, L. E. and Nelson, A. R. 1989).

3.1.3 *Elphidium incertum* (Willliamson, 1858)

Elphidium incertum is in the order *Rotaliinam* superfamily *Elphidiinae* (Armstrong, H. and Brasier, M. 2005). The specie is often found in moderate depths in arctic and subarctic waters. *E. incertum* is particularly found dominant in marine deposits of the later ice ages of the Quaternary (Feyling-Hanssen, R. W. 1971). It is related to proglacial, interstadials and glacial deposits, and reliable indicator of ancient arctic environment (Feyling-Hanssen, R. W. 1972).

3.1.4 *Melonis barleeanum* (Williamson, 1858)

M. barleeanum is in the order *Rotaliina* of superfamily *Nonionoidea*, where the aperture is generally a basal slit (Armstrong, H. and Brasier, M. 2005). It is an infaunal species that feeds on buried organic matter in muddy sediments, which can be an indicator of high surface productivity, and environments rich in organic sediments (Caralp, M. H. 1989, Jennings, A. E. et al. 2004). High abundance of the *M. barleeanum* is therefore related to the food-ability (Caralp, M. H. 1989). In the Arctic regions it is proven to be related to inflows of relatively warm waters in form of the Atlantic waters, and prefers temperatures around 4°C (Hald, M. and Steinsund, P. I. 1992). It is associated with open water conditions to marginal sea conditions and fine sediments (Chauhan, T. et al. 2016).

3.1.5 *Fursenkoina complanata* (Egger, 1893)

F. complanata is an infaunal species which tolerate low-oxygen environments and high organic input (Kawagata, S. et al. 2005), and is therefore found to be abundant in sediments enriched in organic matter and dissolved oxygen levels (Nisha, N. and Singh, A. 2012).

3.2 Planktonic foraminifera

Planktonic foraminifera are holoplanktonic, spending their entire life freely floating in surface waters, except the *Neogloboquadrina pachyderma* which can overwinter in brine channels in sea ice (Spindler, M. and Dieckmann, G. S. 1986) The mixed upper thermocline layer is the most densely populated, while virtually no living individuals are found at depth below 1000 m

(Vincent, E. and Berger, W. 1981). Because of their habitat, planktonic foraminifera can reflect the conditions in the water column, such as surface-water temperature, salinity and food supply (Stein, R. 2008, Katz, M. E. et al. 2010). The foraminifera tests with trochospirally arranged chambers can exhibit either dextral (right handed) or sinistral (left-handed) coiling (Kucera, M. 2007).

3.2.1 *Neogloboquadrina pachyderma* (sinistral) (Ehrenberg, 1861)

The sinistral form of *Neogloboquadrina pachyderma* is a polar species (Chauhan, T. et al. 2016). It has been used as a tool for monitoring Polar Surface Ocean changes and for correlating these changes to atmospheric and thermohaline circulation fluctuations (Kohfeld, K. E. et al. 1996). It is shown to dominate surface sediment assemblages of planktonic foraminifera in the Polar Regions (Pflaumann, U. et al. 1996). *N. pachyderma* is known to avoid low salinity (<32‰) surface layers in the Arctic, and can overwinter in brine channels in sea ice (Spindler, M. and Dieckmann, G. S. 1986, Carstens, J. et al. 1997).

3.2.2 *Neogloboquadrina atlantica* (Berggren, 1972)

N. atlantica is often the most dominant member of the Pliocene planktonic foraminiferal assemblages in the North Atlantic, and are adapted to cool environments (Berggren, W. A. 1972). It exhibits a distinct preference of dextral coiling during late Miocene, and sinistral coiling during Pliocene, and has not been identified with certainty in the Quaternary period (Poore, R. and Berggren, W. 1975).

3.3 Results

3.3.1 Micropaleontology

A total of 172 samples was analyzed in this thesis, where 69 samples did not contain any foraminifera. The near-surface sediments from 0-13 mbsf, contains abundant *N. pachyderma, C. reniforme* and *N. atlantica*. From 13 mbsf to 20 mbsf the same species are still abundant, with presence of *C. neoteretis, M. barleeanum* and *B. elegantissima*. The interval between 20 to 60 mbsf was not prioritized, as it was an interval with few foraminifera that did not show interesting values in δ¹³C in the preliminary work. It is notable that the samples throughout this interval contained abundant biogenic material. The few samples analyzed in the interval 60 to 72 mbsf, contained no foraminifera, with the exception of some *C. neoteretis, M. barleeanum, B. elegantissima* and *E. incertum*. At 67 mbsf there was one sample that contained *Hoeglundina elegans*. There were more abundant assemblage of foraminifera in the interval 72-80 mbsf which include *C. neoteretis, M. barleeanum, F. complanata, B. elegantissima* and *E. incertum*. There are few specimens of *Lagena hexagona* and *Epistominella* at 80 mbsf. Few planktonic foraminifera are present at the interval 72-80mbsf. Below 88 mbsf the specimens are not very well preserved containing mostly broken *C. neoteretis, M. barleeanum* and *B. elegantissima*. White calcite crystals are often found together with the foraminifera in this interval down to 94 mbsf. From 95 mbsf the *M. barleeanum* is less abundant. The species found from 95-113 mbsf are mostly *C. neoteretis* and *E. incertum*.

3.3.2 Foraminiferal δ¹³C measurements

Carbon-isotope composition of the five benthic foraminifera (*C. reniforme, C. neoteretis, M. barleeanum, F. complanata and E. incertum*) and two planktonic foraminifera (*N. pachyderma* and *N. atlantica*) will be listed by species, and summarized at the end. All results are reported relative to the Vienna Pee Dee Belemnite (VPDB). The precision of the samples are ±0,03‰ for δ¹³C (McKay, J. 2015).

3.3.2.1 δ¹³C measurements of *Cassidulina reniforme*

The data from the *C. reniforme* show δ¹³C values that vary in a narrow range from -0,2‰ to -0,8‰ at near surface, to 15 meters below sea level (mbsf), see Figure 18. The values show higher fluctuations between 15 to 20 mbsf. The most negative value is ~-2‰ at 18,68 mbsf.

Measurements between 20 to 70 mbsf are absent because the samples did not contain significant amount of *C. reniforme* to be analyzed. The values range between -0,2‰ to -0,85‰ from 92 mbsf to 134 mbsf, except one strong negative peek (-8,8‰) at 96,37 mbsf.

3.3.2.2 δ¹³C measurements of *Cassidulina neoteretis*

The upper near surface sediments did not contain significant amount of *C. neoteretis* to be analyzed for stable isotopes. The range of measurements between 13 mbsf to 17 mbsf is -2, 1‰ to 0,4‰ δ¹³C. The material contain no measurements between 20 and 60 mbsf. Between 60 to 80 mbsf the δ¹³C values vary in a narrow range from 0‰ to -0,8‰. There is a significant change in the measurements from 80 to 100 mbsf. The range of the δ¹³C values expand in a wide range from 0‰ and up to -13,3‰. The interval from 100 to 112 mbsf show a range between -0,3‰ to -2,5‰ δ¹³C. There are no measurements in the interval from 112 to 130 mbsf, but the values between 130 to 133 meters is ~-0,4‰ δ¹³C.

3.3.2.3 δ¹³C measurements of *Melonis barleeanum*

The upper surface sediments 0-16mbsf contains only three measurements of δ¹³C in *M. barleeanum*, with a value range between -1‰ to -2‰. There are no data between 16 to 70 mbsf because the samples did not contain any significant material of *M. barleeanum*. The interval from 70 to 110 mbsf has a wider range of δ¹³C values between -0, 3 to -5, 6‰. Between 110 to140 mbsf there is only one measurement with a δ¹³C value of -1,2‰.

3.3.2.4 δ¹³C measurements of Neogloboquadrina atlantica

The *N. atlantica* was only found in significant amounts in the upper 20 meters of Hole 912A. The measurements show δ¹³C values between 0,1‰ to -1,2‰. The most negative values are measured between 16-19 mbsf.

3.3.2.5 δ¹³C measurements of *Neogloboquadrina pachyderma (sinistral)*

Like the *N. atlantica,* the *N. pachyderma* was only found in the upper 20 meters of the sediments, in a significant amount to be analyzed. The δ¹³C values show numbers between 0,5‰ to -0,5‰ in intervals between 0 and 13 mbsf. From 13 to 20 mbsf, the values show a wider range in negative values from 0‰ to -1,88‰.

3.3.2.6 δ¹³C measurements of *Fursenkoina complanata*

There was only two isotope data from *F. complanata*. One show a strong negative peak -21,2‰ at 73 mbsf and -0,3‰ at 80 mbsf.

3.3.2.7 δ¹³C measurements of *Elphidium incertum*

There are only data of the *E. incertum* between 80 to 110 mbsf in Hole 912A. All values are between -0,4‰ to -2%. The highest negative peek is at 80 mbsf and are -2‰.
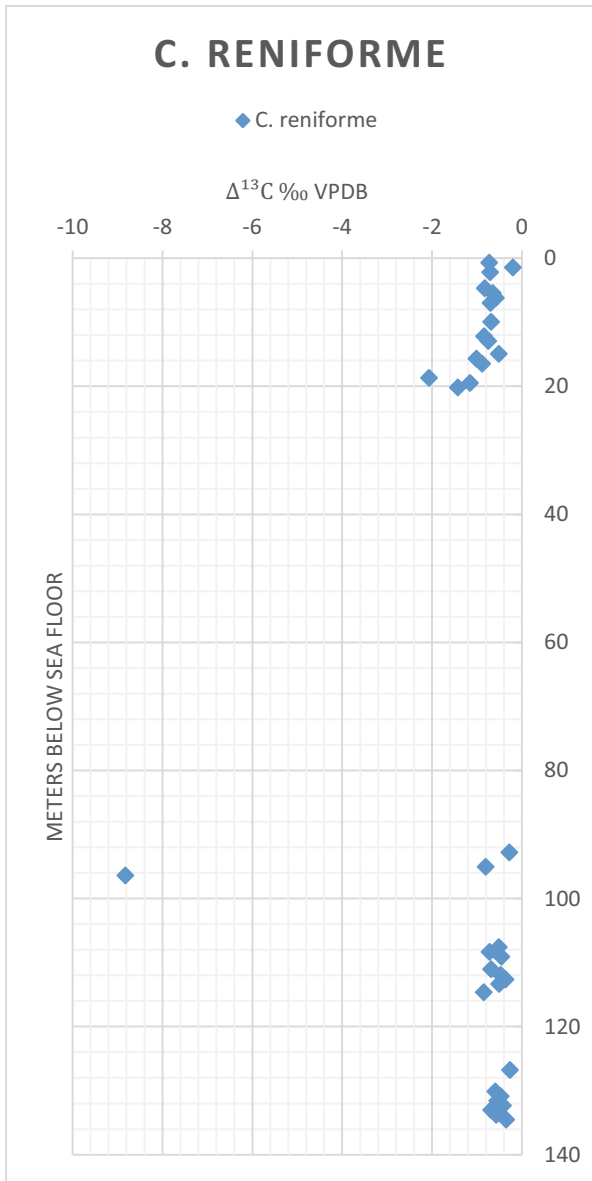
Figure 18: δ¹³C values of C. reniforme and depth below sea floor.
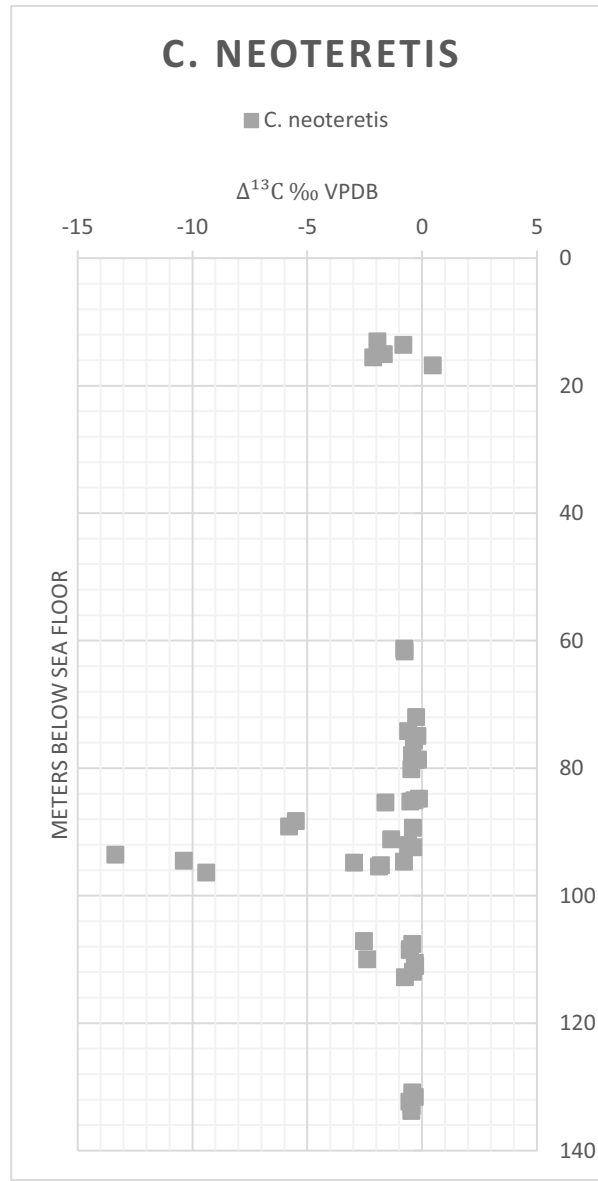
Figure 19: δ¹³C values of C. neoteretis and depth below sea floor.
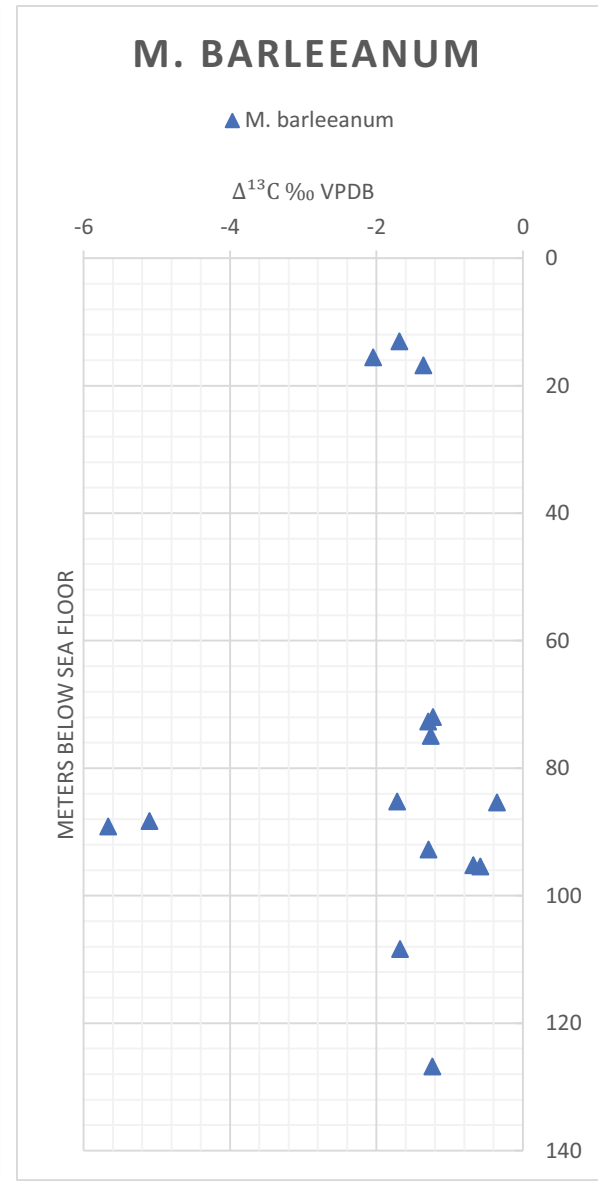
Figure 17: δ¹³C values of M. Barleeanum and depth below sea floor.
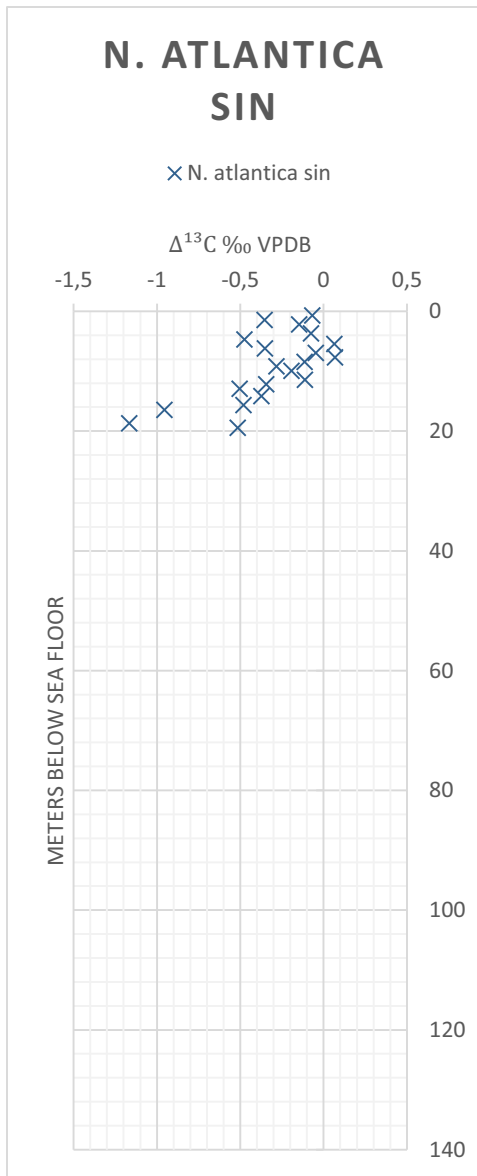
Figure 23: δ¹³C values of N. atlantica and depth below sea floor.
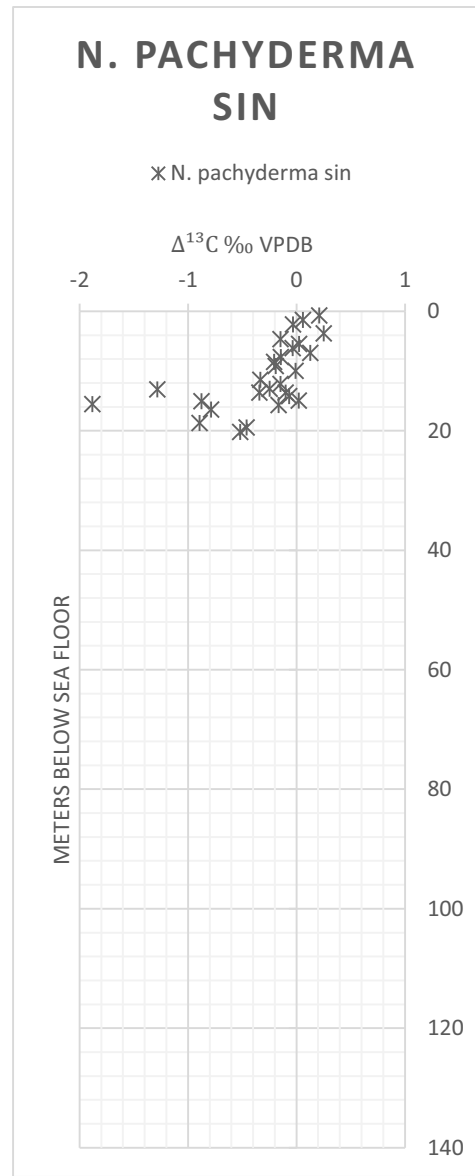
Figure 22: δ¹³C values of N. pachyderma and depth below sea floor.
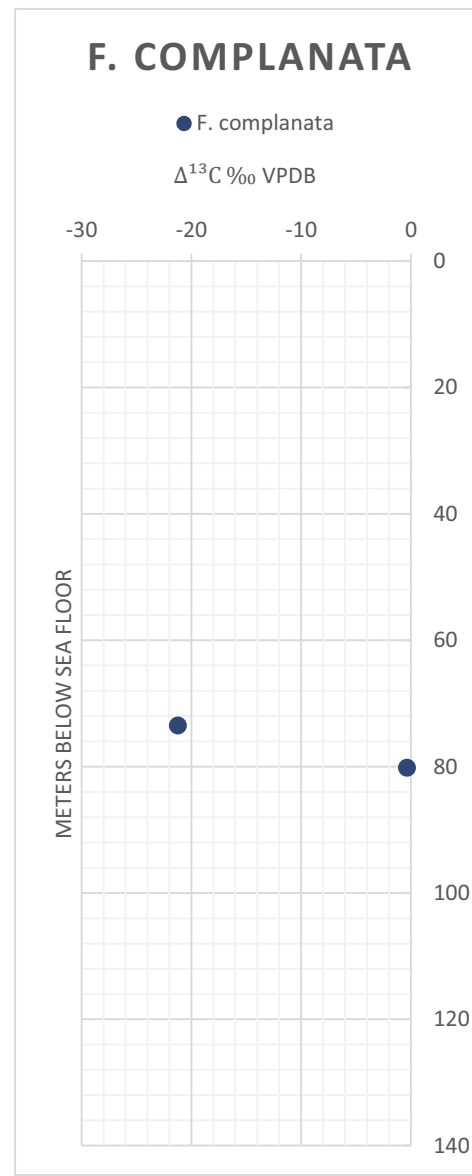
Figure 21: δ¹³C values of F. complanata and depth below sea floor.
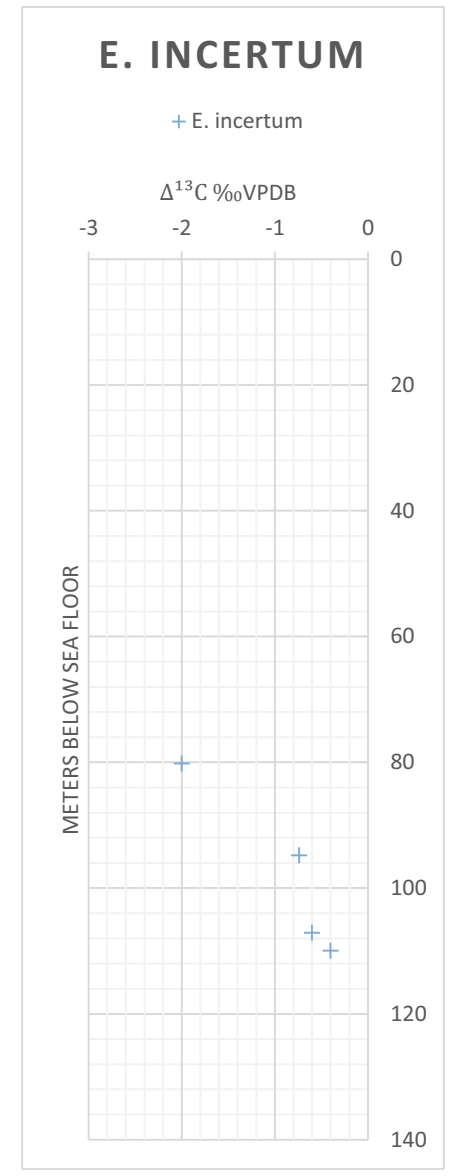
Figure 20: δ¹³C values of E. incertum and depth below sea floor.

41

3.3.2.8 Summary of δ¹³C isotopes in all species

Stable isotope data of $\delta^{13}C$ in the near-surface sediments from 0-13 mbsf, vary within a narrow range from -0,9‰ to 0, 2‰. Below the thirteen meters, the range expand from -2,5‰ to 0,5‰. Measurements between the interval 20 and 60 mbsf are absent, because the samples did not contain significant material to be analyzed. At 73 mbsf, a highly $\delta^{13}C$-depleted value (-21,21‰) are shown in the foraminifera *F. complanata*. The values from 80 to 96 mbsf show the largest range in $\delta^{13}C$-depleted values. At 88 to 89 mbsf the values measured in *M. barleeanum* and *C. neoteretis* are negative (~-5‰). At 93-96 mbsf there are some slightly higher negative values around ~-10‰ in several species. Below 96-107 mbsf there are no measurements. Between 107 to 114 mbsf there are many measurements of $\delta^{13}C$ between -0,3‰ to –2,23‰. Between 114 and 126 mbsf is an empty space with no measurements. Below 126 mbsf most of the values are ~-0,5‰ in average.
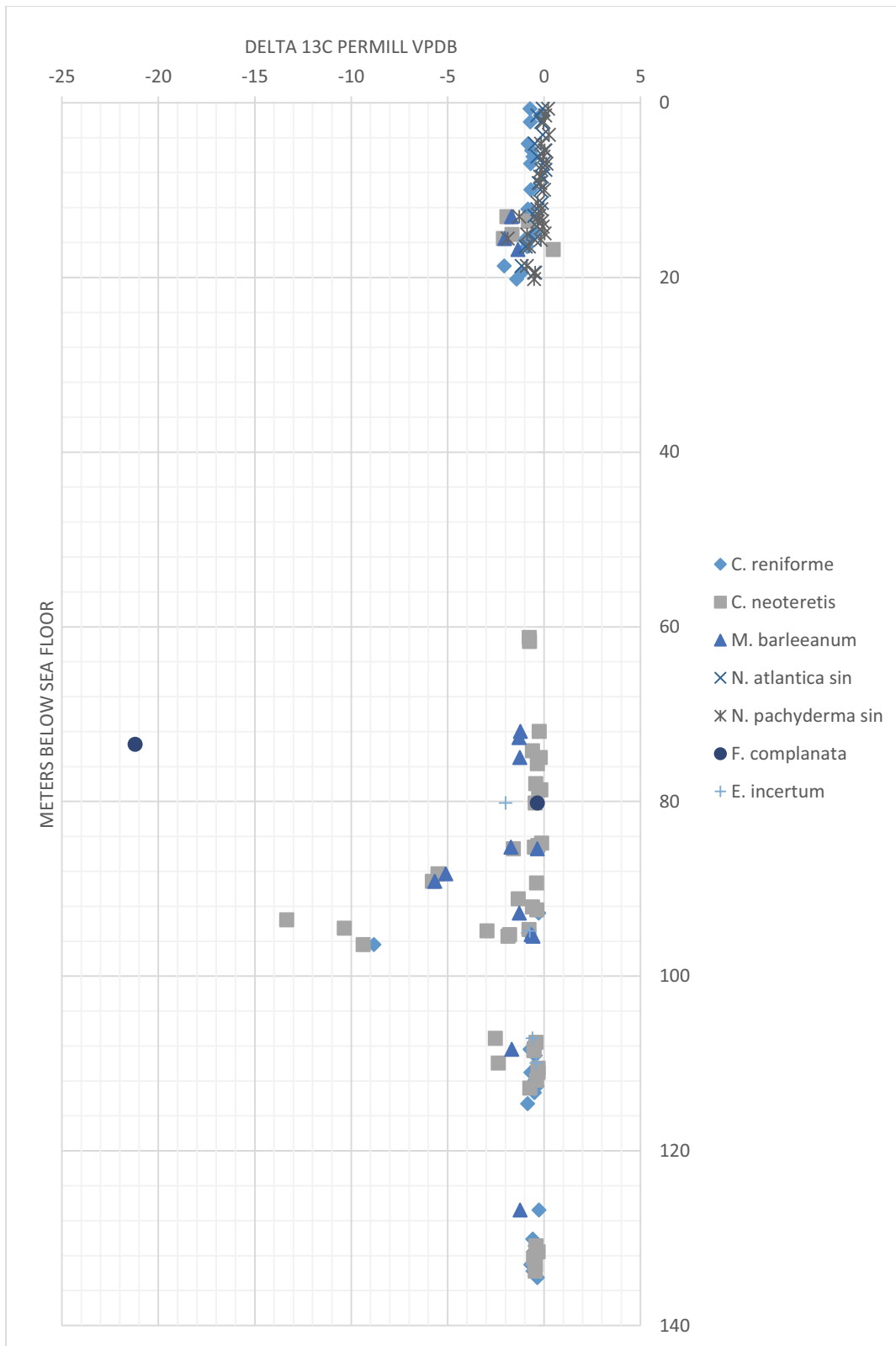
Figure 24: Carbon-isotope values of all foraminifera species in Site 912A, in respect to meters below sea floor.

3.3.3 Foraminiferal δ^{18} O Measurements

The result will first be listed by species, and then a summary of the trend of all the species together. All results are reported relative to the Vienna Pee Dee Belemnite (VPDB). The precision of the samples are ±0,05 ‰ for δ^{18} O (McKay, J. 2015).

3.3.3.1 δ^{18}O measurements of *Cassidulina neoteretis*

The data from *C. reniforme* show fluctuations of δ^{18} O between 3,4‰ to 5,6‰ throughout the core. The uppermost measurement is 13 mbsf that show a value of 5,2‰. The values decrease in an even pattern down to 15 mbsf. There is a small increase in δ^{18} O between 15 and 16,7 mbsf. There are no measurements between 16,7 to 60 mbsf, because the samples did not contain significant amount of *C. reniforme* to be analyzed. The values show an increase in δ^{18} O from 80 to 74 mbsf. From 74,18 to 74,96 mbsf there is a sudden strong decrease in the value down to 3,4‰, which is the lowest value of δ^{18} O in this specie. There is a strong shift from 3,4‰ to 5,5‰ at 75,68 mbsf. The value fluctuates between 5,5‰ to 4,9‰ from 75,68 mbsf down to 84,7 mbsf. Between 84,7 and 96 mbsf the values show higher fluctuations with several peeks that shifts between 3,9 ‰ to 5,6 ‰. There are no measurements between 96 to 107 mbsf, but below 107 mbsf there are several fluctuations between 3,9‰ to 5,1‰ down to 112 mbsf. There are no measurements between 112 to 130 mbsf, but from 130 mbsf there is a decrease from 5,3‰ to 4,7‰ to 133 mbsf. At this point the value increase again to 5,1‰ to the lowest measurement at 133, 8 mbsf.

3.3.3.2 δ^{18}O measurements of *Cassidulina reniforme*

The stable oxygen isotope data in the near-surface sediments vary within a narrow range from 5,4‰ to 5,6‰ at 0 to 6 mbsf. Values between 6 and 20 mbsf show higher fluctuations between 4,8‰ to 6, 7‰. Between 20 to 92 mbsf there are no measurements because the samples did not contain significant amounts of *C. neoteretis*. At 92,78 mbsf the δ^{18} O value is 5,9‰, and decreases to 5,1 ‰ towards 96 mbsf. The values continues to decrease in a stable curve down to 111 mbsf and seems rather stable between 4,6‰ to 4,8‰ down to 113 mbsf, before it shifts to a higher value 5,6 ‰ at 114 mbsf. There are no data between 114 to 126 mbsf. At 126,8 mbsf the value show 4,9 ‰ and increase to 5,6 ‰ at 130 mbsf. Here the value decrease from 5,6‰ at 130 mbsf to 5,0 ‰ at 134, 5mbsf.

3.3.3.3 $\delta^{18}O$ measurements of *Melonis barleeanum*

The data from *M. barleeanum* starts at 13 mbsf with 4,9 ‰ to 17 mbsf with 4,5‰. It shows a decreasing curve between these intervals. Between 17 to 71 mbsf there are no measurements because the samples did not contain a significant amount of *M. barleeanum* that could be analyzed. There are higher fluctuations between 72 to 95 mbsf. At 72 mbsf the value show 5,0‰, where is decrease down to 4, 3 ‰ at 85 mbsf. The measurement show an increase between 72 and 88 mbsf, from 4, 3‰ to 5, 5‰. From 88 to 89 mbsf there is a decrease from 5,5‰ to 4,4‰. At 93 mbsf the value has increased to 5,3‰. The value decreases again to 4,8 ‰ at 95, 5 mbsf. From 95,5 to 108 mbsf the measurements show a small decrease 4,5 ‰. The points between 108 -126 show a rather stable value at ~4,45‰.

3.3.3.4 $\delta^{18}O$ measurements of *Neogloboquadrina atlantica*

The *N. atlantica* was only found in the upper 20 mbsf in significant amounts to be analyzed. The measurements show δ^{18} O values with high fluctuations between 5,8‰ to 3,3‰. The highest shift in values are between 7,5 to 13 mbsf where the value decrease from 5,8 ‰ to 3,3‰.

3.3.3.5 $\delta^{18}O$ measurements of *Neogloboquadrina pachyderma*

The *N. pachyderma* was also only found, with significant amounts to be analyzed, in the upper 20 meters of sediments in the seafloor. The δ^{18} O values show several fluctuations between 5,1‰ to 3,4‰. In the upper 10 mbsf the values fluctuates between 5,1‰ to 4,2 ‰. Between 10 to 20 mbsf the value changes from 3,4‰ to 5,0‰ with lower values in average.

3.3.3.6 δ^{18}O measurements of *Fursenkoina complanata*

There are only two measurements of *F. complanata*, one at 73,5 mbsf where the δ^{18} O value show 5,3‰, and further down at 80 mbsf where the value increases to 6,4‰.

3.3.3.7 δ^{18}O measurements of *Elphidium incertum*

There are measurements of *E. incertum* between 80 to 109 mbsf. Data show variations of δ^{18} O within a narrow range from 5,5‰ to 4,7‰.
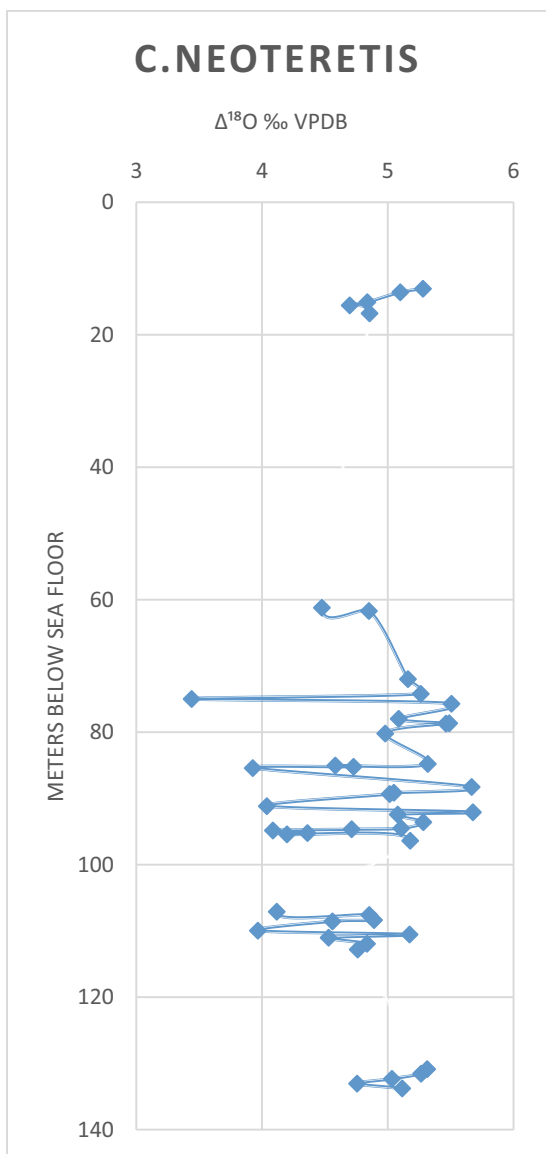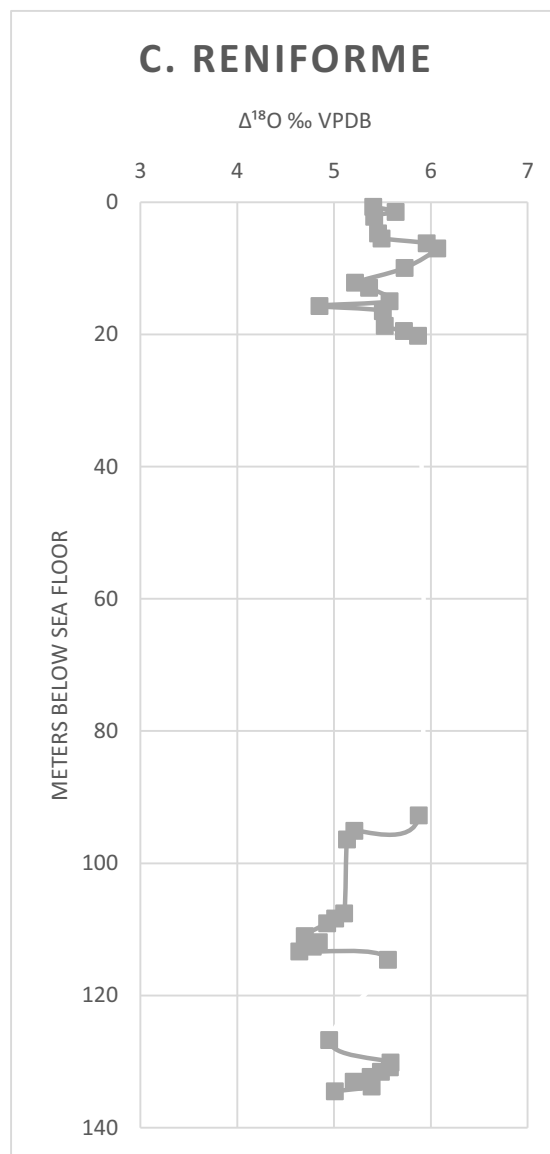
C.NEOTERETIS

Δ¹⁸O ‰ VPDB

Figure 27: δ¹³C values of C. reniforme and depth below sea floor.

C. RENIFORME

Δ¹⁸O ‰ VPDB

Figure 25: δ¹³C values of C. neoteretis and depth below sea floor.

M. BARLEEANUM

Δ¹⁸O ‰ VPDB

Figure 26: δ¹³C values of M. Barleeanum and depth below sea floor.

47
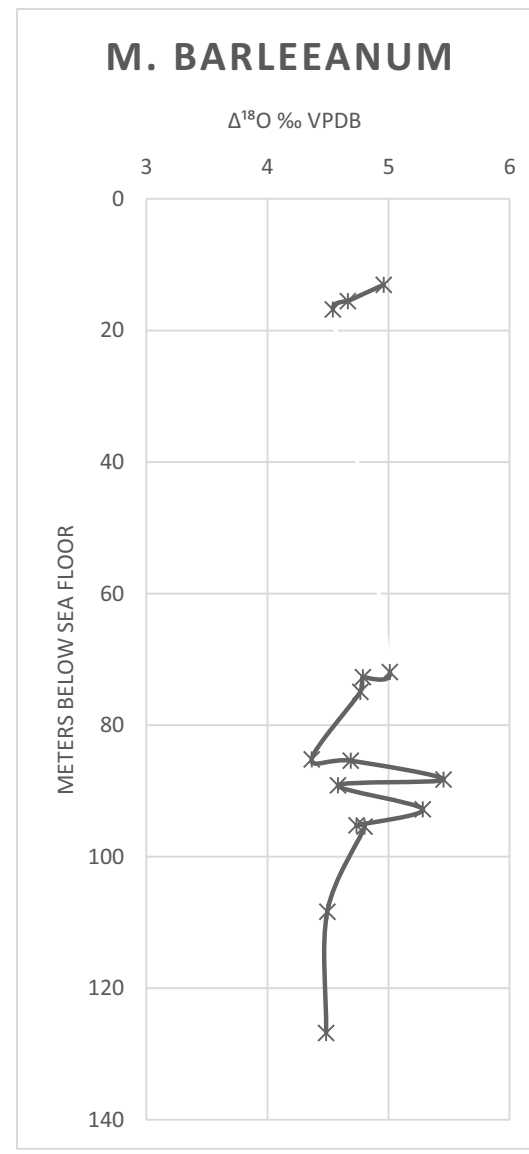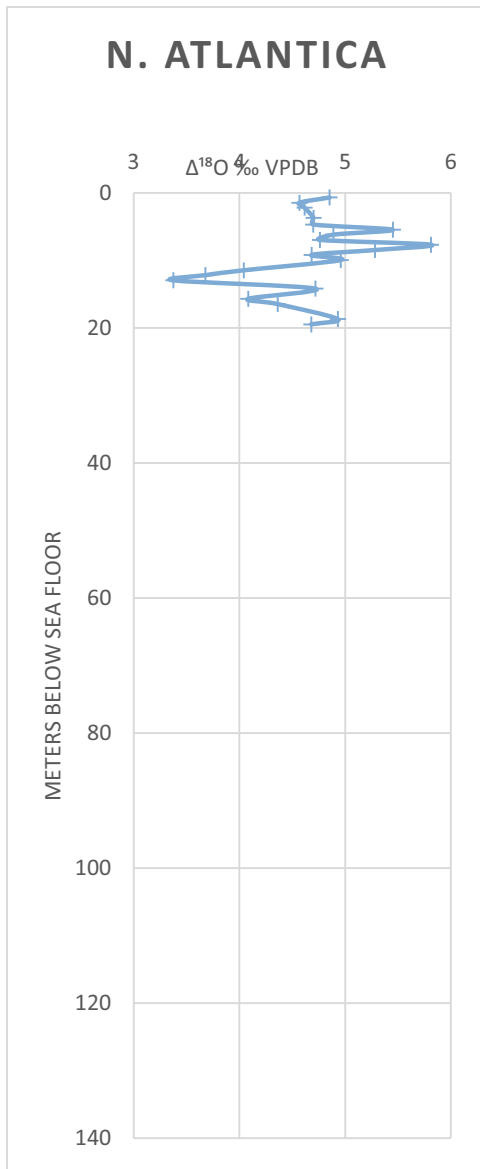
Figure 28: δ¹⁸O values of N. atlantica and depth below sea floor.
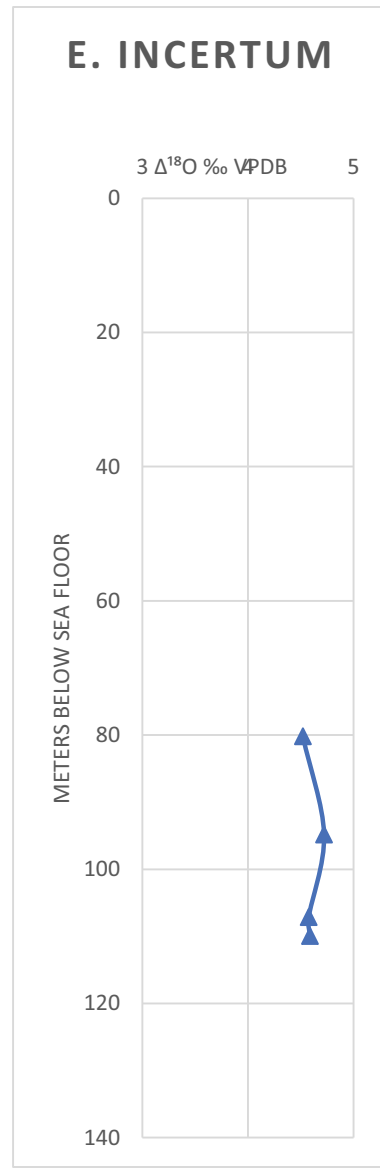
Figure 30: δ¹⁸O values of E. incertum and depth below sea floor.
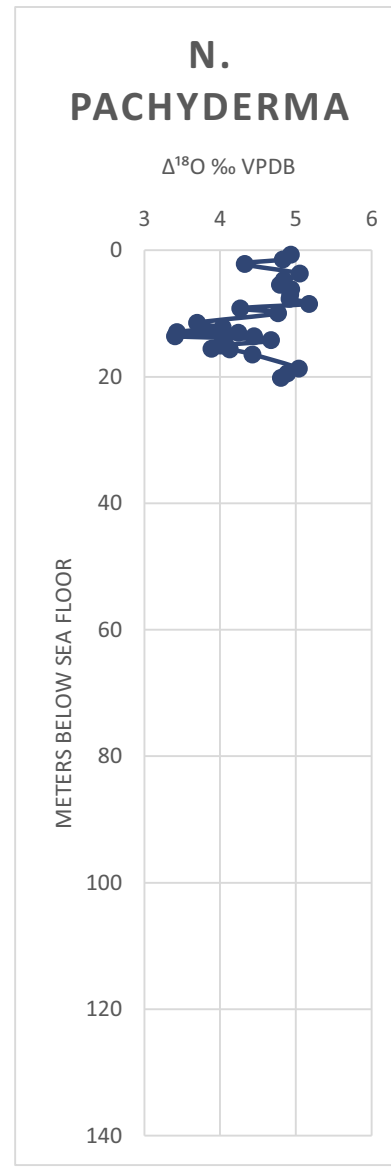
Figure 29: δ¹⁸O values of N. pachyderma and depth below sea floor.
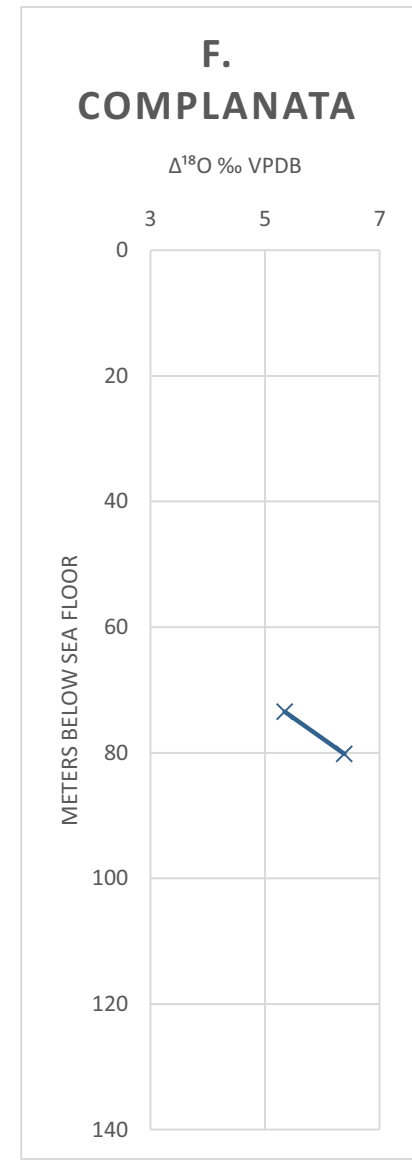
Figure 31: δ¹⁸O values of F. complanata and depth below sea floor.

3.3.3.8 Summary of $\delta^{18}O$ isotopes in all species

There are variations in the δ^{18} O values between the species, but it seems to follow the same trend, see Figure 32. In the upper 8 mbsf, the *N. atlantica* fluctuate with δ^{18} O ratios between 4,5‰ to 5,8‰. The *N. pachyderma* fluctuate less between 4,3‰ to 5,0‰, and the curve do not correlate well with the *N. atlantica*. The *N. atlantica* and the *N. pachyderma* are planktonic species, and will show the δ^{18} O values of the surface water. Between 8 to 20 mbsf the values match well, and fluctuates between 3, 4‰ to 5, 2‰ (*N. pachyderma*), and 3,4‰ to 5,3‰ (*N. atlantica*). The measurement of *C. reniforme* are higher than average with values between 4,8 ‰ to 7,0‰ in the upper 20 mbsf, and follows the curves of *N. atlantica* with less fluctuations. *N. atlantica* and *C. reniforme* have fewer measurements, and are difficult to correlate with the more abundant species. The *C. reniforme* is a benthic specie, and will show the δ^{18} O at the bottom environment. Measurements of *C. neoteretis* are only available between 13 to 17 mbsf, and show a decrease from 5,2‰ at 13 mbsf, to 4,6‰ at 16 mbsf. There is a small increase in value at 16 mbsf to 71 mbsf. Few measurements of *M. barleeanum* in the interval from 13 to 19 mbsf show a decrease from 4,9‰ to 4,5‰. The δ^{18} O data combined from all the species from 0-20 mbsf are presented in Figure 32.
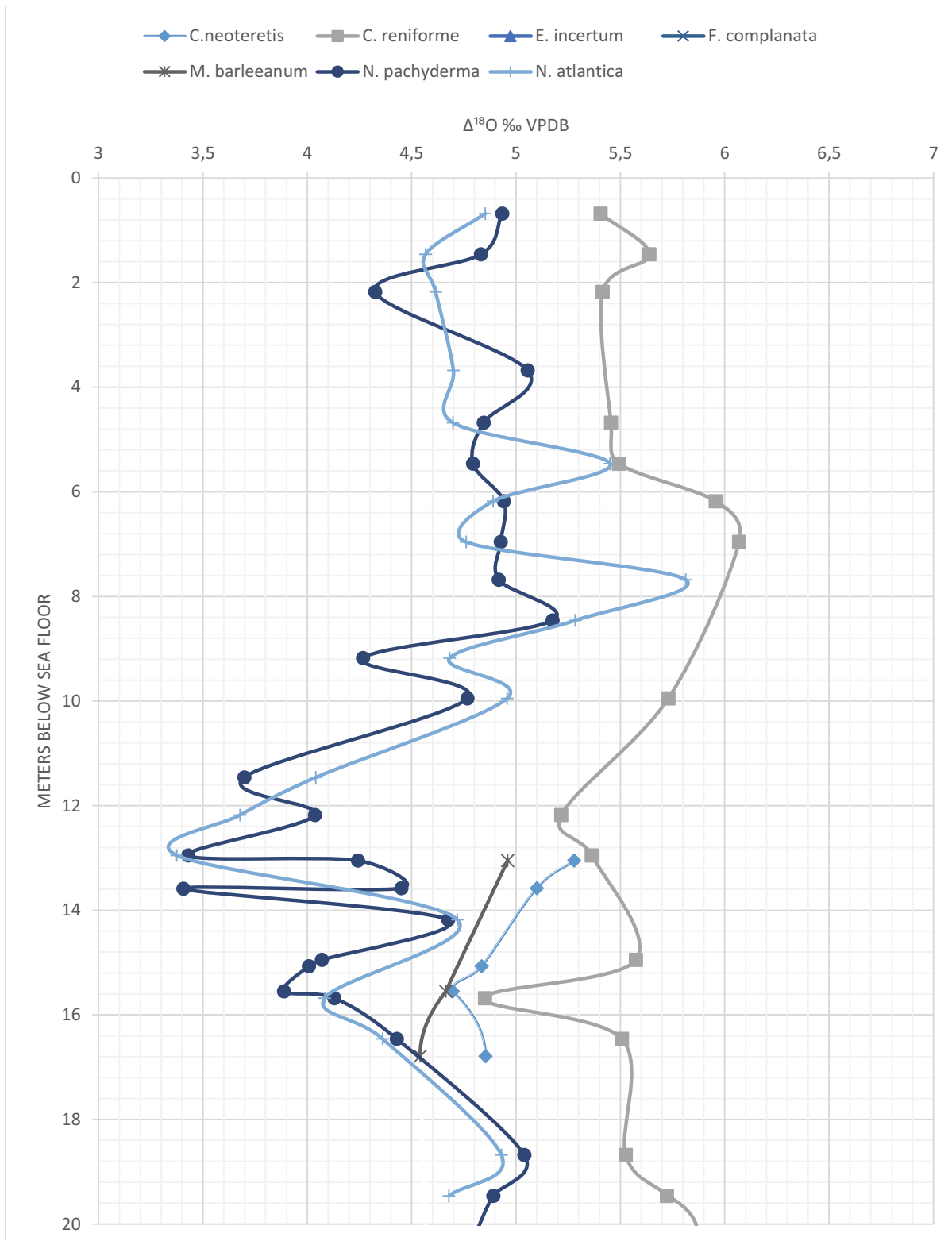
Figure 32: Measurements of $\delta^{18}O$ of all the species in Hole 912A, from 0 to 20 mbsf.

Below 61 mbsf *C. neoteretis* has the most abundant measurement, and show higher fluctuations than the other species. Between 85 to 95 mbsf there are more abundant measurements of *M. barleeanum*, which seems to follow the fluctuations of the *C. neoteretis* measurements. Three analysis of *C. reniforme* between 92 to 96 mbsf imply a decrease in δ^{18} O, which correlates with the other species in that interval. There are only two measurements of *E. incertum* in the interval between 85 to 95 mbsf, making it difficult to correlate to the curves. Between 96 to 107 mbsf there are no measurements. Below 107 mbsf there is an interval with more measurements of the different species. The measurements of *C. reniforme* correlates well with the fluctuations of the more abundant *C. neoteretis* in the interval down to 113 mbsf. There are only one value from *M. barleeanum*, and two measurements of *E. incertum* in this interval. Between 113 to 126 mbsf there are no values. Below 126 to 134 mbsf there are more measurements of *C. reniforme* and *C. neoteretis*. The curves correlate with each other, and the *C. reniforme* show higher ratios of δ^{18} O in average.
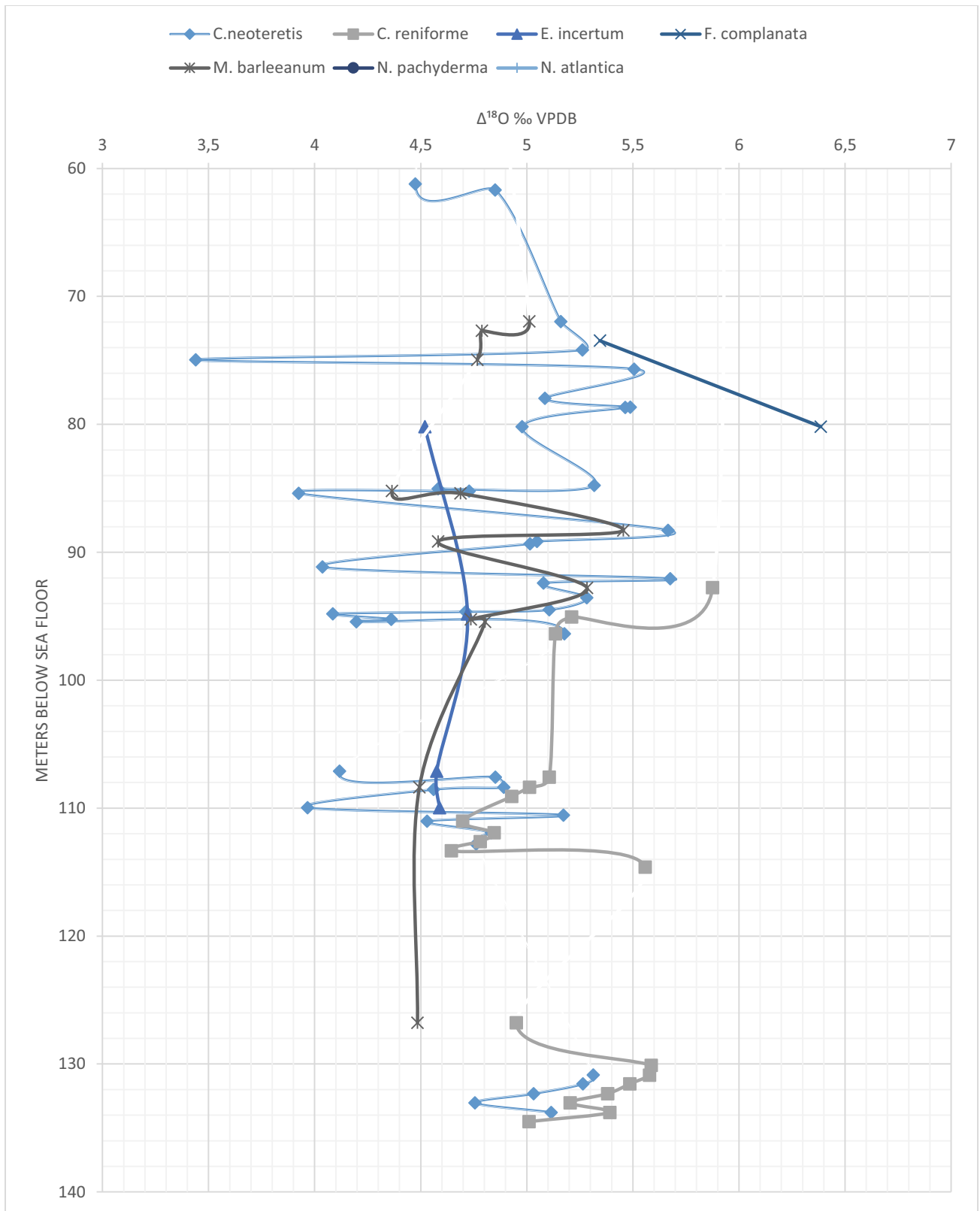
Figure 33: measurements of δ¹⁸O in Hole 912A, from 60 to 140 mbsf.

3.3.4 State of preservation of foraminifera

During the investigation of samples in the light microscope, large differences in preservation state of benthic foraminiferal calcite was observed. The preservation state of the foraminifera tests were further examined by SEM, in order to identify presence of secondary overgrowth of methane derived authigentic carbonate in a selection of specimens.
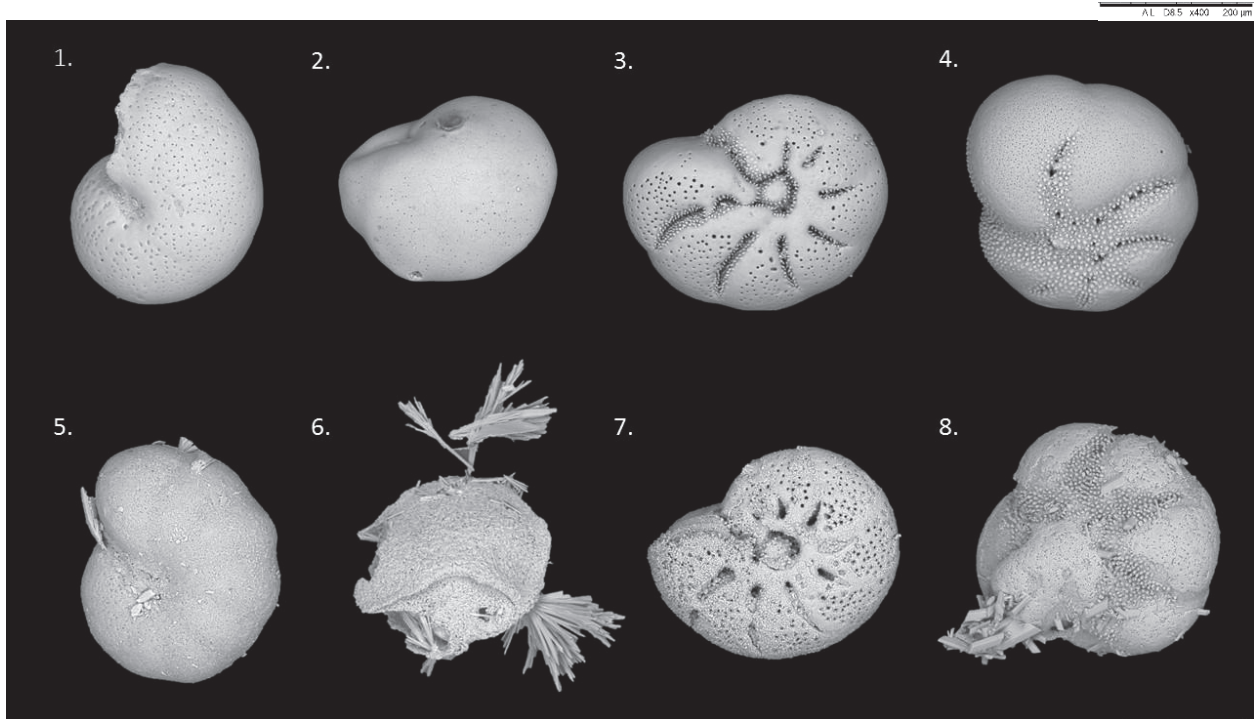
Figure 34: Representative SEM images of different species of foraminifera. (1.) M. barleeanum from 912A-10X at 79,88 mbsf, has a good preservation of the foraminifera test. (2.) C. neoteretis, (3.) E. incertum, (4.) Nonion sp. (1.2.3.) are all from the same sample 912A-8X, at 62, 46 mbsf shows preserved tests with $\delta^{13}C$ values in normal marine range (-0,7‰) in C. neoteretis. (5.) M. barleeanum from 912A-11X at 89, 15 mbsf, showing a test surface with alteration and analyses showed depleted $\delta^{13}C$ values (-5, 66‰) in M. barleeanum. (6.) C. neoteretis from 912A-11X at 89, 15 mbsf, showing surface with precipitation of calcite crystals, and analyzes showed depleted $\delta^{13}C$ values (-5, 79‰) in C. neoteretis. (7.) E. incertum from 912A-9X at 76, 46 mbsf showing test surface with alteration. (8.) Nonion sp. from 912A-9X at 76, 46 mbsf with surface alteration.

In Figure 34 the specimens 1, 2, 3, and 4-, show specimens with good preservation in the tests, picked from intervals showing $\delta^{13}C$ in normal marine range (±1‰). Specimens 5, 6, 7 and 8 are picked from intervals showing depleted values in $\delta^{13}C$, and all specimens have altered test surfaces. The poorly preserved foraminifera test very often showed growth of calcite crystals.

4 Discussion

4.1 State of preservation and stable isotope of foraminifera

In an effort to reconstruct the record of past methane emissions, $\delta^{13}C$ analyses of benthic and planktonic foraminifera has been conducted. Due to preliminary work, the investigation was focused to (1): core 912A-2H and 912A-3H, because of an increased amount of hydrocarbons between 11,5 to 23 mbsf, and (2) core 912A-10X, 912A-11X and 912A-13X, due to depleted $\delta^{13}C$ values previously found at 93,56 mbsf and 96,37mbsf. The results are divided into intervals represented in Figure 36.

4.1.1 Interval I

The interval between 0 to 13,05 mbsf contains planktonic and benthic foraminifera. Micropaleontological analyses showed good preservation of the foraminifera tests, and the carbon isotope measurements revealed $\delta^{13}C$ values in normal marine range (±1‰). The isotope records of the upper 15 meters in Hole 912A has been analyzed by Hevrøy, K., et al. 1996 and are interpreted to represent MIS 1 to MIS 9. The glacial stages 2, 4 and 8 has the highest content of both planktonic and benthic foraminifera. This indicate seasonal open water conditions during glacial periods with high foraminifera production (Hevroy, K. et al.). The $\delta^{13}C$ values found in this interval imply that the foraminifera is unaffected by methane dissociation.

4.1.2 Interval II

In the interval between 13,05 to 20,18 mbsf, both planktonic and benthic foraminifera are present. Micropaleontological analyses showed good preservation of the foraminifera tests. *C. reniforme* has a range in $\delta^{13}C$ between -0,51‰ to -2,07‰ in this interval. *C. neoteretis* has a range between 0,4‰ to -2,11‰. *M. barleeanum* show only two values between 13,05 to 20,18 mbsf, both between -1,68‰ to -2,04‰. *N. atlantica* show values between 0,06‰ to -1,17‰. The *N. pachyderma* was the most abundant foraminifera species in this interval and showed δ^{13} values from 0,02‰ to -1,88‰. The values of $\delta^{13}C$ in both benthic and planktonic foraminifera are in close range of normal marine environment. The more depleted values exhibited by *C. reniforme* at 18,68 mbsf (-2,07‰) and by *C. neoteretis* of 15,55 mbsf (-2,11‰) could imply an early effect of diagenesis near the modern day SMTZ located between 13 to 23 mbsf (Myhre et

al. 1995). Planktonic foraminifera are not expected to record depleted values in the water column, because most of the methane that escapes from the seafloor is consumed by methanotrophic bacteria in the sediments and the water column (Dickens, G. 2001, Reeburgh, W. S. 2007). Planktonic foraminifera are present in this interval, and *N. pachyderma* show values of -1,28‰ at 13, 05 mbsf and -1,88 ‰ at 15, 55 mbsf. The more depleted value of -1,88‰ might be attributed to diagenetic alteration that may stem from methane-derived authigenic carbonates on the foraminiferal tests after their deposition to the seafloor (Torres, M. E. et al. 2003, Millo, C. et al. 2005, Panieri, G. et al. 2009). As both benthic and planktonic foraminifera exhibit negative values of $\delta^{13}C$, the interpretation could be a scenario where the secondary carbonate precipitation has happened after they were buried (Figure 35). Methane-derived authigenic carbonate precipitation occur when the methane flux is low and all the methane is oxidized by AOM within the SMTZ (Borowski, W. S. et al. 1996).

B: How methane flux controls SMTZ (Borowski et al., 1996).

Seawater ↓ SO₄²⁻

SO₄²⁻ Diffusion

SMTZ

Sulfate Reduction Zone

SMTZ

Methane Flux

C: CIE I

AOM-SMTZ

$CH_4 + SO_4^{2-} \rightarrow HCO_3^- + HS^- + H_2O$ (Equation 1)
$Ca^{2+} + 2HCO_3^- \rightarrow CaCO_3 + CO_2 + H_2O$ (Equation 2)

Methane Flux
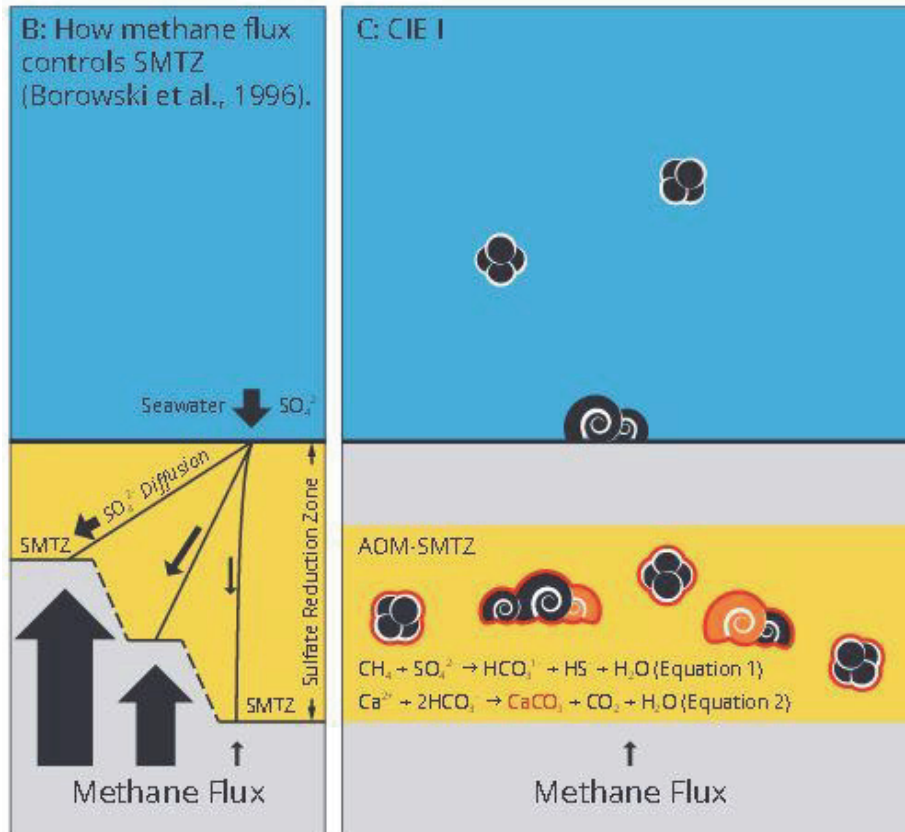
Benthic and planktonic foraminifera with $\delta^{13}C$ in range of normal marine environment

Benthic foraminifera with negative $\delta^{13}C$

Benthic and planktonic foraminifera affected by secondary carbonate ($CaCO_3$) overgrowth

Figure 35: Schematic diagram representing the scenario when the methane flux is low and both planktonic and benthic foraminifera show δ¹³C depletes values caused by precipitation of calcium carbonate on the foraminifera tests after burial (Consolaro, C. et al. 2015).

Hydrocarbon measurements from Hole 912A, done by the Shipboard during the cruise, showed an increase of methane concentration from 18 ppm at 11, 5 mbsf to 40,000 ppm at 23 mbsf. The methane concentration occurs immediately below the depth at which sulfate falls to zero, suggesting that methanogenesis is inhibited by the presence of sulfate and that intense sulfate reduction and methane oxidation occur at the interfaces (Stein, R. et al. 1995). This imply indicate a precence of a modern day SMTZ in the interval. Based on the magnetostatigraphy it is known that the sediments at 24,6 mbsf are correlated with the Brunhes/Matuyama reversal. This means that the sediments in this interval has been deposited after 0,78 Ma.

56

4.1.3 Interval III

The interval between 71,96 mbsf to 80,18 mbsf contained only benthic foraminifera. Micropaleontological investigation under the binocular microscope revealed several samples that did not have well preserved foraminiferal tests. The state of preservation of the foraminifera tests was in general poor and some specimens appeared to be oxidized and had a red color. SEM investigation of *E. incertum* and *Nonion sp.,* from 76, 46 mbsf (number 7 and 8 in Figure 34), confirmed bad preservation in this interval. *M. barleeanum,* from 79, 88 mbsf (number 1 in Figure 34), showed good preservation. Isotope measurements showed $\delta^{13}C$ values in *C. neoteretis* in a range from -0,16‰ to -0,46‰, which are values in normal marine range. *M. barleeanum* in a range between -1,22‰ to -1,30‰. *F. complanata* showed a prominent excursion at 73, 46 mbsf (-21,21‰), whereas the $\delta^{13}C$ value in the same specie is in normal marine range (-0,35‰) at 80,18 mbsf. *E. incertum* showed a value of $\delta^{13}C$ of -2‰ at 80, 18 mbsf, which is the only measurement of this specie in this interval. This extremely negative value in *F. complanata* are clearly due to secondary overgrowth of authigenic carbonate precipitated at SMTZ. However, it cannot be completely excluded that part of the negative signal could be a result of calcification in the presence of ^{13}C-depleted DIC and probably ingestion of ^{13}C-depleted methanotrophic microbes on which foraminifera feed (Consolaro, C. et al. 2015). In this scenario, methane activity is sufficiently high as to surpass the SMTZ and oxidized less efficiently with the consequence of lower AOM rates and higher methane fluxes into the bottom waters.

4.1.4 Interval IV

In the interval between 85 to 97 mbsf, only benthic foraminifera are present. The micropaleontological analyzes revealed crystals of calcite and aragonite sporadically in samples from 88, 10 mbsf to 94,49 mbsf. SEM analyses of foraminifera at 89, 15 mbsf revealed poor preservation of foraminifera tests in *M. barleeanum* and *C. neoteretis* (5 and 6 Figure 34). The interval show measurements of $\delta^{13}C$ in *M. barleeanum* between -0,35‰ and -5,66‰. The range of measurements of *C. neoteretis* is between -0,17‰ to -13,34‰. *C. reniforme* show values between -0,8‰ to -8,82‰.

At 88,28 mbsf, the same sample has $\delta^{13}C$ depleted values in *M. barleeanum* (-5,1‰) and *C. neoteretis* (-5,5‰). Depleted values are also present at 89, 15 mbsf t in *M. barleeanum* (-5,66‰) and *C. neoteretis* (-5,79‰). Between 93, 56 mbsf to 96, 37 mbsf there are several negative values. *C. neoteretis* show depleted values at 93,56 mbsf (-13,35‰), 94,49 mbsf (-10,36‰), 94,81 mbsf (-2,96‰), 95,24 mbsf (-1,79‰), 95,43 mbsf (-1,87‰), and 96,37 mbsf (-9,39‰). At 96, 37 mbsf the *C. reniforme* also have a strong depleted value (-8, 82‰).

This interval show $\delta^{13}C$-depleted values in several species. These negative values cannot be explained without considering precipitation of authigenic calcium carbonate around the foraminifera shells. There is no age-diagnostic in this interval, but the Olduvai Top is interpreted to be at 107,1 mbsf. Based on this, the sediments deposited in this interval are younger than 1,78 Ma.

4.1.5   Interval V

In the interval between 107 and 114, 61 mbsf the micropaleontological analyses revealed poorly preserved foraminifera test. The range $\delta^{13}C$ in this interval in *C. neoteretis* was between -0,3‰ to -2,53‰. At 107, 11 mbsf *C. neoteretis* showed a $\delta^{13}C$ of -2,53‰, and -2,38‰ at 109,96 mbsf. The Olduvai Top is interpreted to be at 107,1 mbsf and the Olduvai base is at 121,6 mbsf. This imply that the sediments in this interval has an age between 1,78 to 1,95 Ma.

4.1.6   Interval VI

In the interval between 126,78 to 133,78, *C. reinforme* and *C. neoteretis* was the most abundant species. The measurements are in the normal marine range (±1‰), except one measurement in *M. barleeanum* at 126, 78 mbsf (-1,24‰). The base of the Olduvai is at 121,6 mbsf, which imply that the sediments deposited in this interval are older than 1,95 Ma. Myhre et al. 1995, interpreted the transition between Quaternary and Pliocene to 135, 8 mbsf, which means that this interval is close to the Gelasian Stage (2,58 Ma).
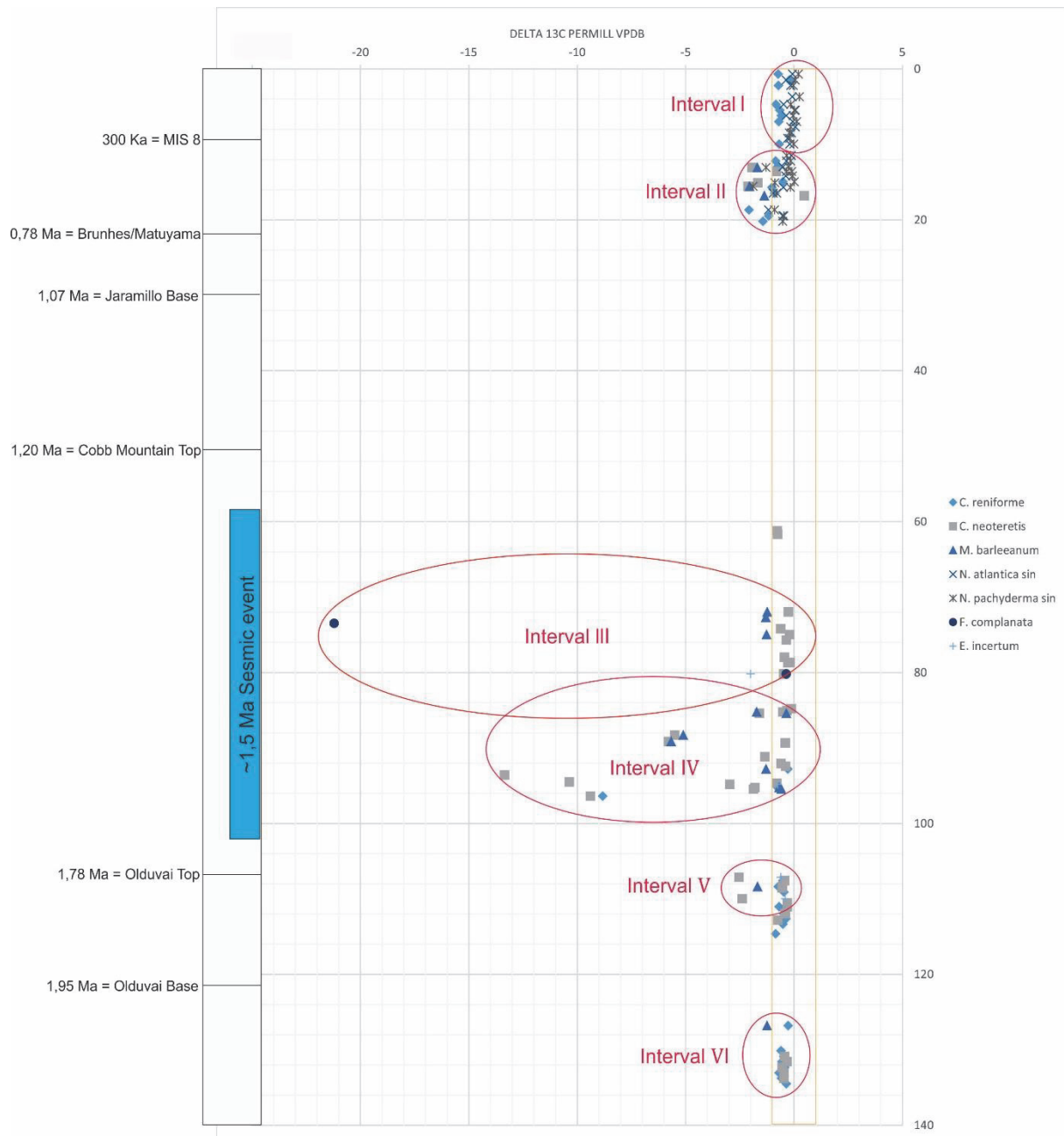
Figure 36: δ¹³C values in normal marine range (±1‰) are shown in orange. Carbon isotope intervals are marked in red ellipses and contain δ¹³C values out of normal marine range.. MIS 8 is dated to 300 ka (Lisiecki, L. E. and Raymo, M. E. 2005) based on data from stable isotope data (Hevroy, K. et al.) at ~12, 7 mbsf. Age-depth fix points from the initial report (Myhre, A. M. et al. 1995) 0,78 Ma at 24,6 mbsf, 1,07 Ma at 36,5 mbsf, 1,20 Ma at 53,8 mbsf, 1,78 Ma at 107,1 mbsf and 1,95 Ma at 121,6 mbsf. The seismic event (Mattingsdal, R. et al. 2014) at ~1,5 Ma is added between the Cobb Mountain Top and the Olduvai Top.

4.2   Yermak Plateau during the Pleistocene

Pleistocene climate is characterized by a persistent succession of glacial-to-interglacial cycles driven by orbital forcing (Bartoli, G. et al. 2005). The northern hemisphere glaciations (NHG) and large scale Arctic Sea ice has only happened since Late Pliocene (~3,2 Ma). Records from the North Atlantic Ocean indicate a large-scale glaciation in the circum Atlantic region spanning from the interval 3,6 to 2,4 Ma (Kleiven, H. F. et al. 2002). Evidences suggest that ice sheets appear to have advanced occasionally during the Quaternary, and is inundated only in the most extensive glaciations (Dowdeswell, J. et al. 2010). The upper boundary of glacial deposits on the Yermak Plateau has an estimated age of ~2,7 Ma according to high-resolution single-channel seismic data seen in Figure 38 (Mattingsdal, R. et al. 2014). The sedimentation rate estimated from Ocean Drilling Program (ODP) Holes 911A, 910C and 912A, seem to have been ~3-10 cm/ka before 2,7 Ma. After the sedimentation rate is estimated to increase to ~9-19 cm/ka. These sedimentation rates has been calculated by using the depths for each fix-points from the three Holes on Yermak Plateau drilled by the ODP. The sediments in all three Holes are dominated with contourite deposition probably sourced by the West Spitsbergen Current from 2,7 Ma to 11 Ma (Mattingsdal, R. et al. 2014). It is suggested that the Svalbard ice sheet reached the shelf break outside NW Svalbard at 2,7 Ma (Mattingsdal, R. et al. 2014). The glacial build up beyond the cost of NW Svalbard at 2,7 Ma is seen in ice-rafted debris (IRD) records for the Yermak Plateau (Knies, J. et al. 2002, Junttila, J. et al. 2008) and Vøring Plateau (Jansen, E. and Sjøholm, J. 1991). The abrupt pulse of IRD is associated with distinct melting derived of icebergs from the Svalbard ice sheet (Knies, J. et al. 2002). The increase in sedimentation rate after 2,7 Ma, is probably due to increase glacial erosion on the Yermak Plateau. There is evidence for a relatively warm Northern Hemisphere climate between 2 and 1,8 Ma (Funder, S. et al. 1985), but sediment transport on the Yermak Plateau is still controlled by the waxing and waning of the Svalbard ice sheet (Knies, J. et al. 2002). According to the magnetostratigraphy in Hole 912A, the base of the section studied paleomagnetically (135 mbsf) was deposited shortly before the Olduvai base at approximately 2 Ma (Myhre, A. M. et al. 1995). Hole 912A show a low abundance of dropstone between 97,2 to 145,5 mbsf (912A-12X to 912A-16X) dated to be Olduvai subcron (1,78 to 1,96 Ma), see Figure 37. This supports the evidence of presence of the Svalbard ice sheet on the Yermak Plateau after the northern hemisphere glaciation at 2,7 Ma. Upper five age fix-points younger than 2 Ma has been established for Hole 912A, and tied to seismic data by correlating

with Hole 912A (Figure 38)(Mattingsdal, R. et al. 2014). There is an increase in dropstone abundance from 97,2 mbsf (Figure 37).
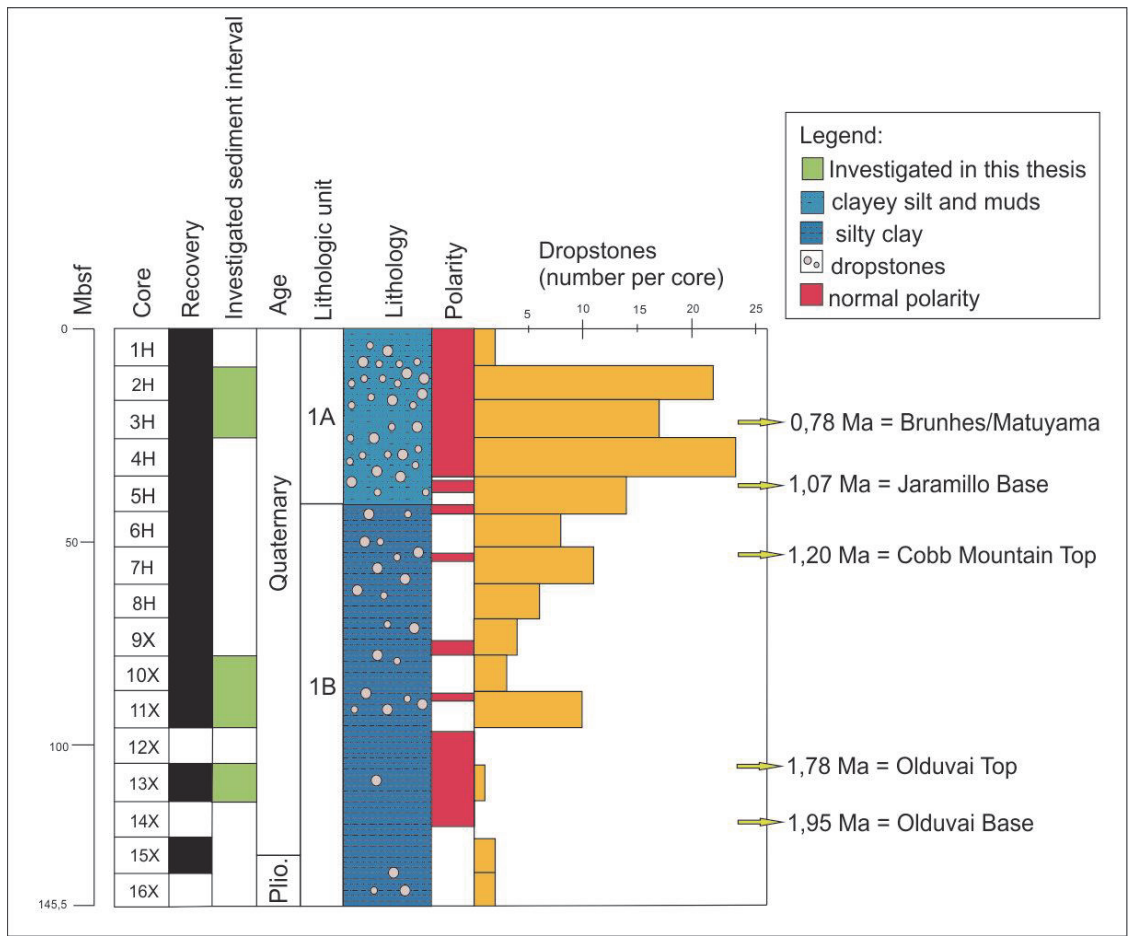
Figure 37: overview of cores at Hole 912A with depth, recovery, age, subunit 1A and 1B, lithology, polarity and number of dropstones. Redrawn form information and figures from (Myhre, A. M. et al. 1995) Added datum from (Myhre, A. M. et al. 1995, Mattingsdal, R. et al. 2014) of polarity events dated with age.

The first glaciation of the Spitsbergen shelf has been dated to between 1.6 and 1.3 Ma, after which glacial advances repeatedly reached the shelf edge. The first signs of extensive glacial erosion on the Yermak Plateau are present from ~1,5 Ma, shown Figure 38 (Mattingsdal, R. et al. 2014) Occurrences of large erosional furrows are interpreted as iceberg plow marks on the southern Yermak Plateau on seismic profiles. The erosional source is primarily from the east and is interpreted as the first shelf break glaciation on the western Barents Sea-Svalbard margin (Mattingsdal, R. et al. 2014). In areas of ice grounding, large scale erosion under the ice is common (Vorren, T. O. et al. 1988). The ~1,5 Ma seismic event is between the Olduvai Top (1,78 Ma) and the Cobb Mountain Top (1,20 Ma) in Hole 912A.

Large-scale glaciation in the Barents Sea occurred after 1 Ma with repeated advances to the shelf edge. The timing is inferred from ice grounding on the Yermak Plateau at about 0.95 Ma, and higher frequencies of gravity-driven mass movements along the western Barents Sea margin associated with expansive glacial growth (Knies, J. et al. 2009). Oxygen isotope records form the circum-Arctic indicate enhanced glacial-interglacial periods between 900 ka (thousands of years before present) to 600 ka, and are thought to reflect more extensive marine Arctic ice sheets (Flower, B. P. 1997). Disintegrating ice sheets at the shelf edge is inferred from massive meltwater pulses during major terminations of the ice sheet suggesting that at least five or six shelf edge glaciations have taken place in the Barents Sea over the past 800.000 years (Knies, J. et al. 2009). Seismic evidence confirms that the Svalbard and the Barents Sea ice sheets were linked during the mid-Quaternary. They may have become decoupled during the late-Quaternary (Solheim, A. et al. 1996, Flower, B. P. 1997). A decrease in the Svalbard ice sheet grounding after 660 ka is suggested, in contrast to the Barents ice sheet which appears to have reached the Yermak Plateau during glacials in the late Quaternary, including the late glacial maximum (Flower, B. P. 1997). Swath bathymetry and sub-bottom acoustic profiling from the Yermak Plateau show ice-produced lineations and iceberg plow marks which is suggested to a MIS 16 (~660 ka) or Saalian age (MIS 6) (Dowdeswell, J. et al. 2010).
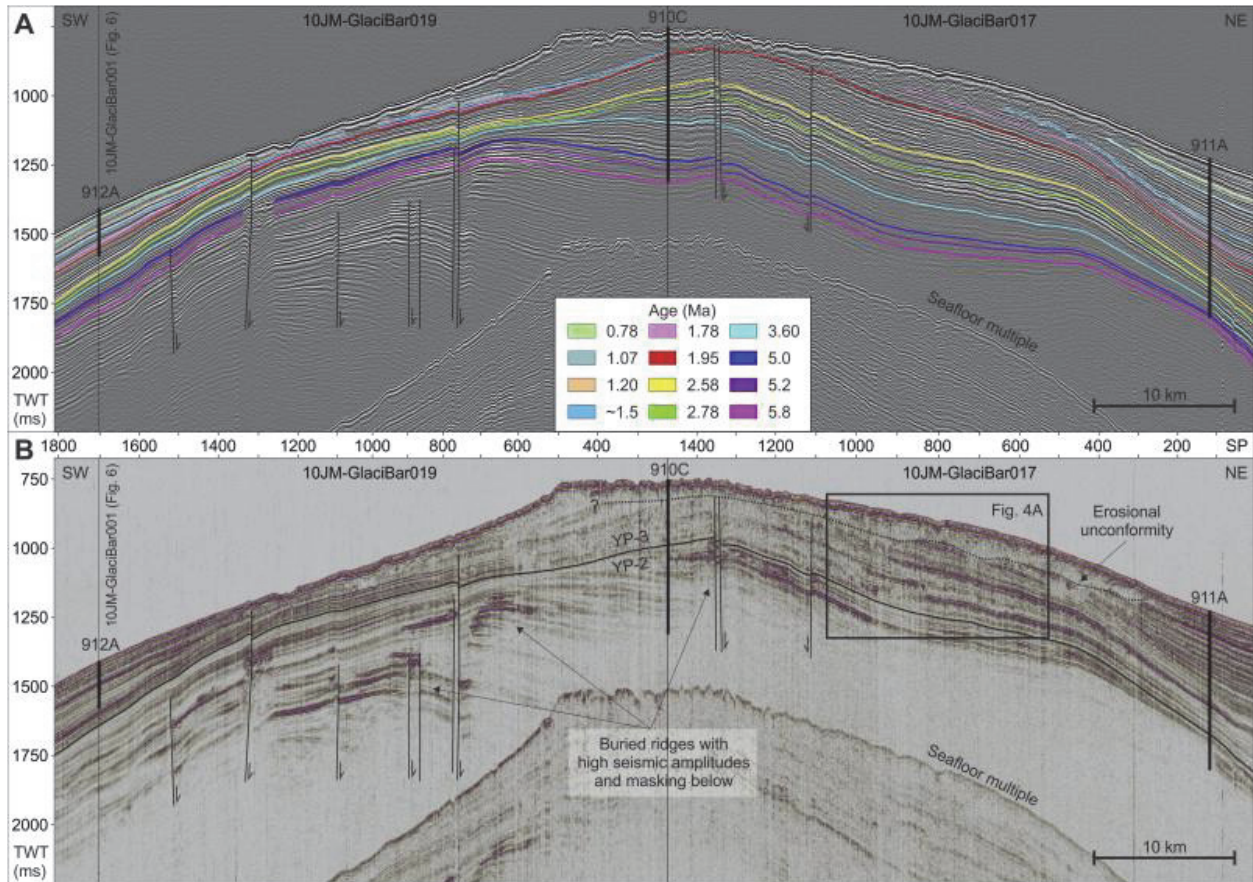
Figure 38: Seismic profile of 2D high-resolution single channel seismic crossing ODP Holes 912A, 910C and 911A on the Yermak Plateau. A) Seismic amplitudes in grayscale with color coded reflectors dated by age fixed-points from the three ODP holes. B) Seismic amplitudes with buried ridges and erosional unconformity indicated. The YP-2 to YP-3 boundary (Eiken, O. and Hinz, K. 1993) corresponds to ~2,5 Ma. Figure from (Mattingsdal, R. et al. 2014).

4.3   Record of Past Methane Fluxes of Yermak Plateau during Pleistocene

The extremely negative calcite $\delta^{13}C$ values in the sediments in intervals III and IV (71 to 97 mbsf) in Hole 912A on the Yermak Plateau, suggest that foraminiferal calcite record past methane seepage on the Yermak Plateau. The air-sea exchange of carbon is not large enough to explain the extreme depletion of $\delta^{13}C$ in foraminifera, and the values cannot be due to the nutrient dynamics of ocean water. The negative values can occur during primary calcification of benthic foraminifera in sediments effected by methane seepage (Rathburn, A. E. et al. 2003, Hill, T. et al. 2004, Panieri, G. et al. 2014, Panieri, G. et al. 2016), but also during secondary precipitation of authigenic calcium carbonate on the calcite wall of foraminifer caused by anaerobic oxidation of methane (AOM) (Torres, M. E. et al. 2003, Torres, M. E. et al. 2010,

Consolaro, C. et al. 2015, Panieri, G. et al. 2016). During times of high methane flux, the secondary overgrowth via AOM can be deposited in near-surface sediments, but also at a subsurface SMTZ. The exceptionally low $\delta^{13}C$ values cannot be produced by biomineralization (Millo, C. et al. 2005), so the signal must be a result of secondary authigenic carbonate precipitation. This was confirmed by SEM investigation of the foraminifera test with low $\delta^{13}C$, which showed internal and external overgrowths of secondary calcite crystals and carbonate patina (Figure 34).

Assuming that light carbon has been incorporated in the tests near the seafloor, the negative excursions evolved by $\delta^{13}C$ of foraminifera seems to coincide with an interval of time between Olduvai Top (1,78 Ma) and Cobb Mountain Top (1,20 Ma). An event showing the first signs of extensive glacial erosion on the Yermak Plateau around ~1,5 Ma between this two age fix points are documented from seismic data (Mattingsdal, R. et al. 2014). It is not certain that the negative $\delta^{13}C$ and the event around ~1,5 Ma correlates, because there are no firm stratigraphic controls in this interval, and we cannot relate periods of high versus low methane flux to specific climate events. But it is known that during periods of warming, methane hydrates accumulated in the subsurface can dissociate, fueling a high methane flux and a shallow SMTZ depths near the seafloor (Panieri, G. et al. 2016).The hypothesized mechanism for the light δ^{13} C expulsion is release of methane from gas hydrates dissociation due to pressure release during ice sheet retreat. The seismic event at 1,5 Ma imply that the investigated area was covered by a grounded ice sheet or tabular icebergs, that caused large scale erosion. Ice retreat and associated isostatic rebound would both reduce the seafloor pressure depending on the change in seafloor depth (Lerche, I. et al. 1997). The retreat of the ice margin could have released enough pressure to dissociate the gas hydrates and expel methane into the overlaying sediments and ocean water (Smith, L. et al. 2001). Additionally, ice retreat would allow the warmer West Spitsbergen Current to flow across the plateau, increasing bottom water temperatures and thus facilitating the dissociation of gas hydrates as suggested for the western Svalbard margin. Similar events invoking both pressure and temperature changes associated with ice shelf retreat as the mechanism for hydrate dissociation has been suggested before (Smith, L. et al. 2001, Chand, S. et al. 2008, Consolaro, C. et al. 2015, Portnov, A. et al. 2016). Influence and increase of pressure and decrease in bottom water/ice temperature due to glaciation on the hydrate stability field in the Barents Sea during the

late Weichselian glacial maximum have been analyzed (Chand, S. et al. 2008). The finding was that the removal of pressure due to ice sheet retreat reduced the GHSZ and resulted in the release of soluble methane. Estimations suggest that the bottom water temperature changed with ~7°C in the south-western Barents Sea (Chand, S. et al. 2008).

5 Conclusions

Foraminiferal isotope and state of preservation in ODP Hole 912A on the Yermak Plateau has been represented in this master thesis. The stable isotope analyzes revealed negative $\delta^{13}C$ values in several intervals in Hole 912A.

Depleted calcite $\delta^{13}C$ values in interval II from 13,05 to 20,18 mbsf could imply an early effect of diagenesis due to a suggested modern day SMTZ located between 13 to 23 mbsf. Benthic and planktonic foraminifera exhibit negative values of $\delta^{13}C$ in the same samples and indicate that the secondary carbonate precipitation has happened after they were buried.

The extremely negative calcite $\delta^{13}C$ values in sediments represented in interval III and IV (71,96 to 97 mbsf) clearly indicate that benthic foraminifera record past methane seepage on the Yermak Plateau. The $\delta^{13}C$ signals have been interpreted as being due to secondary methane-derived authigenic carbonates. SEM investigations confirm the presence of AOM-derived coating by internal and external overgrowths of secondary calcite crystals. The depleted carbon values are represented in sediments in a time interval between 1,20 to 1,95 Ma. A seismic horizon dated to ~1,5 Ma represent iceberg plow marks on the Yermak Plateau, and indicate a regional glacial intensification at this time for the whole Barents Sea-Svalbard region. The interval with depleted $\delta^{13}C$ values coincide with this event. The hypothesis is that the methane hydrate was stable during the shelf break glaciation on the western Barents Sea-Svalbard margin, due to high pressure from ice loading, and low temperatures in the surface bottom. Retreat of the sea ice would release the pressure and allow the West Spitsbergen Current to flow over the region. Evidence of a widening of the Fram Strait in this period would also increase the flow of warmer bottom waters from the Atlantic Ocean. The pressure release and the inflow of warmer bottom waters could have caused dissociation of the methane hydrate.

6 References

Aagaard, K., Foldvik, A. and Hillman, S. R. (1987). "The West Spitsbergen Current - Disposition and Water Mass Transformation." Journal of Geophysical Research-Oceans **92**(C4): 3778-3784.

Armstrong, H. and Brasier, M. (2005). Microfossils (2nd edn), Oxford.

Ascough, P. L., Cook, G. T., Church, M. J., Dugmore, A. J., Arge, S. V. and McGovern, T. H. (2006). "Variability in North Atlantic marine radiocarbon reservoir effects at c. AD 1000." Holocene **16**(1): 131-136.

Barbieri, R. and Panieri, G. (2004). "How are benthic foraminiferal faunas influenced by cold seeps? Evidence from the Miocene of Italy." Palaeogeography, Palaeoclimatology, Palaeoecology **204**(3): 257-275.

Bartoli, G., Sarnthein, M., Weinelt, M., Erlenkeuser, H., Garbe-Schönberg, D. and Lea, D. (2005). "Final closure of Panama and the onset of northern hemisphere glaciation." Earth and Planetary Science Letters **237**(1): 33-44.

Berggren, W. A. (1972). "A Cenozoic time- scale—some implications for regional geology and paleobiogeography." Lethaia **5**(2): 195-215.

Bernard, B. B., Brooks, J. M. and Sackett, W. M. (1978). "Light hydrocarbons in recent Texas continental shelf and slope sediments." Journal of Geophysical Research: Oceans **83**(C8): 4053-4061.

Biastoch, A., Treude, T., Rupke, L. H., Riebesell, U., Roth, C., Burwicz, E. B., Park, W., Latif, M., Boning, C. W., Madec, G. and Wallmann, K. (2011). "Rising Arctic Ocean temperatures cause gas hydrate destabilization and ocean acidification." Geophysical Research Letters **38**.

Blunier, T. and Brook, E. J. (2001). "Timing of millennial-scale climate change in Antarctica and Greenland during the last glacial period." Science **291**(5501): 109-112.

Borowski, W. S., Paull, C. K. and Ussler, W. (1996). "Marine pore-water sulfate profiles indicate in situ methane flux from underlying gas hydrate." Geology **24**(7): 655-658.

Borowski, W. S., Paull, C. K. and Ussler, W. (1999). "Global and local variations of interstitial sulfate gradients in deep-water, continental margin sediments: Sensitivity to underlying methane and gas hydrates." Marine Geology **159**(1-4): 131-154.

Bourke, R. H., Weigel, A. M. and Paquette, R. G. (1988). "The Westward Turning Branch of the West Spitsbergen Current." Journal of Geophysical Research-Oceans **93**(C11): 14065-14077.

Broecker, W. S. (1997). "Thermohaline circulation, the Achilles heel of our climate system: Will man-made CO2 upset the current balance?" Science **278**(5343): 1582-1588.

Brook, E. J., Sowers, T. and Orchardo, J. (1996). "Rapid variations in atmospheric methane concentration during the past 110,000 years." Science **273**(5278): 1087-1091.

Bunz, S., Mienert, J. and Berndt, C. (2003). "Geological controls on the Storegga gas-hydrate system of the mid-Norwegian continental margin." Earth and Planetary Science Letters **209**(3-4): 291-307.

Caralp, M. H. (1989). "Size and Morphology of the Benthic Foraminifer Melonis-Barleeanum - Relationships with Marine Organic-Matter." Journal of Foraminiferal Research **19**(3): 235-245.

Carstens, J., Hebbeln, D. and Wefer, G. (1997). "Distribution of planktic foraminifera at the ice margin in the Arctic (Fram Strait)." Marine Micropaleontology **29**(3): 257-269.

Chand, S., Mienert, J., Andreassen, K., Knies, J., Plassen, L. and Fotland, B. (2008). "Gas hydrate stability zone modelling in areas of salt tectonics and pockmarks of the Barents Sea suggests an active hydrocarbon venting system." Marine and Petroleum Geology **25**(7): 625-636.

Chappellaz, J., Barnola, J. M., Raynaud, D., Korotkevich, Y. S. and Lorius, C. (1990). "Ice-Core Record of Atmospheric Methane over the Past 160,000 Years." Nature **345**(6271): 127-131.

Chauhan, T., Rasmussen, T. L. and Noormets, R. (2016). "Palaeoceanography of the Barents Sea continental margin, north of Nordaustlandet, Svalbard, during the last 74 ka." Boreas **45**(1): 76-99.

Cokelet, E. D., Tervalon, N. and Bellingham, J. G. (2008). "Hydrography of the West Spitsbergen Current, Svalbard Branch: Autumn 2001." Journal of Geophysical Research-Oceans **113**(C1).

Compton, J. S. and Mallinson, D. J. (1996). "Geochemical consequences of increased late Cenozoic weathering rates and the global CO2 balance since 100 Ma." Paleoceanography **11**(4): 431-446.

Consolaro, C., Rasmussen, T. L., Panieri, G., Mienert, J., Bunz, S. and Sztybor, K. (2015). "Carbon isotope (delta C-13) excursions suggest times of major methane release during the last 14 kyr in Fram Strait, the deep-water gateway to the Arctic." Climate of the Past **11**(4): 669-685.

Dickens, G. (2001). "On the fate of past gas: What happens to methane released from a bacterially mediated gas hydrate capacitor?" Geochemistry, Geophysics, Geosystems **2**(1).

Dickens, G. R. (2003). "Methane hydrates in quaternary climate change - The clathrate gun hypothesis." Science **299**(5609): 1017-1017.

Dickens, G. R. and QuinbyHunt, M. S. (1997). "Methane hydrate stability in pore water: A simple theoretical approach for geophysical applications." Journal of Geophysical Research-Solid Earth **102**(B1): 773-783.

Dowdeswell, J., Jakobsson, M., Hogan, K., O'Regan, M., Backman, J., Evans, J., Hell, B., Löwemark, L., Marcussen, C. and Noormets, R. (2010). "High-resolution geophysical observations of the Yermak Plateau and northern Svalbard margin: implications for ice-sheet grounding and deep-keeled icebergs." Quaternary Science Reviews **29**(25): 3518-3531.

Driscoll, N. W. and Haug, G. H. (1998). "A short circuit in thermohaline circulation: A cause for northern hemisphere glaciation?" Science **282**(5388): 436-438.

Eiken, O. and Hinz, K. (1993). "Contourites in the Fram Strait." Sedimentary Geology **82**(1-4): 15-32.

Emiliani, C. (1955). "Pleistocene temperatures." The Journal of Geology: 538-578.

Englezos, P. (1993). "Clathrate Hydrates." Industrial & Engineering Chemistry Research **32**(7): 1251-1274.

Etiope, G. (2015). Natural Gas Seepage, Springer.

Faure, G. and Mensing, T. M. (2005). Isotopes: principles and applications, John Wiley & Sons Inc.

Ferre, B., Mienert, J. and Feseker, T. (2012). "Ocean temperature variability for the past 60 years on the Norwegian-Svalbard margin influences gas hydrate stability on human time scales." Journal of Geophysical Research-Oceans 117.

Feyling-Hanssen, R. W. (1971). "Weichselian interstadial Foraminifera from the Sandnes-Jaeren area." Bulletin of the Geological Society of Denmark 21: 72-116.

Feyling-Hanssen, R. W. (1972). "The foraminifer Elphidium excavatum (Terquem) and its variant forms." Micropaleontology: 337-354.

Flower, B. P. (1997). "Overconsolidated section on the Yermak Plateau, Arctic Ocean: Ice sheet grounding prior to ca. 660 ka?" Geology 25(2): 147-150.

Funder, S., Abrahamsen, N., Bennike, O. and Feyling-Hanssen, R. W. (1985). "Forested arctic: evidence from North Greenland." Geology 13(8): 542-546.

Garming, J. F. L., Bleil, U. and Riedinger, N. (2005). "Alteration of magnetic mineralogy at the sulfate-methane transition: Analysis of sediments from the Argentine continental slope." Physics of the Earth and Planetary Interiors 151(3-4): 290-308.

Gibbard, P. and Cohen, K. M. (2008). "Global chronostratigraphical correlation table for the last 2.7 million years." Episodes 31(2): 243-247.

Gibbard, P. L., Head, M. J., Walkers, M. J. C. and Stratigra, S. Q. (2010). "Formal ratification of the Quaternary System/Period and the Pleistocene Series/Epoch with a base at 2.58 Ma." Journal of Quaternary Science 25(2): 96-102.

Gupta, B. K. S. and Aharon, P. (1994). "Benthic foraminifera of bathyal hydrocarbon vents of the Gulf of Mexico: Initial report on communities and stable isotopes." Geo-Marine Letters 14(2-3): 88-96.

Gupta, B. K. S. and Barun, K. (1999). Modern foraminifera, Springer.

Gupta, B. K. S., Platon, E., Bernhard, J. M. and Aharon, P. (1997). "Foraminiferal colonization of hydrocarbon-seep bacterial mats and underlying sediment, Gulf of Mexico slope." The Journal of Foraminiferal Research 27(4): 292-300.

Hald, M. and Korsun, S. (1997). "Distribution of modern benthic foraminifera from fjords of Svalbard, European Arctic." Journal of Foraminiferal Research 27(2): 101-122.

Hald, M. and Steinsund, P. I. (1992). "Distribution of Surface Sediment Benthic Foraminifera in the Southwestern Barents Sea." Journal of Foraminiferal Research 22(4): 347-362.

Harnung, S. E. and Johnson, M. S. (2012). Chemistry and the Environment, Cambridge University Press.

Harrison, B. K., Zhang, H., Berelson, W. and Orphan, V. J. (2009). "Variations in Archaeal and Bacterial Diversity Associated with the Sulfate-Methane Transition Zone in Continental Margin Sediments (Santa Barbara Basin, California)." Applied and Environmental Microbiology 75(6): 1487-1499.

Hevroy, K., Lavik, G. and Hansen, E. "Quaternary Paleoceanography and Paloclimatology of the Fram Strait." Yermak Plateau Region: Evidence from Sites 909: 469-482.

Hill, T., Kennett, J. and Valentine, D. (2004). "Isotopic evidence for the incorporation of methane-derived carbon into foraminifera from modern methane seeps, Hydrate Ridge, Northeast Pacific." Geochimica et Cosmochimica Acta **68**(22): 4619-4627.

Hunt, J. (1996). "Petroleum geology and geochemistry." Freeman, New York.

Jakobsson, M., Backman, J., Rudels, B., Nycander, J., Frank, M., Mayer, L., Jokat, W., Sangiorgi, F., O'Regan, M., Brinkhuis, H., King, J. and Moran, K. (2007). "The early Miocene onset of a ventilated circulation regime in the Arctic Ocean." Nature **447**(7147): 986-990.

Jansen, E. and Sjøholm, J. (1991). "Reconstruction of glaciation over the past 6 Myr from ice-borne deposits in the Norwegian Sea." Nature **349**(6310): 600-603.

Jennings, A. E., Weiner, N. J., Helgadottir, G. and Andrews, J. T. (2004). "Modern foraminiferal faunas of the southwestern to northern Iceland shelf: Oceanographic and environmental controls." Journal of Foraminiferal Research **34**(3): 180-207.

Judd, A. and Hovland, M. (2009). Seabed fluid flow: the impact on geology, biology and the marine environment, Cambridge University Press.

Junttila, J., Lahtinen, T. and Strand, K. (2008). "Provenance and sea- ice transportation of Mid-Pliocene and Quaternary sediments, Yermak Plateau, Arctic Ocean (ODP Site 911)." Boreas **37**(2): 273-285.

Katz, M. E., Cramer, B. S., Franzese, A., Honisch, B., Miller, K. G., Rosenthal, Y. and Wright, J. D. (2010). "Traditional and Emerging Geochemical Proxies in Foraminifera." Journal of Foraminiferal Research **40**(2): 165-192.

Kawagata, S., Hayward, B. W., Grenfell, H. R. and Sabaa, A. (2005). "Mid-Pleistocene extinction of deep-sea foraminifera in the North Atlantic Gateway (ODP sites 980 and 982)." Palaeogeography Palaeoclimatology Palaeoecology **221**(3-4): 267-291.

Kleiven, H. F., Jansen, E., Fronval, T. and Smith, T. (2002). "Intensification of Northern Hemisphere glaciations in the circum Atlantic region (3.5–2.4 Ma)–ice-rafted detritus evidence." Palaeogeography, Palaeoclimatology, Palaeoecology **184**(3): 213-223.

Knies, J., Matthiessen, J., Vogt, C., Laberg, J. S., Hjelstuen, B. O., Smelror, M., Larsen, E., Andreassen, K., Eidvin, T. and Vorren, T. O. (2009). "The Plio-Pleistocene glaciation of the Barents Sea-Svalbard region: a new model based on revised chronostratigraphy." Quaternary Science Reviews **28**(9-10): 812-829.

Knies, J., Matthiessen, J., Vogt, C. and Stein, R. (2002). "Evidence of 'Mid-Pliocene (similar to 3 Ma) global warmth' in the eastern Arctic Ocean and implications for the Svalbard/Barents Sea ice sheet during the late Pliocene and early Pleistocene (similar to 3-1.7 Ma)." Boreas **31**(1): 82-93.

Kohfeld, K. E., Fairbanks, R. G., Smith, S. L. and Walsh, I. D. (1996). "Neogloboquadrina pachyderma (sinistral coiling) as paleoceanographic tracers in polar oceans: Evidence from northeast water Polynya plankton tows, sediment traps, and surface sediments." Paleoceanography **11**(6): 679-699.

Kucera, M. (2007). "Planktonic foraminifera as tracers of past oceanic environments." Developments in marine geology **1**(6): 213-262.

Kvenvolden, K. A. (1988). "Methane Hydrate - a Major Reservoir of Carbon in the Shallow Geosphere." Chemical Geology **71**(1-3): 41-51.

Kvenvolden, K. A. (1993). "Gas Hydrates - Geological Perspective and Global Change." Reviews of Geophysics **31**(2): 173-187.

Kvenvolden, K. A. (1995). "A review of the geochemistry of methane in natural gas hydrate." Organic Geochemistry **23**(11-12): 997-1008.

Lerche, I., Yu, Z., Tørudbakken, B. and Thomsen, R. (1997). "Ice loading effects in sedimentary basins with reference to the Barents Sea." Marine and Petroleum Geology **14**(3): 277-338.

Lisiecki, L. E. and Raymo, M. E. (2005). "A Pliocene- Pleistocene stack of 57 globally distributed benthic δ18O records." Paleoceanography **20**(1).

Loeng, H. (1991). "Features of the Physical Oceanographic Conditions of the Barents Sea." Polar Research **10**(1): 5-18.

Lowe, J. J., Walker, M. J. and Walker, M. J. (1997). Reconstructing quaternary environments, Longman Londres.

Mackensen, A. and Hald, M. (1988). "Cassidulina-Teretis Tappan and Cassidulina-Laevigata Dorbigny - Their Modern and Late Quaternary Distribution in Northern Seas." Journal of Foraminiferal Research **18**(1): 16-24.

Mackensen, A., Sejrup, H. P. and Jansen, E. (1985). "The Distribution of Living Benthic Foraminifera on the Continental-Slope and Rise Off Southwest Norway." Marine Micropaleontology **9**(4): 275-306.

Manley, T. O. (1995). "Branching of Atlantic Water within the Greenland-Spitsbergen Passage - an Estimate of Recirculation." Journal of Geophysical Research-Oceans **100**(C10): 20627-20634.

Mattingsdal, R., Knies, J., Andreassen, K., Fabian, K., Husum, K., Grosfjeld, K. and De Schepper, S. (2014). "A new 6 Myr stratigraphic framework for the Atlantic-Arctic Gateway." Quaternary Science Reviews **92**: 170-178.

McKay, J. (2015). "Carbonate Analysis δ13C and δ18O."   Retrieved 29.03., 2016, from http://stable-isotope.coas.oregonstate.edu/methods/carbonate%20analysis/carbonateanal.html.

Meincke, J., Rudels, B. and Friedrich, H. J. (1997). "The Arctic ocean Nordic seas thermohaline system." Ices Journal of Marine Science **54**(3): 283-299.

Millo, C., Sarnthein, M., Erlenkeuser, H. and Frederichs, T. (2005). "Methane-driven late Pleistocene delta C-13 minima and overflow reversals in the southwestern Greenland Sea." Geology **33**(11): 873-876.

Millo, C., Sarnthein, M., Erlenkeuser, H., Grootes, P. M. and Andersen, N. (2005). "Methane-induced early diagenesis of foraminiferal tests in the Southwestern Greenland Sea." Marine Micropaleontology **58**(1): 1-12.

Muench, R. D., Mcphee, M. G., Paulson, C. A. and Morison, J. H. (1992). "Winter Oceanographic Conditions in the Fram Strait Yermak Plateau Region." Journal of Geophysical Research-Oceans **97**(C3): 3469-3483.

Murray, J. W. (2001). "The niche of benthic foraminifera, critical thresholds and proxies." Marine Micropaleontology **41**(1-2): 1-7.

Myhre, A., Thiede, J. and Firth, J. (1995). "1. NORTH ATLANTIC-ARCTIC GATEWAYS1."

Myhre, A. M., Thiede, J., Firth, J. V., Johnson, G. L. and Ruddiman, W. F. (1995). "Site 912." Proc. ODP, Init. Repts **151**: 319–343.

Nisha, N. and Singh, A. (2012). "Benthic foraminiferal biofacies on the shelf and upper continental slope off North Kerala (Southwest India)." Journal of the Geological Society of India **80**(6): 783-801.

Osterman, L. E. and Nelson, A. R. (1989). "Latest Quaternary and Holocene Paleoceanography of the Eastern Baffin Island Continental-Shelf, Canada - Benthic Foraminiferal Evidence." Canadian Journal of Earth Sciences **26**(11): 2236-2248.

Panieri, G. (2006). "Foraminiferal response to an active methane seep environment: A case study from the Adriatic Sea." Marine Micropaleontology **61**(1-3): 116-130.

Panieri, G., Camerlenghi, A., Cacho, I., Cervera, C. S., Canals, M., Lafuerza, S. and Herrera, G. (2012). "Tracing seafloor methane emissions with benthic foraminifera: Results from the Ana submarine landslide (Eivissa Channel, Western Mediterranean Sea)." Marine Geology **291**: 97-112.

Panieri, G., Camerlenghi, A., Conti, S., Pini, G. A. and Cacho, I. (2009). "Methane seepages recorded in benthic foraminifera from Miocene seep carbonates, Northern Apennines (Italy)." Palaeogeography Palaeoclimatology Palaeoecology **284**(3-4): 271-282.

Panieri, G., Graves, C. A. and James, R. H. (2016). "Paleo- methane emissions recorded in foraminifera near the landward limit of the gas hydrate stability zone offshore western Svalbard." Geochemistry, Geophysics, Geosystems.

Panieri, G., James, R. H., Camerlenghi, A., Westbrook, G. K., Consolaro, C., Cacho, I., Cesari, V. and Cervera, C. S. (2014). "Record of methane emissions from the West Svalbard continental margin during the last 23.500 yrs revealed by delta C-13 of benthic foraminifera." Global and Planetary Change **122**: 151-160.

Pflaumann, U., Duprat, J., Pujol, C. and Labeyrie, L. D. (1996). "SIMMAX: A modern analog technique to deduce Atlantic sea surface temperatures from planktonic foraminifera in deep-sea sediments." Paleoceanography **11**(1): 15-35.

Polyak, L., Korsun, S., Febo, L. A., Stanovoy, V., Khusid, T., Hald, M., Paulsen, B. E. and Lubinski, D. J. (2002). "Benthic foraminiferal assemblages from the southern Kara Sea, a river-influenced Arctic marine environment." Journal of Foraminiferal Research **32**(3): 252-273.

Poore, R. and Berggren, W. (1975). "The morphology and classification of Neogloboquadrina atlantica (Berggren)." The Journal of Foraminiferal Research **5**(2): 76-84.

Portnov, A., Vadakkepuliyambatta, S., Mienert, J. and Hubbard, A. (2016). "Ice-sheet-driven methane storage and release in the Arctic." Nature communications **7**.

Rathburn, A. E., Pérez, M. E., Martin, J. B., Day, S. A., Mahn, C., Gieskes, J., Ziebis, W., Williams, D. and Bahls, A. (2003). "Relationships between the distribution and stable isotopic composition of living benthic foraminifera and cold methane seep biogeochemistry in Monterey Bay, California." Geochemistry, Geophysics, Geosystems **4**(12).

Reeburgh, W. S. (2007). "Oceanic methane biogeochemistry." Chemical Reviews **107**(2): 486-513.

Rudels, B., Bjork, G., Nilsson, J., Winsor, P., Lake, I. and Nohr, C. (2005). "The interaction between waters from the Arctic Ocean and the Nordic Seas north of Fram Strait and along the East Greenland Current: results from the Arctic Ocean-02 Oden expedition." Journal of Marine Systems **55**(1-2): 1-30.

Ruppel, C. (2011). "Methane hydrates and contemporary climate change." Nature Education Knowledge **3**(10): 29.

Schmiedl, G., Mackensen, A. and Muller, P. J. (1997). "Recent benthic foraminifera from the eastern South Atlantic Ocean: Dependence on food supply and water masses." Marine Micropaleontology **32**(3-4): 249-287.

Shakhova, N., Semiletov, I., Salyuk, A., Yusupov, V., Kosmach, D. and Gustafsson, O. (2010). "Extensive Methane Venting to the Atmosphere from Sediments of the East Siberian Arctic Shelf." Science **327**(5970): 1246-1250.

Slubowska-Wodengen, M., Rasmussen, T. L., Koc, N., Klitgaard-Kristensen, D., Nilsen, F. and Solheim, A. (2007). "Advection of Atlantic Water to the western and northern Svalbard shelf since 17,500 cal yr BP." Quaternary Science Reviews **26**(3-4): 463-478.

Smith, L., Sachs, J., Jennings, A., Anderson, D. and DeVernal, A. (2001). "Light δ13C events during deglaciation of the East Greenland continental shelf attributed to methane release from gas hydrates." Geophysical Research Letters **28**(11): 2217-2220.

Snyder, G. T., Hiruta, A., Matsurnoto, R., Dickens, G. R., Tomaru, H., Takeuchi, R., Komatsubara, J., Ishida, Y. and Yu, H. (2007). "Pore water profiles and authigenic mineralization in shallow marine sediments above the methane-charged system on Umitaka Spur, Japan Sea." Deep-Sea Research Part Ii-Topical Studies in Oceanography **54**(11-13): 1216-1239.

Solheim, A., Andersen, E., Elverhøi, A. and Fiedler, A. (1996). "Late Cenozoic depositional history of the western Svalbard continental shelf, controlled by subsidence and climate." Global and Planetary Change **12**(1): 135-148.

Spiegler, D. (1993). Planktonic foraminifer Cenozoic biostratigraphy of the Arctic Ocean, Fram Strait (Sites 908-909), Yermak Plateau (Sites 910-912), and East Greenland Margin (Site 913). PROCEEDINGS-OCEAN DRILLING PROGRAM SCIENTIFIC RESULTS, NATIONAL SCIENCE FOUNDATION.

Spielhagen, R. F., Werner, K., Sorensen, S. A., Zamelczyk, K., Kandiano, E., Budeus, G., Husum, K., Marchitto, T. M. and Hald, M. (2011). "Enhanced Modern Heat Transfer to the Arctic by Warm Atlantic Water." Science **331**(6016): 450-453.

Spindler, M. and Dieckmann, G. S. (1986). "Distribution and abundance of the planktic foraminifer Neogloboquadrina pachyderma in sea ice of the Weddell Sea (Antarctica)." Polar Biology **5**(3): 185-191.

Stein, R. (2008). Arctic Ocean Sediments: Processes, Proxies, and Paleoenvironment: Processes, Proxies, and Paleoenvironment, Elsevier.

Stein, R., Brass, G., Graham, D., Pimmel, A. and Party, S. S. (1995). "Hydrocarbon measurements at Arctic Gateways Sites (ODP-Leg 151)." Initial Reports ODP **151**: 385-396.

Steinsund, P. I. and Hald, M. (1994). "Recent Calcium-Carbonate Dissolution in the Barents Sea - Paleoceanographic Applications." Marine Geology **117**(1-4): 303-316.

Thiede, J., Myhre, A. and Firth, J. (1995). Cenozoic northern hemisphere polar and subpolar ocean paleoenvironments (summary of ODP Leg 151 drilling results). Proceedings of the Ocean Drilling Program. Initial reports, Ocean Drilling Program.

Thiede, J., Myhre, A. M., Firth, J. V., Johnson, G. L. and Ruddiman, W. F. (1996). "Introduction to the north Atlantic-Arctic Gateways: Plate Tectonic-Paleoceanographic history and significance." Proceedings of the Ocean Drilling Program, Scientific Results **151**.

Torres, M. E., Martin, R. A., Klinkhammer, G. P. and Nesbitt, E. A. (2010). "Post depositional alteration of foraminiferal shells in cold seep settings: New insights from flow-through time-resolved analyses of biogenic and inorganic seep carbonates." Earth and Planetary Science Letters **299**(1): 10-22.

Torres, M. E., Mix, A. C., Kinports, K., Haley, B., Klinkhammer, G. P., McManus, J. and de Angelis, M. A. (2003). "Is methane venting at the seafloor recorded by delta C-13 of benthic foraminifera shells?" Paleoceanography **18**(3).

Vincent, E. and Berger, W. (1981). "Planktonic foraminifera and their use in paleoceanography." The sea **7**: 1025-1119.

Vorren, T. O., Hald, M. and Lebesbye, E. (1988). "Late cenozoic environments in the Barents Sea." Paleoceanography **3**(5): 601-612.

Wefer, G. and Heinze, P.-M. (1994). "Clues to ancient methane release." Nature **369**: 282.

Wefer, G., Heinze, P. M. and Berger, W. H. (1994). "Clues to Ancient Methane Release." Nature **369**(6478): 282-282.

Zachos, J. C., Rohl, U., Schellenberg, S. A., Sluijs, A., Hodell, D. A., Kelly, D. C., Thomas, E., Nicolo, M., I, R., Lourens, L. J., McCarren, H. and Kroon, D. (2005). "Rapid acidification of the ocean during the Paleocene-Eocene thermal maximum." Science **308**(5728): 1611-1615.

Appendix 1

Sample no.	SITE HOLE	CORE	SEC	DEPTH	MBSF	C. reniforme (	delta 13C (permil VPDB)	delta 18O (permil VPDB)
1a	151-912A	1	1	68-72	0,68	17	-0,726	5,405
2a	151-912A	1	1	146-150	1,46	17	-0,201	5,639
3a	151-912A	1	2	68-72	2,18	15	-0,707	5,415
5a	151-912A	2	1	68-72	4,68	16	-0,829	5,455
6a	151-912A	2	1	146-150	5,46	6	-0,649	5,493
7a	151-912A	2	2	68-72	6,18	15	-0,58	5,957
8a	151-912A	2	2	146-150	6,96	11	-0,696	6,069
12a	151-912A	2	4	145-149	9,95	10	-0,681	5,73
14a	151-912A	2	6	68-72	12,18	10	-0,843	5,217
15a	151-912A	2	6	145-149	12,95	15	-0,75	5,363
18a	151-912A	3	1	145-149	14,95	8	-0,51	5,575
19a	151-912A	3	2	68-72	15,68	15	-1,008	4,851
20a	151-912A	3	2	146-150	16,46	14	-0,883	5,507
21a	151-912A	3	4	68-72	18,68	15	-2,067	5,526
22a	151-912A	3	4	146-150	19,46	12	-1,156	5,723
23a	151-912A	3	5	68-72	20,18	11	-1,424	5,87
						N. pachyderma sin. (no. of specimen)		
1b	151-912A	1	1	68-72	0,68	15	0,211	4,934
2b	151-912A	1	1	146-150	1,46	15	0,06	4,832
3b	151-912A	1	2	68-72	2,18	15	-0,031	4,326
4b	151-912A	1	3	68-72	3,68	15	0,253	5,056
5b	151-912A	2	1	68-72	4,68	15	-0,148	4,845
6b	151-912A	2	1	146-150	5,46	14	0,025	4,794
7b	151-912A	2	2	68-72	6,18	15	-0,033	4,942
8b	151-912A	2	2	146-150	6,96	15	0,128	4,927
9b	151-912A	2	3	68-72	7,68	8	-0,143	4,917
10b	151-912A	2	3	146-150	8,46	10	-0,205	5,175
11b	151-912A	2	4	68-72	9,18	15	-0,19	4,267
12b	151-912A	2	4	145-149	9,95	15	-0,007	4,767
13b	151-912A	2	5	146-150	11,46	15	-0,332	3,698
14b	151-912A	2	6	68-72	12,18	15	-0,146	4,037
15b	151-912A	2	6	145-149	12,95	15	-0,248	3,43
16b	151-912A	2	7	59-63	13,59	8	-0,342	3,406
17b	151-912A	3	1	68-72	14,18	15	-0,067	4,675
18b	151-912A	3	1	145-149	14,95	12	0,021	4,07
19b	151-912A	3	2	68-72	15,68	12	-0,163	4,129
20b	151-912A	3	2	146-150	16,46	15	-0,786	4,429
21b	151-912A	3	4	68-72	18,68	15	-0,893	5,04
22b	151-912A	3	4	146-150	19,46	15	-0,46	4,891
23b	151-912A	3	5	68-72	20,18	11	-0,518	4,806
						N. atlantica sin. (no. of specimen)		
1c	151-912A	1	1	68-72	0,68	15	-0,068	4,853
2c	151-912A	1	1	146-150	1,46	15	-0,354	4,567
3c	151-912A	1	2	68-72	2,18	15	-0,147	4,615
4c	151-912A	1	3	68-72	3,68	14	-0,075	4,7
5c	151-912A	2	1	68-72	4,68	15	-0,475	4,698
6c	151-912A	2	1	146-150	5,46	15	0,064	5,45
7c	151-912A	2	2	68-72	6,18	15	-0,352	4,89
8c	151-912A	2	2	146-150	6,96	15	-0,047	4,761
9c	151-912A	2	3	68-72	7,68	15	0,068	5,813
10c	151-912A	2	3	146-150	8,46	10	-0,114	5,283
11c	151-912A	2	4	68-72	9,18	14	-0,283	4,682
12c	151-912A	2	4	145-149	9,95	15	-0,192	4,957
13c	151-912A	2	5	146-150	11,46	15	-0,112	4,041
14c	151-912A	2	6	68-72	12,18	16	-0,345	3,678
15c	151-912A	2	6	145-149	12,95	15	-0,504	3,375
17c	151-912A	3	1	68-72	14,18	14	-0,373	4,719
19c	151-912A	3	2	68-72	15,68	15	-0,481	4,083
20c	151-912A	3	2	146-150	16,46	15	-0,956	4,361
21c	151-912A	3	4	68-72	18,68	15	-1,166	4,93
22c	151-912A	3	4	146-150	19,46	15	-0,516	4,679

Sample no.	SITE HOLE	CORE	SEC	DEPTH	MBSF	C. reniforme (	delta 13C (permil VPDB)	delta 18O (permil VPDB)
2a	151-912A	11	4	68-72	92,78	10	-0,279	5,876
4a	151-912A	11	5	146-150	95,06	15	-0,805	5,211
5a	151-912A	11	6	127-131	96,37	15	-8,824	5,135
6a	151-912A	13	1	68-72	107,58	15	-0,51	5,106
7a	151-912A	13	1	146-150	108,36	15	-0,721	5,013
8a	151-912A	13	2	68-72	109,08	15	-0,457	4,929
11a	151-912A	13	3	120-124	111,02	15	-0,683	4,698
12a	151-912A	13	4	68-72	111,92	15	-0,472	4,846
13a	151-912A	13	4	137-141	112,61	12	-0,363	4,78
14a	151-912A	13	5	68-72	113,34	9	-0,505	4,644
15a	151-912A	13	6	45-49	114,61	15	-0,847	5,558
16a	151-912A	15	1	68-72	126,78	8	-0,263	4,951
17a	151-912A	15	3	146-150	130,11	10	-0,589	5,586
18a	151-912A	15	4	72-76	130,87	15	-0,467	5,578
19a	151-912A	15	4	141-145	131,56	18	-0,547	5,485
20a	151-912A	15	5	72-76	132,32	15	-0,423	5,381
21a	151-912A	15	5	144-148	133,04	15	-0,682	5,204
22a	151-912A	15	6	68-72	133,78	15	-0,569	5,391
23a	151-912A	15	6	140-144	134,5	14	-0,351	5,01
						C. teretis (no. of specimen)		
1b	151-912A	11	3	146-150	92,06	9	-0,596	5,676
3b	151-912A	11	4	146-150	93,56	15	-13,345	5,283
5b	151-912A	11	6	127-131	96,37	15	-9,388	5,177
6b	151-912A	13	1	68-72	107,58	7	-0,425	4,852
7b	151-912A	13	1	146-150	108,36	7	-0,521	4,891
10b	151-912A	13	3	72-76	110,54	8	-0,303	5,173
11b	151-912A	13	3	120-124	111,02	10	-0,302	4,53
12b	151-912A	13	4	68-72	111,92	13	-0,398	4,833
18b	151-912A	15	4	72-76	130,87	10	-0,426	5,314
19b	151-912A	15	4	141-145	131,56	13	-0,311	5,264
20b	151-912A	15	5	72-76	132,32	15	-0,54	5,032
21b	151-912A	15	5	144-148	133,04	15	-0,451	4,756
22b	151-912A	15	6	68-72	133,78	14	-0,457	5,115
						M. barleeanum (no. of specimen)		
2c	151-912A	11	4	68-72	92,78	6	-1,288	5,284
7c	151-912A	13	1	146-150	108,36	5	-1,678	4,494
16c	151-912A	15	1	68-72	126,78	11	-1,238	4,485

Appendix 1: Values from the preliminary work (Baranwal, S., unpublished data).

Appendix 2

Sample	Site Hole	Core	Sec	Depth	Foranminifera	Count	MASS 44 (mV)	δ¹³C ‰	δ¹⁸O ‰
6160CN	151-912A	2	7	13,05	Cassidulina neoteretis	20	4636,833333	-1,93412	5,279309
6160NP	151-912A	2	7	13,05	Negloboquadrina pachyderma (si	40	4568,166667	-1,28308	4,242087
6160MB	151-912A	2	7	13,05	Melonis barleeanum	20	4854,666667	-1,68712	4,96028
6156NP	151-912A	3	1	13,58	Negloboquadrina pachyderma (si	40	4793,833333	-0,09832	4,451289
6156CN	151-912A	3	1	13,58	Cassidulina neoteretis	15	2552,333333	-0,80647	5,099539
6162CN	151-912A	3	2	15,07	Cassidulina neoteretis	22	2582,166667	-1,65938	4,835563
6162NP	151-912A	3	2	15,07	Negloboquadrina pachyderma (si	30	2664	-0,87457	4,007585
6164NP	151-912A	3	2	15,55	Negloboquadrina pachyderma (si	40	3845,5	-1,88286	3,888133
6164MB	151-912A	3	2	15,55	Melonis barleeanum	19	3469,666667	-2,0439	4,664399
6164CN	151-912A	3	2	15,55	Cassidulina neoteretis	20	4557,5	-2,11411	4,696871
6169MB	151-912A	3	3	16,79	Melonis barleeanum	18	2170,5	-1,3591	4,540705
6169CN	151-912A	3	3	16,79	Cassidulina neoteretis	22	5810,333333	0,476154	4,853674
84B CN	151-912A	8	1	61,22	Cassidulina neoteretis	10	4200,666667	-0,76543	4,475432
85B CN	151-912A	8	1	61,68	Cassidulina neoteretis	20	4009,666667	-0,75028	4,850698
99B CN	151-912A	9	2	71,96	Cassidulina neoteretis	12	2470,333333	-0,25738	5,160257
99B MB	151-912A	9	2	71,96	Melonis barleeanum	9	3148,666667	-1,22626	5,012487
100B MB	151-912A	9	2	72,68	Melonis barleeanum	13	3569,166667	-1,29552	4,788428
101B F	151-912A	9	3	73,46	Fursenkoina	13	2037,5	-21,2108	5,344484
102B CN	151-912A	9	3	74,18	Cassidulina neoteretis	20	4131,5	-0,60468	5,26266
103B CN	151-912A	9	4	74,96	Cassidulina neoteretis	20	5059,333333	-0,199	3,439458
103B MB	151-912A	9	4	74,96	Melonis barleeanum	10	4330,5	-1,25751	4,766502
104B CN	151-912A	9	4	75,68	Cassidulina neoteretis	18	4558,666667	-0,35291	5,505795
107B CN	151-912A	9	6	77,96	Cassidulina neoteretis	20	4153,5	-0,43824	5,085682
108B CN	151-912A	10	1	78,66	Cassidulina neoteretis	16	3833,333333	-0,16785	5,488078
109B CN	151-912A	10	1	78,68	Cassidulina neoteretis	9	1755,666667	-0,27699	5,463624
111B CN	151-912A	10	2	80,18	Cassidulina neoteretis	13	2720,333333	-0,46639	4,978186
111B E	151-912A	10	2	80,18	Elphidium	16	4866,166667	-1,99955	4,5198
111B F	151-912A	10	2	80,18	Fursenkoina	20	2145,666667	-0,35481	6,385671
117B CN	151-912A	10	5	84,77	Cassidulina neoteretis	20	2907,666667	-0,1249	5,318028
5971 CN	151-912A	10	5	85,04	Cassidulina neoteretis	25	3688,833333	-0,31895	4,581964
5973 CN	151-912A	10	5	85,22	Cassidulina neoteretis	24	3289	-0,50724	4,727777
5973 MB	151-912A	10	5	85,22	Melonis barleeanum	15	5088,833333	-1,71806	4,364505
5975 CN	151-912A	10	5	85,4	Cassidulina neoteretis	20	2161,5	-1,59119	3,92499
5975 MB	151-912A	10	5	85,4	Melonis barleeanum	6	2175,833333	-0,35286	4,687858
119B CN	151-912A	11	1	88,28	Cassidulina neoteretis	30	3571	-5,4974	5,665938
119B MB	151-912A	11	1	88,28	Melonis barleeanum	13	5788	-5,10156	5,45498
6123 CN	151-912A	11	2	89,15	Cassidulina neoteretis	20	5721,666667	-5,78938	5,047709
6123 MB	151-912A	11	2	89,15	Melonis barleeanum	19	5563,5	-5,66341	4,581803
6125 CN	151-912A	11	2	89,33	Cassidulina neoteretis	22	5495,666667	-0,39711	5,015411
5996 CN	151-912A	11	3	91,15	Cassidulina neoteretis	10	2431,833333	-1,34141	4,036486
5960 CN	151-912A	11	4	92,41	Cassidulina neoteretis	15	5563,5	-0,37886	5,078867
6082 CN	151-912A	11	5	94,49	Cassidulina neoteretis	12	4633,333333	-10,3637	5,105534
6077 CN	151-912A	11	5	94,65	Cassidulina neoteretis	23	4256,666667	-0,78782	4,712065
6074 CN	151-912A	11	5	94,81	Cassidulina neoteretis	20	5640,333333	-2,96059	4,085543
6074 E	151-912A	11	5	94,81	Elphidium	20	5480,166667	-0,73954	4,720684
6080 CN	151-912A	11	6	95,24	Cassidulina neoteretis	21	5321,5	-1,79271	4,361318
6080 MB	151-912A	11	6	95,24	Melonis barleeanum	12	4042,166667	-0,67713	4,735852
6085 CN	151-912A	11	6	95,43	Cassidulina neoteretis	25	5630,166667	-1,86905	4,196807
6085 MB	151-912A	11	6	95,43	Melonis barleeanum	15	3525,333333	-0,57996	4,803096
6105CN	151-912A	13	1	107,11	Cassidulina neoteretis	20	3980	-2,52988	4,118051
6105 E	151-912A	13	1	107,11	Elphidium	9	1234,333333	-0,6008	4,57548
6106 CN	151-912A	13	2	108,54	Cassidulina neoteretis	12	1364,833333	-0,53485	4,560412
6110 CN	151-912A	13	3	109,96	Cassidulina neoteretis	20	3428,5	-2,38083	3,966398
6110 E	151-912A	13	3	109,96	Elphidium	14	1960	-0,40002	4,588593
6119 CN	151-912A	13	5	112,8	Cassidulina neoteretis	16	5942,666667	-0,73843	4,761312

Appendix 2: Samples from the Stable Isotope Laboratory at Oregon State University in the USA conducted in this mater thesis.